# Seismic Analysis and Design for Enhanced Performance of Nonstructural Components in Steel Buildings

# Seismic Analysis and Design for Enhanced Performance of Nonstructural Components in Steel Buildings

By
NEDA SALARI, BSC, MSC

Faculty of Engineering
Department of Civil Engineering

A Thesis Submitted to the School of Graduate Studies in Partial Fulfilment of the Requirements for the Degree of Doctor of Philosophy

McMaster University


TITLE: SEISMIC ANALYSIS AND DESIGN FOR ENHANCED PERFORMANCE OF NONSTRUCTURAL COMPONENTS IN STEEL BUILDINGS

AUTHOR: Neda Salari
SUPERVISORS: Dr. Michael Tait
Dr. Dimitrios Konstantinidis

NUMBER OF PAGES: pages (i-145)

## Abstract

Large economic losses and downtime due to nonstructural damage in recent earthquakes have highlighted the need for improving the seismic performance of nonstructural components (NSCs). Recognizing this, many studies have focused on evaluating the seismic demands of NSCs supported on structures of various types. However, previous studies considered the supporting structure as a single-degree-of-freedom (SDOF) system or as a simplified multi-DOF frame. More advanced nonlinear modeling techniques able to capture damage-induced deterioration must be considered to arrive at more realistic estimates of the response of various structural system types. In addition, demand estimation methods must be complemented with appropriate design procedures that enable the reduction of seismic losses associated with NSCs.

The first main objective of this thesis is to better quantify the seismic demands imposed on acceleration-sensitive components mounted in steel buildings with common lateral force resisting systems, including Special Concentrically Braced Frame (SCBF) and Special Moment Frame (SMF) structures. The second main objective focuses on developing a simplified performance-based design procedure centered on NSC losses. To achieve the first objective, eleven archetypes with varying heights and vibration properties are numerically modeled using state-of-the-art validated methods. Then, the absolute floor acceleration responses are used to generate floor acceleration spectra for various NSC damping and ductility levels. The thesis presents qualitative and quantitative aspects of the NSC demands, as well as practical formulas for relevant design parameters, including the ratio of peak floor acceleration (PFA) to peak ground acceleration (PGA), and the ratio of peak component acceleration (PCA) to PFA. The thesis proceeds with using FEMA P-58 procedures to develop a simplified NSC-loss-based design approach for SCBF structures. This approach is based on NSC loss spectra that allow in-advance selection of the design base shear coefficient so that acceptable exceedance probabilities can be met for multiple loss levels.

## Acknowledgments

This research would not have been possible without the support, advice, and guidance from Dr. Dimitrios Konstantinidis. I greatly appreciate his knowledge and commitment to research. I would like to express my sincere gratitude to Dr. Michael Tait for his continuous support in different stages of my graduate studies at McMaster University.

I also would like to thank the members of my supervisory committee, Dr. Lydell Wiebe and Dr. Tracy Becker, for their valuable comments and suggestions throughout this research work.

It is difficult for me to find appropriate words to thank my parents and my sister, Hoda. I can never forget the support and encouragement from my love, Ashkan. Also, I would like to express my gratitude to my best friends Mehdi and Nooshin, and my sweetheart niece, Noojhan, who have gifted motivation and happiness to my Ph.D. life.

# Table of Contents

Chapter 1. Introduction ..... 14

1.1. Background and Motivation ..... 14

1.2. State of the art in NSC performance evaluation ..... 3

1.2.1. General Subjects ..... 4

1.2.2. FRS generation Methods ..... 7

1.2.3. NSC performance evaluation methods ..... 8

1.3. The knowledge gaps in performance evaluation of NSCs ..... 9

1.4. Research Objectives ..... 11

1.5. Thesis structure ..... 12

1.6. References ..... 13

Chapter 2. Demands on Acceleration-Sensitive Nonstructural Components in Special Concentrically Braced Frame and Special Moment Frame Buildings……...17

2.1. Introduction ..... 18

2.2. Overview of Building Archetype Designs ..... 22

2.1. Modeling Approach ..... 24

2.2. Verification of the Models ..... 27

2.3. Earthquake Ground Motions ..... 28

2.4. Floor Acceleration Demands ..... 29

2.4.1. PFA/PGA Ratio ..... 29

2.4.2. Fourier Amplitude Spectra of Floor Accelerations ..... 34

2.5. Modified Equation for the PFA/PGA Ratio ..... 37

2.6. Floor Response Spectra ..... 40

2.7. Component Amplification Factor ..... 45

2.8. Conclusions ..... 50

2.9. References ..... 51

Chapter 3. Seismic Demands on Inelastic Nonstructural Components in Steel Buildings ..... 56

3.1. Introduction ..... 57

3.2. Analysis Methods ..... 60

3.2.1. Summary of Building Designs, Structural Modeling, and Ground Motions ..... 60

3.2.2. Modeling of Inelastic NSCs ..... 61

3.3. Floor Response Spectra for Inelastic NSC ..... 62

3.3.1. Effect of NSC Damping Ratio on the Roof Response Spectra. ..... 62

3.4. Effect of NSC Ductility on the Component Amplification Factor ..... 65

3.5. Effect of NSC Damping Ratio on the Roof Response Spectra ..... 66

3.6. Damping Modification Factor Formula ..... 67

3.7. Component Amplification Factor Formula for NSCs Mounted on SCBF and SMF Buildings ..... 68

3.8. Comparison of NSC Seismic Design Force Values Based on Different Methods ..... 70

3.9. Conclusions ..... 74

3.10. References ..... 75

Chapter 4. Simplified Seismic Nonstructural Loss-Based Design of Special Concentric Braced Frames ..... 90

4.1. Introduction ..... 91

4.2. Methodology ..... 95

4.3. Initial design evaluations ..... 101

4.4. The loss and MID spectra ..... 108

4.5. Design Example ..... 116

4.6. Conclusions ..... 117

4.7. *References* ..... 119

Chapter 5. Summary and Recommendations ..... 140

5.1. Summary ..... 140

5.2. Recommendations for Future Study ..... 143

# List of Figures

Fig. 1-1. Overturned nonstructural components [10, 11]..... 2
Fig. 1-2. Examples of nonstructural components [12]..... 2
Fig. 1-3. A Chronological view of the studies conducted on NSCs utill 2019; a)keyword repetitions, and b) overall quantity of related papers published in each year [15]..... 4
Fig. 1-4. Example numerical evaluation on acceleration-sensitive NSCs by [20]; a) building layout, b) input ground motion spectra..... 5
Fig. 2-1. Plan views of the (a) 3- and 6-story SCBF buildings (b) 12-story SCBF buildings (c) SMF buildings ..... 23
Fig. 2-2. Elevation views of the (a) chevron SCBFs (b) TSX SCBFs (c) SMF……..24
Fig. 2-3. Results of the verification for (a) SCBF [52], (b) RBS steel moment connection [53] ..... 28
Fig. 2-4. Acceleration response spectra of the $MCE_R$-scaled ground motions for the 6-story SCBFs (5% damping) ..... 29
Fig. 2-5. Distributions of PFA/PGA and peak story drift ratio of the SCBF systems (a) 3-chevron (b) 3-TSX (c) 6-chevron (d) 6-TSX (e) 12-chevron (f) 12-TSX ..... 32
Fig. 2-6. Distributions of PFA/PGA and peak story drift ratio of the SMF systems (a) 4-ELF (b) 4-RSA (c) 8-RSA (d) 12-RSA (e) 20-RSA ..... 33
Fig. 2-7. Fourier spectra of the (a) fourth floor of the 6-TSX structure, 1992 Landers earthquake, Coolwater record (b) fourth floor of the 12-chevron structure, Imperial Valley earthquake, Delta record (c) $11^{th}$ floor of the 12-TSX structure, Imperial Valley earthquake, El Centro Array #11 record (DE level) ..... 36
Fig. 2-8. Profile of PFA/PGA over building height for seismic design of acceleration-sensitive NSC (DE level) ..... 40
Fig. 2-9. Median floor response spectra for SCBF archetype buildings under DE level (5% damping), (a) 3-chevron (b) 3-TSX (c) 6-chevron (d) 6-TSX (e) 12-

chevron (f) 12-TSX, vertical dashed lines show the first few structural periods ..... 42
Fig. 2-10. Median floor response spectra for SMF archetype buildings under DE level (5% damping), (a) 4-ELF (b) 4-RSA (c) 8-RSA (d) 12-RSA (e) 20-RSA, vertical dashed lines show the first few structural periods ..... 43
Fig .2-11. Median of PCA/PFA under DE level, 5% component damping ratio, (a) 3-TSX (b) 12-chevron (c) 4-ELF (d) 12-RSA..... 46
Fig. 2-12. Effect of the modal period on the component amplification factor 47
Fig. 2-13. Maximum PCA/PFA curves of the 11 archetype buildings together with the median of all buildings and a regression formula ..... 49
Fig. 3-1. Plan and elevation views of the SCBF buildings ..... 80
Fig. 3-2. Plan and elevation views of the SMF buildings ..... 81
Fig. 3-3. Constant-ductility floor response spectra for NSCs mounted on the SCBF structures ($\beta_{comp}$ = 2%) ..... 83
Fig. 3-4. Constant-ductility floor response spectra for NSCs mounted on the SMF structures ($\beta_{comp}$ = 2%) ..... 83
Fig. 3-5. Component amplification factor spectra for NSCs mounted at the roof levels of 6-TSX and 8-RSA ($\beta_{comp}$ = 2%) ..... 84
Fig. 3-6. Component amplification factor as a function of target ductility for NSC mounted at the roof level ($\beta_{comp}$ = 2%)..... 84
Fig. 3-7. Effect of NSC damping ratio on roof-level response spectra ($\mu_{comp}$ = 1.5) ..... 85
Fig. 3-8. Effect of NSC damping ratio on roof-level response spectra ($\mu_{comp}$ = 2.0) ..... 85
Fig. 3-9. Effect of ductility level on PCA reduction from $\beta_{comp}$=1% to $\beta_{comp}$=7%.....86
Fig. 3-10. Damping modification factor (DMF) at the roof level..... 86
Fig. 3-11. Median component amplification factor PCA/PFA ($\beta_{comp}$ = 5%) as a function of the ratio of component period to resonant structural period, $T_p / T_r$: (a) SCBF (b) SMF (c) Combined..... 87

Fig. 3-12. Comparison of the component amplification factor ($\beta_{comp}$ = 5%) for in-resonance NSCs in ASCE 7-22/ATC-120, and this study for NSC (a) supported at grade plane (b) supported above grade plane ..... 87
Fig. 3-13. Deviation of seismic design force predicted by: (a) the ATC-120 formula [adapted from Figure 4-42 in (NIST 2018)], and (b) this study's prediction formula, from the seismic design force values computed by NLRHA ..... 87
Fig. 3-14. Comparison of the normalized design force for NSCs supported at grade plane ..... 88
Fig. 3-15. Comparison of the normalized design force for NSCs supported at the roof level ..... 89
Fig. 4-1.The proposed flowchart for simplified design based on Loss/MID-MAFE design spectra. ..... 96
Fig. 4-2. The IDA-based procedure used for generating the design spectra. ..... 98
Fig. 4-3. The simplified pushover-based approach used for extracting structural demand distributions. ..... 98
Fig. 4-4. Plan layout of the SCBF archetypes along with the elevation layout of the 12-story SCBFs (Salari et al., 2022). ..... 99
Fig. 4-5. Static pushover curves obtained for the structures. ..... 103
Fig. 4-6. Median MID-$S_a$ curves obtained for the chevron SCBFs obtained using IDA and SPO methods. ..... 104
Fig. 4-7. Median PSDRs obtained for the chevron SCBFs at the 0.5MCC $S_a$ level using IDA and SPO methods. ..... 107
Fig. 4-8. Median PFAs obtained for the chevron SCBFs at the 0.5MCC $S_a$ level using IDA and SPO methods. ..... 108
Fig. 4-9. The utilized seismic hazard curves. ..... 109
Fig. 4-10. MID-MAFE spectra obtained for the chevron SCBFs at the 0.5MCC $S_a$ level using IDA and SPO methods. ..... 111
Fig. 4-11. Spectra of repair cost MAFE obtained for seismic NSCs using the IDA and SPO-based methods. ..... 113
Fig. 4-12. Spectra of parallel repair time MAFEs obtained for seismic NSCs using the IDA and SPO-based methods. ..... 114

Fig. 4-13. Regions of the loss-MAFE curves. ..... 115
Fig. 4-14. a) the pushover curve and b) the NSC repair cost probability curve, of the 5-story chevron SCBF designed versus $C_y$=0.22. ..... 117
Fig. 4-15. IDA-based spectra of repair cost MAFEs (seismic NSCs). ..... 121
Fig. 4-16. IDA-based spectra of parallel repair time MAFEs (seismic NSCs)……..122
Fig. 4-17. IDA-based spectra of sequential repair time MAFEs (seismic NSCs)……..123
Fig. 4-18. IDA-based spectra of repair cost MAFE (non-seismic NSCs)..... 124
Fig. 4-19. IDA-based spectra of parallel repair time MAFEs (non-seismic NSCs). ..... 125
Fig. 4-20. IDA-based spectra of sequential repair time MAFEs (non-seismic NSCs). ..... 126
Fig. 4-21. Pushover-based spectra of repair cost MAFE (seismic NSCs). .... 127
Fig. 4-22. Pushover-based spectra of parallel repair time MAFEs (seismic NSCs). ..... 128
Fig. 4-23. Pushover-based spectra of sequential repair time MAFEs (seismic NSCs). ..... 129
Fig. 4-24. Pushover-based spectra of repair cost MAFE (non-seismic NSCs).130
Fig. 4-25. Pushover-based spectra of parallel repair time MAFEs (non-seismic NSCs). ..... 131
Fig. 4-26. Pushover-based spectra of sequential repair time MAFEs (non-seismic NSCs). ..... 132

# List of Tables

Table 2-1. Member sections ..... 25

Table 3-1. Modal and resonant periods of the buildings with SCBF and SMF seismic force resisting systems (SFRS) ..... 79

Table 3-2. Parameters used to calculate the maximum PCA based on Eq. (5) and as required per ASCE 7-22 (Horizontal lines in Figs. 3 and 4) ..... 79

Table 3-3. Regression coefficient values of the proposed DMF formula [Eq. (4)]……..…..78

Table 3-4. Component ductility categories (adapted from ASCE/SEI 7-22, Table C13.3-1) ..... 80

Table 4-1. $C_y$ values regarded for developing the design maps. ..... 99

Table 4-2. The variables used in the accompanying "extractPlots.m" MATLAB script. ..... 138

## Co-Authorship

This thesis has been prepared in accordance with the regulations for a "sandwich" thesis format as stipulated by the School of Graduate Studies at McMaster University. Chapters 2 through 4 consist of journal articles co-authored with the supervisors[1] and collaborators as detailed below:

Chapter 2: Demands on Acceleration-Sensitive Nonstructural Components in Special Concentrically Braced Frame and Special Moment Frame Buildings

Authors: N. Salari, D. Konstantinidis, V. Mohsenzadeh, L. Wiebe

The analytical model and analysis were carried out by Neda Salari under the supervision of Dr. Konstantinidis. Equations for the PFA/PGA ratio and NSC amplification factor, which account for the dynamic characteristics of the buildings, are developed based on regression analysis of the generated data. Conceptualization, methodology, software, validation, formal analysis and investigation were carried out by N. Salari. Conceptualization, methodology, writing - review & editing, supervision, project administration and funding acquisition are provided by Dr. Konstantinidis. Dr. Mohsenzadeh and Dr. Wiebe had contributions in methodology, software, writing - review & editing. This chapter has been published in *Engineering Structures*.

Chapter 3: Seismic Demands on Inelastic Nonstructural Components in Steel Buildings

Authors: N. Salari, D. Konstantinidis

Conceptualization, methodology, software, validation, formal analysis and investigation were carried out by N. Salari under the supervision of Dr. Konstantinidis. The manuscript was prepared by N. Salari under the supervision of Dr. Konstantinidis. This chapter has been submitted for publication in the *Journal of Structural Engineering*.

[1] Initially, Dr. Konstantinidis served as the sole supervisor until his departure from McMaster University in December 2018. In January 2019, Dr. Tait assumed the primary supervisor role, while Dr. Konstantinidis continued to lead the technical supervision.

Chapter 4: Simplified Seismic Nonstructural Loss-based Design of Special Concentric Braced Frames

Authors: N. Salari, D. Konstantinidis, L. Wiebe, M. Tait

The conceptualization was done by Neda Salari. The methodology was developed by Neda Salari with advice from Drs. Konstantinidis, Wiebe, and Tait. The first draft was prepared by N. Salari, and subsequent versions were edited with feedback from Drs. Konstantinidis, Wiebe, and Tait. This chapter is ready to be submitted for publication in *Engineering Structures*.

# Chapter 1. INTRODUCTION

## 1.1. Background and Motivation

Significant losses and downtime due to the failure of architectural components, electrical and mechanical equipment, collectively referred to as nonstructural components (NSC), have been reported after past seismic events [1-5]. Damage to NSCs initiates at lower seismic intensity levels compared to structural elements and can result in downtime and casualty even when the structural system performs well. Maintaining functionality during and after the seismic event is vital for critical facilities, including hospitals, emergency operations centers, and fire stations. As the investment in NSC accounts for 80 to 90% of the total cost of a building [6, 7], losses due to damage in these components were greater than losses due to structural damage in many strong earthquakes [8]. Fig. 1-1 illustrates the overturned components in an office building. Even in the case of ordinary residential, commercial, or office buildings, the cost and time related to the repair or replacement of NSCs may be comparable to or exceed those of the structural system itself [6, 7]. This is especially true when high-tech facilities such as high-performance computers and other expensive electrical systems are contained in the building. According to the loss evaluation reports following the 2001 El Salvador earthquake, NSC damage led to functionality loss in hospitals, while only limited damage to structural systems was reported [9]. The NSC losses in the February 28, 2001, Nisqually (Seattle Olympia) earthquake [10] and the 2010 Bio-Bio Chilean earthquake [11] have also been reported to account for a considerable portion of the economic seismic losses, especially for the healthcare system. Therefore, it is important to ensure that NSC mounted in buildings can resist the force and displacement demands on them due to seismic excitations.

Fig. 1-2 shows examples of typical nonstructural components. To assess their damage vulnerability, NSCs can be classified into two categories: (a) Acceleration-sensitive components, such as suspended ceilings, fire sprinkler piping, and light

fixtures and (b) displacement-sensitive components such as vertical pipes running floor to floor, floor-to-ceiling partition walls, and cladding. The performance of acceleration-sensitive components is controlled by the supporting structure's acceleration, while displacement-sensitive components are vulnerable to damage because of the interstory drift response of the supporting structure [8].

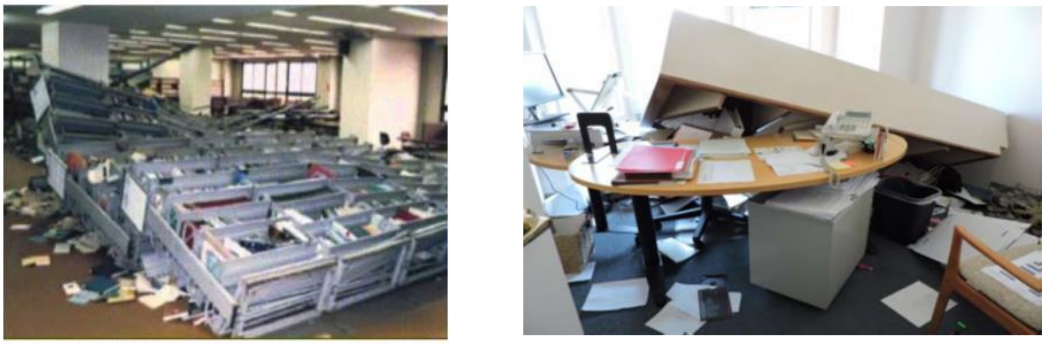

***Fig. 1-1. Overturned nonstructural components [10, 11].***

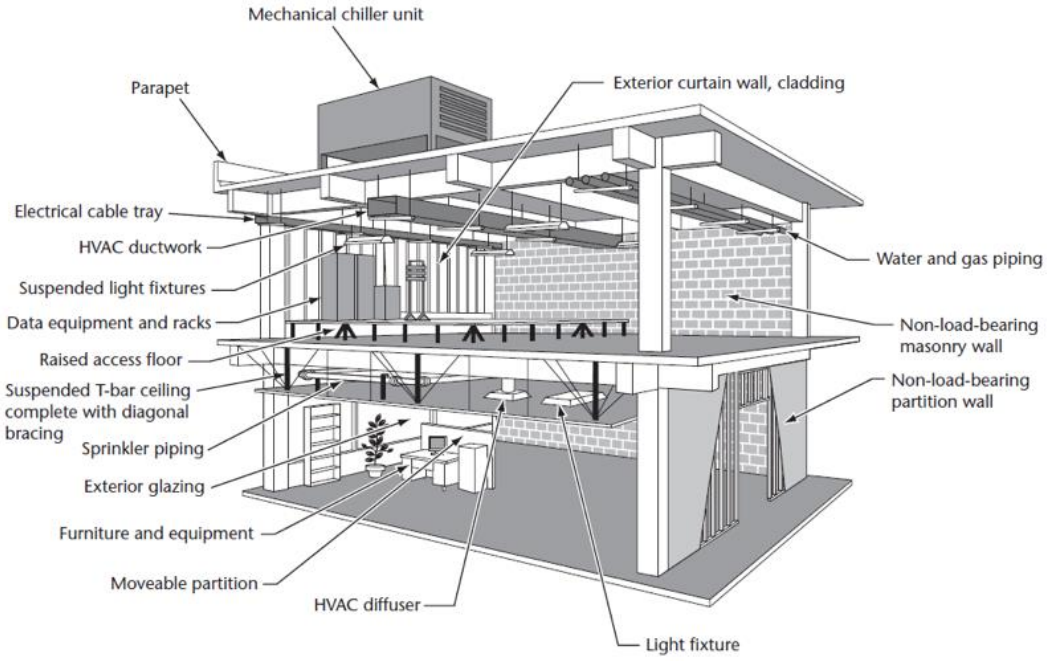


***Fig. 1-2. Examples of nonstructural components [12]***

Along with the development of structural evaluation methods, the damage to NSCs caused by the structural response (drifts and accelerations) came into the spotlight. Design standards, such as ASCE 7, included provisions regarding the seismic force demands on NSCs. A detailed review of these provisions and the research supporting them is provided in the next section. In general, the acceleration demands

on NSCs with different vibration periods and located at various heights of structures were the subject of research on NSC performance and code-based requirements. The structural design methods have started to replace force-based demand estimations with performance predictions that are more and more expressed in terms of the interests of the owners and stockholders. The seismic loss parameter is a key representative of buildings' seismic performance which includes NSC losses as a main part. However, the NSC design requirements do not currently account for NSC losses by considering parameters such as the response of the supporting structure. [8,10].

The development of a performance-based NSC design approach is a key requirement according to the key roles NSCs play in many critical buildings and facilities. These buildings include hospitals, emergency management services, power plants, governmental decision-making centers and so on. In such buildings, NSCs are expected to remain operational during and after seismic events. In other building occupancies, NSC damage may be allowed as far as it does not lead to loss of life. In general, there are wide ranges of NSC types and building occupancies and a loss estimation procedure should align itself to these variables. To allow the design scenario to address different intensity and response levels, structural analysis should be repeated for various intensity levels pushing the structure to various response and damage levels. Considering the requirements of a performance-based design method, the current approach of the standards may be inadequate since it does not provide a metric to estimate the level of damage to NSCs under given seismicity levels.

Before presenting the objectives and the methodology used in this thesis for supporting a future performance-based NSC design approach, a review of the state of the art in predicting the seismic performance of the NSCs is presented. Next, the goal of the study and the steps taken to address it throughout the chapters are presented.

### 1.2. State of the art in NSC performance evaluation

Many studies have been carried out in recent years to evaluate seismic demands on NSCs in buildings. A chronological review of these studies classified with respect to several related keywords until 2019 was presented by Wang et al [15] and is illustrated in Fig. 1-3. According to this figure, the number of studies performed in this area has continuously increased and reached a total number of 410 based on the SCI-

EXPANDED database, updated on May 10, 2019 [15]. A brief review of some of these studies is presented in this section. More detailed reviews are provided in the later sections of this dissertation with respect to the subject of those sections.

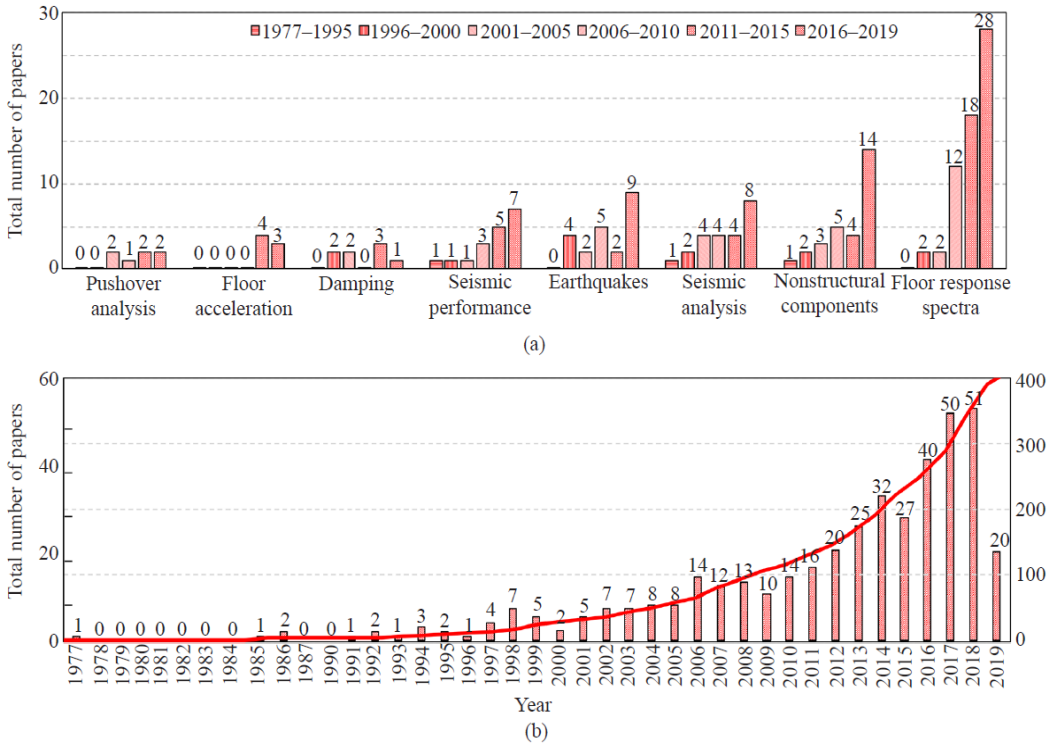


***Fig. 1-3. A Chronological view of the studies conducted on NSCs utill 2019; a)keyword repetitions, and b) overall quantity of related papers published in each year [15].***

### *1.2.1. General subjects*

Although there are plentiful information and guidelines available for the design of structural systems, the seismic design of NSCs is still unexplored for different performance levels [16]. Due to the large economic losses caused by NSCs during earthquakes, the post-earthquake downtime and repair costs associated with NSC damage have been studied in the context of the seismic resilience of buildings [17-18]. These studies have reported difficulties in orchestrating the response of NSCs with that of the supporting structures due to the different mechanical properties of the two types of components. Thus, identifying the vibration characteristics of the floor, where the NSC is located on, forms one of the key steps in evaluating NSCs performance.

Due to the complete compatibility between the drift response of the drift-sensitive NSCs and the supporting structures, the seismic response of these components

can be estimated in a straightforward way from the structure's interstory drifts. However, the relation between the response of acceleration-sensitive NSCs and the supporting floor is associated with complexities related to the dynamic properties dominating the vibration of both the supporting floor and the mounted NSC. Thus, acceleration-sensitive components have been the focus of most previous studies. These studies have generated floor response spectra (FRS) and assessed the effect of various parameters influencing the FRS. The results of an investigation examining the effect of floor number and NSC vibration period are shown in Fig. 1-4. This figure shows typical results of response history analyses on a four-story moment-resisting frame provided in the later chapters of this dissertation. Other descriptions about the data given in this figure will be provided in the next chapters.

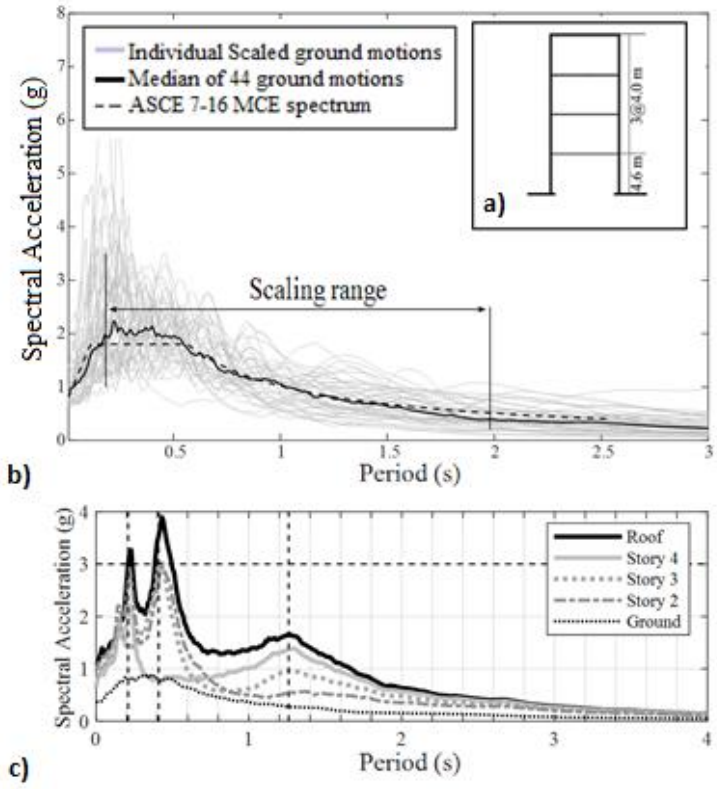


***Fig. 1-4. Example numerical evaluation on acceleration-sensitive NSCs by [20]; a) building layout, b) input ground motion spectra.***

The floor acceleration spectra are affected by the dynamic properties of the structure and the intensity and frequency content of the applied ground motion. Considering an earthquake as a collection of acceleration pulses imposed one after another, the excitation pulses with periods near the period of the structure are amplified

while the remaining pulses are filtered out [21]. Various studies have been conducted to develop FRS for the seismic design of NSCs. Medina et al. [22] evaluated the effects of different parameters that influence the shape of the FRS in frame structures, including the damping ratio of the component, the location of the component, and the modal periods of the structure. The effect of NSC location was also evaluated by Ray-Chaudhuri and Villaverde [23], in which the authors conducted a parametric study on acceleration responses of NSCs in steel moment frames, showing that the widespread nonlinear behavior of the supporting structure generally reduces the peak acceleration responses, except for a few cases in which NSCs located on lower floors have periods in resonance with the second and third modal periods of the structure. Medina et al. [22] modeled NSCs as single-degree-of-freedom (SDOF) oscillators located on a variety of stiff and flexible moment frames modeled using nondeteriorating elements, which are called generic models. Anajafi and Medina [24] evaluated the ASCE 7-16 seismic design force formula for NSCs through modeling simplified structural systems and concluded that the acceleration responses of NSCs are a function of NSC location along the height, seismic intensity, and the ratio between the period of the NSC and structural period. In addition, studies were carried out in which the effect of damping ratios of the supporting structures and of the NSCs were examined [21, 25-27]. The effect of nonlinear behavior of the structural system was evaluated in a number of studies [22, 28-30]. Some other topics evaluated by past researchers include the effect of torsion [26], diaphragm flexibility [25], and type of lateral load-resisting system [26, 31-33] in the supporting building.

Although considerable efforts have been spent on improving the simplified design approach for attached NSCs, only a few studies have considered the actual observations made for the response of the floors supporting NSCs in evaluating their seismic performance [28, 34-35]. The results of these studies were based on recorded data from instrumented buildings subjected to ground motions that were significantly weaker than the design level earthquakes [24, 34-35]. In addition to these observation-based studies, the effect of NSC inelasticity has been addressed in a number of numerical researches [23-24, 35-40]. Further details regarding the methods used by these studies are presented in the next section.

### *1.2.2. FRS generation methods*

Generally, the methods used in the literature to define the FRS can be classified as SDOF-based methods, MDOF-based methods, amplification factor methods and methods directly defining FRS. The earliest studies used the SDOF-based method, where the supporting structure is modeled as an SDOF system [41-42]. The SDOF-based studies use a spring model which represents the damped fundamental mode and the yielding base shear obtained by applying the first vibration mode as the load pattern. On the other hand, modal superposition was used by MDOF-based methods, in which SDOF-based FRS are obtained for multiple modes, instead of the first mode, and are then combined using modal superposition techniques such as SRSS and CQC [43].

Numerical prediction of the FRS for NSCs supported on elastic and inelastic SDOF models was the subject of work done by Sullivan et al., 2013 [21]. The floor acceleration spectra were quantified as a function of the vibration period, the extent of experienced inelasticity, and the damping ratio of the supporting structure. They also employed results of dynamic inelastic analyses to propose an equation for predicting the dynamic amplification factor. The uncertainties associated with modal characteristics of the supporting structures were the focus of the study by Haymes et al. [44], who estimated elastic FRS through a modal superposition method. The proposed method was adequately simple for design purposes and could enhance the reliability of the estimated FRS compared with methods neglecting higher mode effects. The proposed method was validated against the spectra recorded for instrumented buildings in New Zealand. Evaluations on inelastic SDOF models were performed by Vukobratović and Fajfar [45], in which the NSC properties including vibration period, ductility demand level, and damping ratio were considered. A study by Kazantzi et al. [46] represented the effect of dynamic characteristics of the supporting structure by modifying the NSC damping ratio using a factor which was correlated to the NSC period normalized by the building period. In a recent evaluation, Merino et al. [47] aimed to improve the accuracy of the equation proposed by Sullivan et al. [21] by enhancing the consistency between absolute acceleration and relative displacement FRS through conducting inelastic dynamic analyses at various ground motion intensity levels.

### *1.2.3. NSC performance evaluation methods*

The final objective of the demand estimation methods proposed for NSCs is to enable evaluation of losses during a seismic event. In general, the term "loss" addresses conditions in which a system or a component fails to fulfill the desired performance and leaves economic, social and environmental consequences. The loss associated with NSC was pursued initially in prescriptive standards that proposed design methods for limiting the NSC's damage. The first NSC design guideline was published by the Applied Technology Council (ATC) [48]. Following that, the ratio of peak floor acceleration to peak ground acceleration (PFA/PGA) was introduced by design standards, such as ASCE 7-10 (2010). The design formulas proposed by these documents were later evaluated by research studies. Fathali and Lizundia [49] employed data from the California Strong Motion Instrumentation Program database and showed the conservatism of the ASCE 7-10 PFA/PGA ratio, expressed as the so-called height factor, against the recorded data. The same database was used by Anajafi and Medina [26] to extend the ASCE 7-16 formula to include various factors, including diaphragm deformability, torsional effects, and the type of lateral force resisting system.

In line with the developments proposed for structural systems, evolving the code-based prescriptive design methods into performance-based guidelines could allow better addressing of the interests of the building owners and stockholders. One of the guidelines addressing the seismic performance of NSCs is FEMA P-58 [52]. This guideline provides a loss-based performance assessment calculation tool (PACT) that can support a performance-based seismic design (PBSD) procedure. Such procedures require the computation of NSC losses when the structure is subjected to probabilistic seismic analyses. Thus, the findings of the previous studies in estimating NSC demands should be accompanied by fragility and loss functions that rely on observed damage and losses for NSCs when subjected to various levels and types of acceleration excitation.

Currently, there is a gap between the implementation of the loss-based NSC design procedures (such as FEMA P-58) and the NSC demand estimation methods proposed by previous researchers. FEMA P-58 provides a database for NSCs that are commonly used in residential and office buildings. This database contains fragility functions that estimate the probability that a damage state of an NSC will be reached

conditioned on the floor shaking intensity, represented by an engineering demand parameter (EDP). The predicted damage is next mapped to probabilistic consequences which can be monetary, downtime, casualty or environmental type. The NSCs potential damage is currently evaluated based on one of three EDPs: peak floor acceleration, peak interstory drift, and, rarely, peak floor velocity. Thus, the component acceleration, which is the focus of the reviewed literature, is not readily useable in state-of-the-art NSC loss estimation procedures. This is mainly due to the previously mentioned lack of component damage acceleration relations.

### 1.3. The knowledge gaps in performance evaluation of NSCs

This section highlights limitations and knowledge gaps related to the performance evaluation and design of NSCs:

- Accounting for the effects of structural system inelasticity

The previous studies on the demand (mainly acceleration) of NSCs have either used elastic models or inelastic models simplified as SDOF or MDOF models. According to seismic design criteria proposed by standards like ASCE 7-22, a considerable level of inelasticity is expected to occur even under the design basis earthquake. Many experimental evaluations have revealed that local damage starts to appear in the members just as soon as they enter the inelastic range. Upon damage initiation, the strength and stiffness of the members also start to deteriorate as the deflection is amplified or the absorbed energy is increased by applying repeated loading reversals. This evidence supports the need for utilizing inelastic deteriorating models even when intensities as low as DE are considered.

On the other hand, using inelastic SDOF models might not be sufficient because higher vibration modes are known to play a crucial role in the demands on NSCs. Prescriptive seismic design codes focus on a performance objective at which the NSC damage is only prevented at the DE level. At the MCE level, prevention of life losses forms the focus of these codes, thereby allowing extensive damage to the NSCs. From a performance-based design view, selection of the performance objective is due to the building owner. Therefore, NSC damage prevention is also likely to become a concern at the MCE level, as it is actually necessary for buildings with specialized NSC contents. Considering the yield strengths of the story members and the distributed story drifts at

intensities higher than DE, some members enter into their inelastic range while others behave elastically. This alters the distribution of the stiffness throughout the structure and the vibration modes determining the response of the building to the ground motion excitation. Continual plasticity accumulation in yielded members eventually leads to damage and total stiffness loss in the members. Therefore, it can be said that the response of the stories supporting the NSCs is a result of the changes in the stiffness distribution due to yielding and local damage. While a story with reduced stiffness undergoes larger drifts, it will vibrate with lower acceleration, compared to stories with higher stiffness. Accounting for these phenomena is only possible when accurate simulation of yielding and local buckling is allowed by the model.

Replacing SDOF models with generic inelastic MDOF models is also associated with some approximations. These models are commonly one-bay equivalent frames that only represent the overall shear/flexural force-deformation behavior of the actual story members. Thus, these frames cannot account for phenomena such as local or global buckling of plates or braces. They also neglect the accurate distribution of response in the horizontal direction. This distribution is important when the axial column forces are computed using the flexural demands imposed on the stories. That is, using equivalent lateral dimension misleads computation of the structure's slenderness (the height-to-width ratio) which affects the significance of p-delta moments and the domination of either shear or flexural deformations in the lateral response. Generic models are also incapable to account for the actual redundancy of the structure due to the concentration of resisting mechanisms via a few springs.

According to the above descriptions, In line with an accurate representation of the structural system’s behavior, the geometrical and mechanical aspects of the structures should be specifically addressed. In fact, the use of SDOF and generic MDOF models by previous studies had made it difficult to focus on the geometrical and mechanical aspects of the structures. A widely used structural system, in which deterioration of structural members is highly probable, is the SCBF system. Besides the SCBFs, which are characterized by highly deteriorating behavior, steel moment frames (SMFs) form the most frequent structural system employed in urban construction. Developing system-specific NSC demand models needs to be prioritized for these structural systems.

- NSC response inelasticity

In addition to the supporting structure, the maximum demand on the NSCs depends on the yielding-induced stiffness changes they undergo during an excitation. The NSC stiffness affects its vibration period which in turn influences the degree to which NSC is in resonance with the vibration of the supporting structure. The yielding-induced period changes have also been neglected in the previous studies on NSC demand estimations.

- Design procedures that use NSC damage estimations

While the reviewed studies have focused on estimating the NSC demands, utilization of their findings in a practical performance-based design procedure is not yet established, especially when the monetary and casualty losses form the direct interests of the decision-makers. As mentioned before, a design procedure makes use of pertinent performance estimation tools and proposes optimum methods for adjustment of the building so that the estimated performance reaches the design goal.

- NSC damage-demand relations

As mentioned before, accounting for NSC losses in a performance-based design procedure needs fragilities that map the estimated NSC demands to probable damage levels. Mapping the damage prediction to loss measures such as repair cost and downtime should be next done using appropriate consequence functions. Such fragility and consequence functions are currently provided by FEMA P-58 for limited NSCs and by relying on demands that are computed for the structural system rather than for the NSCs.

Among the above knowledge gaps, the last one is found to be apart from the path of this study due to its dependence on lacking experimental data. However, addressing the former items makes the objectives of this research.

### 1.4. Research objectives

The goal of this study is to generate knowledge about improving the seismic performance of nonstructural components in steel buildings. Its findings aim at informing the development of a new generation of either prescriptive or performance-based design approaches for nonstructural components.

In the first part, we concentrate on developing structural system-specific demand models for acceleration-sensitive elastic and inelastic NSCs. These demand models are to be proposed as regression formulas, which facilitate a straightforward integration with the structure of existing seismic provisions for NSCs. For this purpose, the absolute floor acceleration responses of SCBF and MRF structures are simulated considering ground motion uncertainties. The simulated data are next used for generating the NSC acceleration spectra that account for accurate structural behavior. These spectra are subjected to regression analysis in order to generate a formula that predicts the PCA/PFA ratio.

The objective of the second part is to develop a simplified a NSC-loss-based design approach and to showcase its application on SCBF structures. To achieve this, the study introduces the concept of NSC loss spectra, which allow in-advance selection of the design base shear coefficient so that multiple loss levels and their acceptable exceedance probabilities can be met. The fragility and loss functions provided by FEMA P-58 [50] are used for filling the mentioned knowledge gap between the NSC demand formulas and the NSC loss functions. Other aspects of the loss estimation procedure proposed by FEMA P-58 are also used for developing the NSC loss spectra.

### 1.5. Thesis structure

In Chapter 2, the demands on acceleration-sensitive elastic NSCs mounted on various floors of SCBF and MRF structures with different heights are investigated. The seismic behavior of these structural systems is accurately modeled in OpenSees and validated against available experimental findings. The models are subjected to nonlinear response history analyses under a suite of ground motion records. The simulated floor acceleration histories are then used to generate the acceleration spectra for elastic NSCs. The generated spectra are finally used for deriving regression equations that predict the PCA/PFA ratio for varying conditions including the damping ratio of the NSC and the structure's fundamental period.

In Chapter 3, the findings of Chapter 2 are extended for NSCs with nonlinear responses and the PCA/PFA results are used for deriving separate regression equations. The findings are used for evaluation of the recommendations of the most recent seismic

design standard ASCE 7-22 (ASCE 2022). The accuracy of this standard is assessed for various NSC ductility levels. Predictive regression formulas are also provided for the damping modification factor and strength-reduction factor for inelastic NSCs mounted on the roof level of the archetype buildings.

Chapter 4 addresses the performance-based design procedure of structures using NSC losses. For this purpose, a set of design spectra are provided that express the exceedance probability for various NSC loss levels when different design base shear coefficients, denoted by $C_y$, are considered. To develop these design spectra, a total number of 36 SCBF structures with 3, 6 and 12 stories are designed for a range of $C_y$ values, and the FEMA P-58 (FEMA 2018) procedure is followed for estimating the probabilistic NSC loss curves. The accuracy and applicability of two alternative structural demand estimation methods proposed by FEMA P-58, based on incremental dynamic analysis (IDA) and static pushover (SPO), are evaluated and discussed. The SPO-based method is finally adopted for developing the NSC loss-based design spectra, according to its better consistency with the $C_y$-based proportioning procedure.

Chapter 5 is devoted to a summary of the findings and proposing potential topics for future studies.

**References**

[1] Federal Emergency Management Agency (FEMA). Reducing the risks of nonstructural earthquake damage – A practical guide, Fourth edition. FEMA E-74 2011.

[2] Soong T. Seismic performance of nonstructural elements during the Loma Prieta earthquake. Report NIST SP 796, Proceedings of the 22nd Joint Meeting U.S.-Japan Cooperative Program in Natural Resources Panel on Wind and Seismic Effects, National. Institute of Standards and Technology, Gaithersburg, Maryland, PP. 331-336, 1990.

[3] Soong T., Chen G., Wu Z., Zhang R., Grigoriu M. Assessment of the 1991 NEHRP provisions for nonstructural components and recommended revisions. Report NCEER-93-0003, National Center for Earthquake Engineering Research, Buffalo, N.Y. 1993. 25

[4] Reitherman R., Sabol T. Northridge earthquake of January 17, 1994: reconnaissance report -nonstructural damage. Earthquake Spectra. 11. PP.453-514 EERI 1995.

[5] Phipps M. The impact of nonstructural damage on building performance: reflections on the 1994 Northridge earthquake. Report UCB/EERC- 97/05, The EERC-CUREE Symposium in Honor of Vitelmo V. Bertero, Earthquake Engineering Research Center, University of California, Berkeley, California, 173-178. 1997.

[6] Taghavi S., and Miranda E. Response assessment of nonstructural building elements. The University of California, Berkeley, CA, Report No. 2003/05, 2003.
[7] Comerio M. PEER testbed study on a laboratory building: exercising seismic performance assessment. Report No. PEER 2005-12 Pacific Earthquake Engineering Research Center, University of California, Berkeley, CA, 2005.
[8] Filiatrault A., and Sullivan T. Performance-based seismic design of nonstructural building components: The next frontier of earthquake engineering," Earthquake Engineering and Engineering Vibration. 13(1): PP. 17-46. 2014.
[9] Boroschek, R. L. (2004). Seismic vulnerability of the healthcare system in El Salvador and recovery after the 2001 earthquakes. Natural Hazards in El Salvador, 375, 269.
[10] Filiatrault, A., Perrone, D., Merino, R. J., & Calvi, G. M. (2021). Performance-based seismic design of nonstructural building elements. Journal of Earthquake Engineering, 25(2), 237-269.
[11] Mitrani-Reiser, J., Mahoney, M., Holmes, W. T., De La Llera, J. C., Bissell, R., & Kirsch, T. (2012). A functional loss assessment of a hospital system in the Bío-Bío province. Earthquake Spectra, 28(1_suppl1), 473-502.
[12] CSA S832-06 (2006), Seismic Risk Reduction of Operational and Functional Components (OFCs) of Buildings, Canadian Standards Association, Mississauga, Ontario, Canada
[13] ASCE-7. 2016. ASCE 7-16: Minimum design loads and associated criteria for buildings and other structures. In. American Society of Civil Engineers, Reston, Virginia.
[14] ASCE-7. 2022. ASCE 7-22: Minimum design loads and associated criteria for buildings and other structures. In. American Society of Civil Engineers, Reston, Virginia.
[15] Wang, T., Shang, Q., & Li, J. (2021). Seismic force demands on acceleration-sensitive nonstructural components: a state-of-the-art review. Earthquake Engineering and Engineering Vibration, 20(1), 39-62.
[16] O'Reilly, G J., et al. Seismic assessment and loss estimation of existing school buildings in Italy. Engineering Structures 168 (2018), 142-162.
[17] Bruneau, M., Chang, S. E., Eguchi, R. T., Lee, G. C., O'Rourke, T. D., Reinhorn, A. M., Von Winterfeldt, D. (2003). A framework to quantitatively assess and enhance the seismic resilience of communities. Earthquake Spectra, 19(4), 733-752.
[18] Myrtle, R. C., Masri, S. F., Nigbor, R. L., & Caffrey, J. P. (2005). Classification and prioritization of essential systems in hospitals under extreme events. Earthquake Spectra, 21(3), 779-802.
[19] Wang, T., Shang, Q., & Li, J. (2020). Case Study of Floor Acceleration Response Spectra in Reinforced Concrete Frames Using Different Methods. Paper presented at the 17th World Conference on Earthquake Engineering.
[20] Salari, N, Konstantinidis D, Mohsenzadeh V, Wiebe L. Demands on acceleration-sensitive nonstructural components in special concentrically braced frame and special moment frame buildings. Engineering Structures 260 (2022), 114031.
[21] Sullivan, T. J., Calvi, P. M., & Nascimbene, R. (2013). Towards improved floor spectra estimates for seismic design. Earthquakes and Structures, 4(1), 109-132.

[22] Medina, R. A., Sankaranarayanan, R., & Kingston, K. M. (2006). Floor response spectra for light components mounted on regular moment-resisting frame structures. Engineering Structures, 28(14), 1927-1940.
[23] Chaudhuri, S. R., and Villaverde, R. Effect of building nonlinearity on seismic response of nonstructural components: a parametric study. Journal of structural engineering 134.4 (2008), 661-670.
[24] Anajafi, H. and Medina, R. A. (2018). Evaluation of ASCE 7 equations for designing acceleration-sensitive nonstructural components. Paper presented at the 11th US National Conference on Earthquake Engineering.
[25] Anajafi, H., & Medina, R. A. (2019). Damping modification factor for elastic floor spectra. Bulletin of Earthquake Engineering, 17(11), 6079-6108.
[26] Anajafi, H., & Medina, R. A. (2019). Lessons learned from evaluating the responses of instrumented buildings in the United States: the effects of supporting building characteristics on floor response spectra. Earthquake Spectra, 35(1), 159-191.
[27] Clayton, J. S., & Medina, R. A. (2012). Proposed method for probabilistic estimation of peak component acceleration demands. Earthquake Spectra, 28(1), 55-75.
[28] Chaudhuri, S. R., & Villaverde, R. (2008). Effect of building nonlinearity on seismic response of nonstructural components: a parametric study. Journal of Structural Engineering, 134(4), 661-670.
[29] Sankaranarayanan, R., & Medina, R. A. (2008). Statistical models for a proposed acceleration-response modification factor for nonstructural components attached to inelastic structures. Paper presented at the Proceedings of 14th world conference on earthquake engineering, Beijing, China.
[30] Taghavi, S., & Miranda, E. (2012). Probabilistic study of peak floor acceleration demands in nonlinear structures. Paper presented at the Proceedings of the 15th world conference on earthquake engineering (15WCEE), Lisbon, Portugal.
[31] Anajafi, H., & Medina, R. A. (2018a). Effects of Supporting Building Characteristics on Nonstructural components Acceleration Demands. Paper presented at the 11th US National Conference on Earthquake Engineering.
[32] Miranda, E., & Taghavi, S. (2003). Response assessment of nonstructural building elements. Pacific Earthquake Engineering Research Center, University of California Berkeley, California, USA.
[33] Taghavi, S., & Miranda, E. (2006). Seismic demand assessment on acceleration-sensitive building nonstructural components. Paper presented at the Proceedings of the 8th National Conference on Earthquake Engineering, San Francisco, California, USA.
[34] Kazantzi, A., Vamvatsikos, D., & Miranda, E. (2018). Effect of yielding on the seismic demands of nonstructural elements. Paper presented at the Proceedings of 16th European conference on earthquake engineering, Thessaloniki, Greece.
[35] Anajafi, H., Medina, R. A., & Santini-Bell, E. (2020). Inelastic floor spectra for designing anchored acceleration-sensitive nonstructural components. Bulletin of Earthquake Engineering, 18(5), 2115-2147.
[36] Adam, C., & Fotiu, P. (2000). Dynamic analysis of inelastic primary–secondary systems. Engineering Structures, 22(1), 58-71.
[37] Igusa, T. (1990). Response characteristics of inelastic 2-DOF primary-secondary system. Journal of Engineering Mechanics, 116(5), 1160-1174.

[38] Obando, J., & Lopez-Garcia, D. (2018). Inelastic displacement ratios for nonstructural components subjected to floor accelerations. Journal of Earthquake Engineering, 22(4), 569-594.
[39] Toro, G. R., McGuire, R. K., Cornell, C. A., & Sewell, R. T. (1989). Linear and nonlinear response of structures and equipment to California and Eastern United States earthquakes. Retrieved from
[40] Villaverde, R. (2006). Simple method to estimate the seismic nonlinear response of nonstructural components in buildings. Engineering Structures, 28(8), 1209-1221.
[41] Kapur, K. K., & Shao, L. C. (1973). Generation of seismic floor response spectra for equipment design. Paper presented at the Structural Design of Nuclear Plant Facilities 1973.
[42] Penzien, J., & Chopra, A. K. (1965). Earthquake response of appendage on a multi-story building. Paper presented at the Proceedings, 3rd World Conference on Earthquake Engineering.
[43] Igusa, T., D. Kiureghian, A. and Sackman J. L. (1984). Modal decomposition method for stationary response of non-classically damped systems. Earthquake Engineering & Structural Dynamics 12(1), 121-136.
[44] Haymes, K., Sullivan, T., Chandramohan, R. A practice-oriented method for estimating elastic floor response spectra. Bulletin of the New Zealand Society for Earthquake Engineering 53.3 (2020), 116-136.
[45] Vukobratović, V., & Fajfar, P. (2017). Code-oriented floor acceleration spectra for building structures. Bulletin of Earthquake Engineering, 15(7), 3013-3026.
[46] Kazantzi, A., Vamvatsikos D., and Miranda E. The effect of damping on floor spectral accelerations as inferred from instrumented buildings. Bulletin of Earthquake Engineering 18.5 (2020), 2149-2164.
[47] Merino, R. J., Perrone, D., Filiatrault A. Consistent floor response spectra for performance-based seismic design of nonstructural elements. Earthquake Engineering & Structural Dynamics 49.3 (2020), 261-284.
[48] Applied Technology Council, and Structural Engineers Association of California. Tentative Provisions for the Development of Seismic Regulations for Buildings: A Cooperative Effort with the Design Professions, Building Code Interests, and the Research Community. No. 6. Department of Commerce, National Bureau of Standards, 1978.
[49] Fathali S, Lizundia B. Evaluation of current seismic design equations for nonstructural components in tall buildings using strong motion records. The Structural Design of Tall and Special Buildings 2011; 20 30-46. DOI:10.1002/tal.736.
[50] NIST. NIST GCR 18-917-43. 2018. Recommendations for Improved Seismic Performance of Nonstructural Components.
[51] Salari, N, Konstantinidis. Seismic Demands on Inelastic Nonstructural Components in Steel Buildings. Under review.
[52] FEMA P-58. (2018). Seismic Performance Assessment of Buildings. Volume 1 Methodology. Washington, D.C.

# Chapter 2. Demands on Acceleration-Sensitive Nonstructural Components in Special Concentrically Braced Frame and Special Moment Frame Buildings

Reproduced with permission from Elsevier

Salari, N, Konstantinidis D, Mohsenzadeh V, Wiebe L. Demands on acceleration-sensitive nonstructural components in special concentrically braced frame and special moment frame buildings. *Engineering Structures*, 260 (2022): 114031

## Abstract

This study investigates demands on acceleration-sensitive nonstructural components (NSCs) in code-compliant Special Concentrically Braced Frame (SCBF) and Special Moment Frame (SMF) structures. Previous studies have highlighted that the assumption of ASCE 7-22 for the ratio of Peak Floor Acceleration (PFA) to Peak Ground Acceleration (PGA) is overly conservative. In most previous studies, the results were based on generic analytical models with non-deteriorating structural behavior or recorded data from instrumented buildings subjected to ground motions that were significantly weaker than the design-level earthquakes. This study evaluates the acceleration demands on NSCs in 11 archetype buildings modeled using advanced techniques. The ground motions used elicit inelastic response in the frames at the level expected by ASCE 7-16 compliant designs. The study examines the effect of the ratio of NSC period to structural period, NSC damping ratio, and NSC vertical location on these demands. Results of this investigation are compared with the provisions of ASCE 7-16 and the recommendations of the recently completed effort by the Applied Technology Council (ATC-120 project). Equations for the PFA/PGA ratio and NSC amplification factor, which account for the dynamic characteristics of the buildings, are developed based on regression analysis of the generated data. Results of the analyses

indicate that the NSC seismic design force formula recommended by ATC-120, which includes building nonlinearity effects through a constant building ductility reduction factor, underestimates the PFA/PGA ratio for most of the considered archetypes, especially in the lower floors. At the same time, results show that the design force equation recommended by ATC-120 is conservative for SCBF archetypes, while it underestimates the design force for the SMFs.

## 2.1. INTRODUCTION

Past earthquakes have underscored that damage to acceleration-sensitive nonstructural components (NSCs) can result in significant economic losses and partial or total loss of building functionality [1-5]. Loss of functionality can be especially detrimental in the case of critical facilities like hospitals [6-9].

Current seismic design codes, such as ASCE 7-16 [10], permit an equivalent static approach for the design of acceleration-sensitive NSCs. The ASCE 7-16 [10] formula for the seismic design force of NSCs assumes that peak floor acceleration (PFA) varies linearly from the Peak Ground Acceleration (PGA) at the ground level to three times the PGA at the roof. Owing to its simplistic nature, the ASCE 7-16 approach does not adequately factor in all aspects that affect the acceleration response of NSCs, e.g., the structural periods, the location of the NSC in the building, and the NSC period and damping ratio [11].

Investigations have been conducted to better estimate the PFA/PGA ratio, considering the parameters that are expected to influence it, such as structural periods, lateral force-resisting system (LFRS), and earthquake intensity [12-14]. Fathali and Lizundia [14] used recorded floor motions of the California Strong Motion Instrumentation Program to evaluate the PFA/PGA ratio from ASCE 7-10 [15], and they concluded that it was overly conservative. They recommended new formulas for both the PFA/PGA ratio and the component amplification factor, i.e., the ratio of Peak Component Acceleration (PCA) to PFA. More recently, Anajafi and Medina [16] conducted a study on the same instrumented buildings used by Fathali and Lizundia [14] to evaluate the effects of various factors that are not considered in the seismic design force formula for NSCs in ASCE 7-16, including diaphragm flexibility, torsional effects, and the type of LFRS. The evaluation concluded that the shear- and flexure-

dominated behavior of the buildings can affect the roof response spectra. In another study, Anajafi and Medina [11] evaluated the ASCE 7-16 seismic design force formula for NSCs through modeling simplified archetype buildings and concluded that the PCA/PGA ratio is a function of NSC location along the height, ground motion intensity, and the ratio between the period of the NSC and structural period. When considering instrumented buildings, they reported that the ratio of the measured PGA to the design PGA (which is equal to $0.4S_{DS}$ in the code) was smaller than unity in most of the cases. Specifically, the ratio was less than 0.5 and 0.75 for 85% and 96% of the records, respectively, which implies that the instrumented buildings were likely responding in their elastic range [11]. Kazantzi et al. [17] proposed a simplified equation to estimate the NSC amplification factor using the floor motions recorded for the instrumented buildings. It was also concluded that the NSC amplification factor used in the ASCE 7-16 standard considerably underestimates the acceleration responses for the components tuned with the modal periods of the structures.

Medina et al. [18] considered NSCs as single-degree-of-freedom (SDOF) oscillators mounted on a variety of stiff and flexible moment frames modeled using non-deteriorating frame elements, referred to as *generic* models therein. Based on this, they introduced recommendations for estimating the peak acceleration demands on NSCs in nonlinear moment resisting frames, concluding that the energy dissipation through the nonlinear action of the supporting structure provides valuable benefit in reducing the maximum acceleration responses experienced by the NSCs. D'Angela et al. [19] evaluated the seismic damage to the unanchored NSCs mounted on the reinforced concrete buildings. Flores et al. [20] evaluated floor acceleration demands on NSCs mounted on moment resisting frames modeled using elastic and inelastic frames. The effect of gravity frame modeling and different levels of partially restrained connections in the gravity frames were also assessed. Ray-Chaudhuri and Villaverde [21] conducted a parametric study on acceleration responses of NSCs in steel moment frames, illustrating that the widespread nonlinear action of the supporting structure generally reduces the peak acceleration responses, except for a few cases in which NSCs located on lower floors had periods in resonance with the second and third modal periods of the structure. Taghavi and Miranda [22] investigated a set of structures with different periods and LRFS types. Results indicated that when the supporting structure

behaved in the linear range, the ground accelerations were amplified at the floor levels, while when the structures were pushed into the inelastic range, the floor accelerations were smaller than the ground acceleration. Also, they concluded that the saturation of the floor acceleration keeps the peak roof acceleration below the peak ground acceleration. Wieser et al. [23] proposed an improved equation for the PFA/PGA ratio considering period and ductility level of the buildings through modeling 3-, 9-, and 20-story three-dimensional moment frames.

Flores et al. [24] evaluated the acceleration demands on NSCs attached to special steel moment frames represented by models with different degrees of complexity. Results showed that the modeling approach does not greatly affect the acceleration demands on NSCs, but simple models that did not include strength degradation were unable to capture large drifts. Ray-Chaudhuri and Hutchinson [25] evaluated the effect of nonlinearity of moment frames on the horizontal peak floor accelerations, finding that the PFA of nonlinear frames was overestimated in IBC 2003 [26]. Similar to the results of the earlier studies, the nonlinearity of the frames generally resulted in PFA reduction.

Sullivan et al. [27] presented a set of calibrated equations to predict the Floor Response Spectrum (FRS) of elastic and inelastic SDOF supporting structures. To define the shape and magnitude for the floor spectra, different factors were considered, including natural period, nonlinearity level, and damping ratio of the supporting system. Moreover, an empirical formula for estimating the dynamic amplification factor was recommended based on nonlinear response history analysis results. Haymes et al. [28] proposed a modal superposition method to estimate elastic FRS considering uncertainty in modal properties. The method showed a reliable estimation while keeping simplicity for practical design purposes. Comparison between the generated FRS with the recorded spectra from instrumented buildings in New Zealand confirmed the effectiveness of the proposed approach. Vukobratovic and Fajfar [29] proposed a method for generating FRS considering the inelastic behavior of supporting SDOF structures. They evaluated the effects of the natural period of the structure, ductility, and damping ratio of the NSC on the FRS. The effect of the NSCs viscous damping ratio on the FRS has been evaluated by Kazantzi et al. [30] and a damping modification factor as a function of a normalized NSC period by the building modal period has been proposed. More recently,

Merino et al. [31] showed that the proposed methodology by Sullivan et al. [27] does not precisely predict consistent absolute acceleration and relative displacement FRS, and they proposed a new procedure to achieve that. The FRS generated from the results of the nonlinear response history analyses confirmed the effectiveness of the procedure for both 70-year and 2475-year ground motions.

One of the most comprehensive projects on the seismic performance of nonstructural components to-date was conducted by the Applied Technology Council (ATC) project ATC-120, culminating in the publication of the NIST GCR 18-917-43 report [36]. The objectives of the project included the development of an improved nonstructural design force formula. The formula recommended by ATC-120 depends on various factors, among them the PFA/PGA and PCA/PFA factors, recommendations for which were also presented. The recommended PFA/PGA factor is based on both the variation in PFA/PGA recorded in instrumented buildings and computed from simplified continuous models consisting of a flexural beam coupled with a shear beam [22, 32]. However, as discussed earlier, the data from instrumented buildings correspond largely to scenarios where the intensity level of the input ground motions was not sufficiently large to elicit inelastic response in the buildings [11], and the analytically derived PFA/PGA profiles were based on elastic models. To account for the effect on inelastic action in the buildings on the PFA/PGA profile, ATC-120 recommended the use of a constant reduction factor ($R_{\mu bldg}$) based on the building's global ductility. However, the use of a constant factor to modify the elastic PFA/PGA profile reduces that profile uniformly up the structure, and thus may not realistically represent the profile shape that results due to the inelastic action expected at the design earthquake level.

The results of this study are compared with the current state of the art as presented in the ATC-120 project [36]. This comparison has not been considered in previous studies. Also, only a limited number of investigations have been conducted to assess the adequacy of the ASCE 7-16 and Eurocode 8 design formula for NSCs using code-designed SCBF [33], SMF [20, 23] and RC buildings [34]. The seismic demand on NSCs recommended by ASCE 7-16 and Eurocode 8 is also compared with the results of the current study.

The present study focuses on quantifying the effects of nonlinear structural behavior on the in-structure amplification factor and nonstructural amplification factor in SCBF and SMF structures. Demands on acceleration-sensitive NSCs in 11 archetype buildings, designed per ASCE 7-16 [10] are evaluated based on NSC-related ASCE 7-16 provisions and ATC-120 recommendations [36]. Detailed OpenSees models are developed for 3-, 6-, and 12-story SCBF structures including chevron and Two-Story X (TSX) configurations and 4- (two designs), 8-, 12-, and 20-story SMF structures, which have the same plans as one of the buildings considered in the NIST GCR 10-917-8 report [37]. Nonlinear response history analyses are carried out using the FEMA P695 [38] suite of ground motions scaled to two seismic intensity levels to compute the floor accelerations in the buildings. The ratio of the PGA of the ground motions to the design PGA is greater than one for 87% of the ground motions used, thus resulting in the buildings behaving in the inelastic range. PFA/PGA profiles and FRS are developed to quantify acceleration demands on attached NSCs. The seismic design forces calculated based on the findings of the present study are compared to the recommendations of ATC-120.

## 2.2. OVERVIEW OF BUILDING ARCHETYPE DESIGNS

The plan and elevation of the building designs considered in this study are from the NIST GCR 10-917-8 report [37]. The buildings are located in San Francisco (site coordinates: 37.783$^{o}$N, 122.392$^{o}$W), on Site Class D soil. The NIST GCR 10-917-8 designs were used as the basis for this study but were redesigned for an office occupancy (Risk category II and importance factor $I_e$ = 1) and Seismic Design Category (SDC) D in accordance with the provisions of ASCE 7-16 [10], ANSI/AISC 341-16 [39], and ANSI/AISC 360-16 [40]. The mapped spectral accelerations at 0.2 s and 1 s are $S_S$ = 1.5 g and $S_1$ = 0.6 g, respectively. The drift ratio limit is 2% for the SCBF and SMF buildings, except for the buildings with fewer than four stories, where the limit is 2.5%.

The SCBF buildings have 9.14 m spans in each direction, and a story height of 4.57 m. A dead load of 4.0 kPa and 3.2 kPa and a live load of 2.4 kPa and 0.96 kPa are uniformly distributed over the floors and roof, respectively. As shown in Fig. 2-1(a,b), the buildings have a rectangular plan with one bay of SCBF in each direction for the 3- and 6-story buildings, and two bays of SCBFs for the 12-story building. The SCBFs are

designed with a response modification factor *R* of 6. Two different configurations are considered for the SCBFs: chevron and TSX bracing systems. The labeling scheme for the SCBFs in this study includes the number of stories and the SCBF configuration, i.e., 3-chevron, 3-TSX, 6-chevron, 6-TSX, 12-chevron, and 12-TSX. Fig. 2(a,b) shows elevation views of the SCBF buildings. The columns are fixed at the base and oriented to bend about the strong axis. The braces consist of circular Hollow Structural Section (HSS) with slenderness and $D/t$ ratios that satisfy ANSI/AISC 341-16 [39] criteria for seismically compact sections.

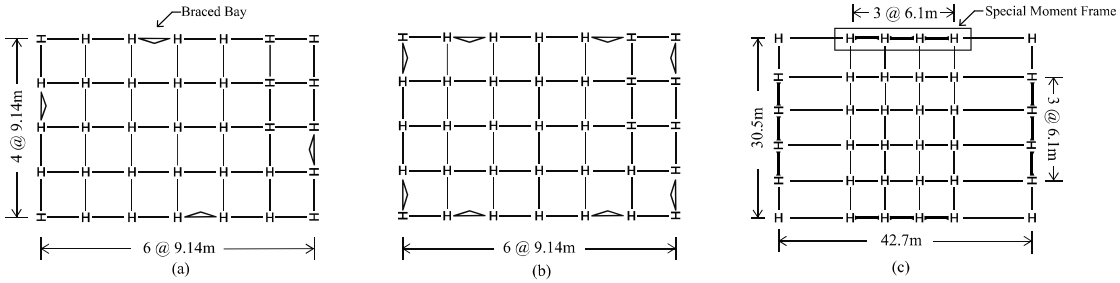


***Fig. 2-1. Plan views of the (a) 3- and 6-story SCBF buildings (b) 12-story SCBF buildings (c) SMF buildings***

As shown in Fig. 2-1(c), the SMF buildings have a bay width of 6.1 m for the SMF spans. The first floor has a height of 4.6 m, and floors two and above have a height of 4.0 m. The SMF systems are designed for the dead load of 4.3 kPa, which is applied on all floors. A live load of 2.4 kPa and 0.96 kPa is applied on the floors and roof, respectively. In addition, a cladding load of 1.2 kPa is considered as a perimeter load. A Response Spectrum Analysis (RSA) procedure is used for designing the 8-, 12-, and 20-story SMF buildings, while the 4-story building is designed using both an Equivalent Lateral Force (ELF) and a RSA method to study the differences in acceleration responses for the designs resulting from each design. The SMF designs are labeled 4-ELF, 4-RSA, 8-RSA, 12-RSA, and 20-RSA, with elevation views shown in Fig. 2-2(c). The column bases are assumed to be fixed. The seismic compactness of the W sections is checked to satisfy the ratio in ANSI/AISC 341-16 [39]. Reduced Beam Sections (RBS) are designed based on ANSI/AISC 341-16 [39] criteria for all the connections. In accordance with FEMA P695 [38], the deflection amplification factor $C_d$ is considered to be equal to the response modification factor *R* of 8. Therefore, the building designs are based on $C_d = 8$, instead of the value of 5.5 in ASCE 7-16.

The steel of the frame members and braces in this study is assumed to have a characteristic yield strength of 345 MPa and 318 MPa, respectively [37]. The beam, column, and brace member sizes of the SCBFs and exterior SMFs are summarized in Table 2-1.

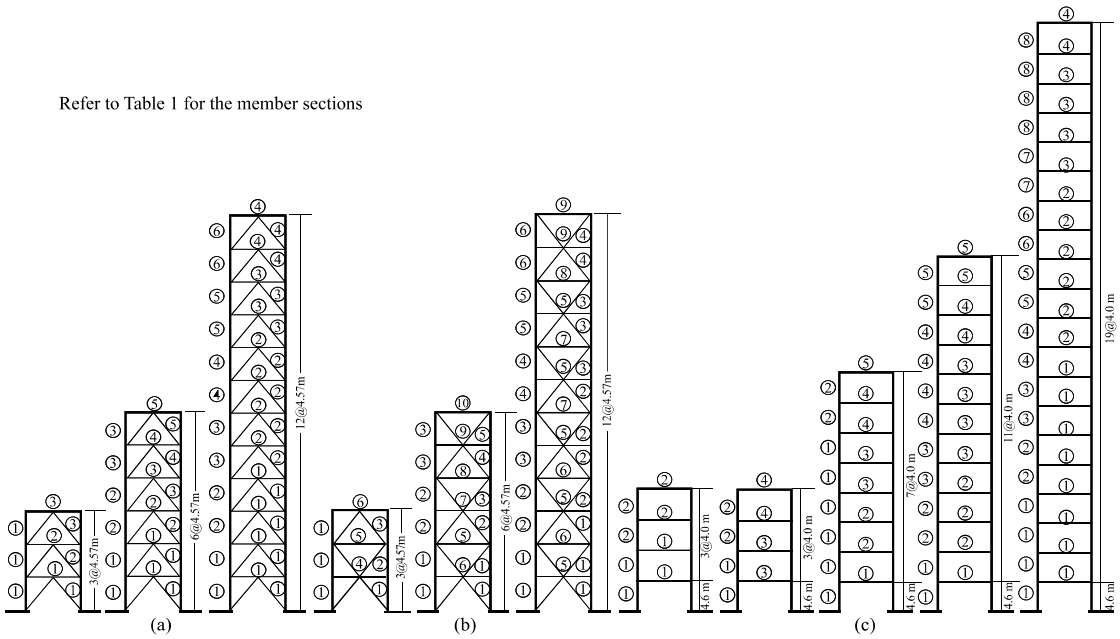


***Fig. 2-2. Elevation views of the (a) chevron SCBFs (b) TSX SCBFs (c) SMFs***

## 2.1. MODELING APPROACH

Two-dimensional models of the SCBF and SMF structures are developed in OpenSees [41]. Force-based fiber beam-column elements are used to model the beams, columns, and braces. It is assumed that all the beams and columns are fixed at their connections. All elements use the 'Steel02' material that represents the Giuffre-Menegotto-Pinto model with a 3% strain-hardening ratio. The P-Delta geometric transformation formulation is included considering a leaning column, placed parallel to the main frame to account for P-Δ effects. The gravity load of the tributary area of each floor is supported by the leaning column, which is pinned at its base. The plastic moment, the moment of inertia, and the stiffness of each gravity column are multiplied by the number of gravity columns in the tributary area. Furthermore, the mass of the tributary area of the gravity columns is also lumped at the nodes of the leaning column. Tangent-stiffness-proportional Rayleigh damping of 3% is assigned to the first and third modal periods, as recommended by Mohsenzade and Wiebe [49] and NIST GCR 10-

917-8 report [37]. Table 2-2 lists the periods of the first three lateral modes of the SCBF and SMF systems.

***Table 2-1. Member sections***

| Lateral System | Columns (Exterior for the SMFs) | Beams | Braces |
|---|---|---|---|
| 3-chevron<br>3-TSX | ① W12x120 | ①W30x261<br>②W30x235<br>③W30x211<br>④W18x65<br>⑤W21x111<br>⑥W30x173 | ①HSS9.625x0.5<br>②HSS8.75x0.5<br>③HSS7.5x0.5 |
| 6-chevron<br>6-TSX | ①W14x342<br>②W14x176<br>③W14x68 | ①W36x361<br>②W33x354<br>③W30x292<br>④W30x261<br>⑤W30x211<br>⑥W21x62<br>⑦W24x146<br>⑧W18x76<br>⑨W24x131<br>⑩W18x97 | ①HSS12.5x0.625<br>②HSS11.25x0.625<br>③HSS10.75x0.5<br>④HSS9.625x0.5<br>⑤HSS7.5x0.5 |
| 12-chevron<br>12-TSX | ①W14x550<br>②W14x398<br>③W14x283<br>④W14x193<br>⑤W14x99<br>⑥W12x45 | ①W30x261<br>②W30x235<br>③W30x191<br>④W27x161<br>⑤W18x35<br>⑥W18x71<br>⑦W18x65<br>⑧W18x60<br>⑨W18x55 | ①HSS9.625x0.5<br>②HSS8.625x0.5<br>③HSS8.75x0.375<br>④HSS6.625x0.312 |
| 4-ELF<br>4-RSA | ①W24x103<br>②W24x76 | ①W24x103<br>②W24x76<br>③W21x73<br>④W21x57 | - |
| 8-RSA | ①W24x131<br>②W24x94 | ①W30x108<br>②W30x116<br>③W27x94<br>④W24x84<br>⑤W21x68 | - |
| 12-RSA | ①W24x207<br>②W24x162<br>③W24x146<br>④W24x131<br>⑤W24x84 | ①W30x124<br>②W30x132<br>③W30x116<br>④W27x94<br>⑤W24x84 | - |
| 20-RSA | ①W14x426<br>②W14x398<br>③W14x370<br>④W14x311<br>⑤W14x283<br>⑥W14x233<br>⑦W14x159<br>⑧W14x132 | ①W33x169<br>②W33x141<br>③W30x108<br>④W24x62 | - |

**1.** A rainflow counting approach using strain history in each individual fiber was followed in this study. Zero stiffness was assigned to the fibers that exceeded the low-cycle fatigue limit, as recommended by Karamanci and Lignos [42]. Sixteen force-based nonlinear beam-column elements with fiber-based sections are used for modeling the braces. An out-of-straightness initial imperfection of 0.1% of the brace length is applied at the middle of the braces to initiate buckling. The gusset plates are modeled

using fiber beam-column elements with three integration points and a length equal to twice the thickness of the gusset plate.

***Table 2-2 Periods of the first four lateral modes for the SCBF and SMF systems***

| Lateral System | Configuration | $T_1$ (s) | $T_2$ (s) | $T_3$ (s) |
|---|---|---|---|---|
| SCBF | 3-chevron | 0.53 | 0.21 | 0.13 |
| | 3-TSX | 0.56 | 0.24 | 0.15 |
| | 6-chevron | 0.92 | 0.32 | 0.26 |
| | 6-TSX | 0.99 | 0.37 | 0.28 |
| | 12-chevron | 1.83 | 0.60 | 0.39 |
| | 12-TSX | 1.95 | 0.63 | 0.39 |
| SMF | 4-ELF | 1.26 | 0.41 | 0.21 |
| | 4-RSA | 1.56 | 0.49 | 0.25 |
| | 8-RSA | 2.28 | 0.79 | 0.44 |
| | 12-RSA | 3.11 | 1.08 | 0.61 |
| | 20-RSA | 4.45 | 1.59 | 0.91 |

The nonlinear behavior of the SMFs is produced by three components: the RBS, plastic hinges in the columns, and the panel zones. The steel beams and columns in the SMFs are represented by elastic elements with two plastic hinges at their ends to concentrate the inelastic behavior. The moment-rotation behavior of the plastic hinges, which was previously obtained by Lignos and Krawinkler [43], is used for the RBS and columns in this study. A deterioration model named ‘other than RBS’ beam is considered for the column bases [44]. The ‘Bilin’ material is used in OpenSees to represent the modified Ibarra-Medina-Krawinkler deterioration model [45]. The parallelogram model with eight rigid elements is used to model the panel zone [46], with two bilinear springs to model the tri-linear backbone curve representing the shear force-shear deformation behavior of the joint panel zone [45]. The characteristics of the backbone curve including the strength cap, the post-yield stiffness, and deformation range for the post-capping region are obtained from ATC 72-1 [47].

The significance of gravity systems on the collapse performance of SMF systems was evaluated by Flores et al. [20]. The effect of the contribution of gravity framing on the response of SCBFs was also investigated by Hsiao et al. [48] and Mohsenzadeh and Wiebe [49]. In this study, for the sake of simplicity, only the stiffness of the gravity columns is simulated in the analytical models, while the effect of beam-column connections in the gravity system has been ignored. The effect of composite floor slab is also not considered in this study.

The dynamic interaction between primary and secondary components in buildings has been studied extensively in the past and shown to be negligible when the secondary-to-primary mass ratio is less than 0.01 [22, 50]. The present study assumes that the NSCs are sufficiently light to allow a decoupled dynamic analysis approach.

This study does not consider soil-structure interaction effects. Recent work by Cruz and Miranda [51] has concluded that soil-structure interaction can affect the viscous damping ratios, and thus floor accelerations, in elastically behaving structures. However, in inelastic structures, as those considered in the present study, energy dissipation is governed mainly by inelastic action rather than inherent (viscous) damping and in this case the effects on soil-structure interaction are not clear. Future research would be needed to evaluate how soil-structure interaction and building nonlinearity together affect acceleration demands on nonstructural components.

## 2.2. VERIFICATION OF THE MODELS

The fidelity of the models is evaluated by comparing their predicted cyclic behavior with experimental results. For this purpose, an OpenSees model of the two-story concentrically braced frame tested by Uriz and Mahin [52] is considered. The modeled frame has a chevron configuration with HSS braces, which is similar to the SCBFs used in this study, and the same modeling approach is used. Fig. 2-3(a) compares the global hysteretic behavior to the experimental results, showing a good agreement for the deterioration of stiffness and strength. It can be seen from Fig. 2-3(a) that the maximum resistance of the analytical model is within 5% of the experimental results.

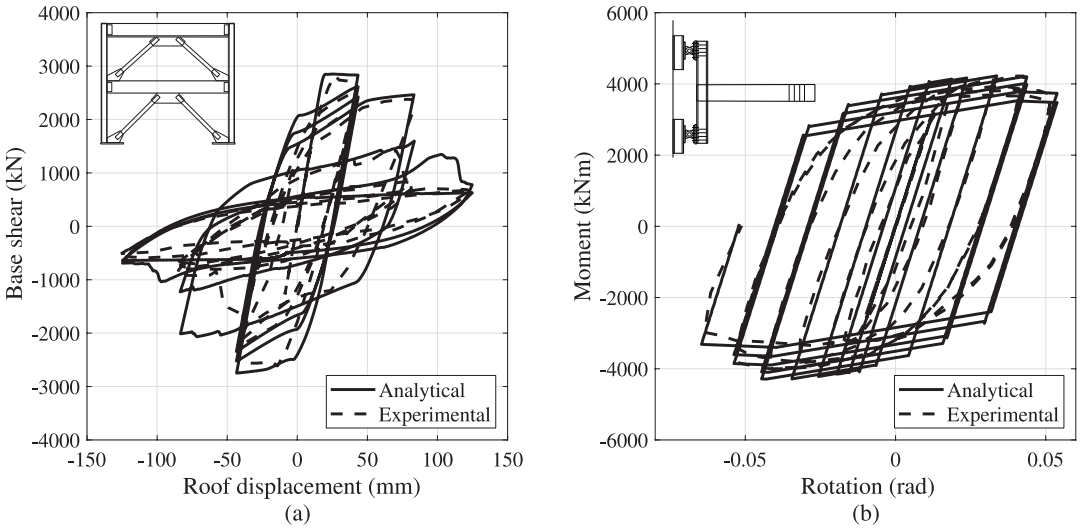


***Fig. 2-3. Results of the verification for (a) SCBF [52], (b) RBS steel moment connection [53]***

To verify the fidelity of the modeling approach taken for the RBS in the SMFs, a numerical simulation of the experimental test by Lee et al. [53] is performed in OpenSees [41]. The approach used for modeling the SMF archetype buildings is followed in this numerical simulation. Fig. 2-3(b) illustrates the moment-rotation behavior of the modeled specimen DB700-SW [53], which showed an acceptable rotation capacity without fracture under the SAC standard loading. The hysteresis predicted by the analytical model is close to that recorded in the experiment in terms of peak strength, though the reloading stiffness is less rounded in the model.

## 2.3. EARTHQUAKE GROUND MOTIONS

This study uses the FEMA P695 suite of 22 far-field ground motions, each consisting of a pair of orthogonal horizontal records [38]. Although the design of NSCs in ASCE 7-16 is based on the Design Earthquake (DE), in this study the evaluation of the PFA/PGA ratio in the code is performed at both DE and risk-targeted maximum considered earthquake ($MCE_R$) levels to investigate the effect of large nonlinear action in the structures.

Each pair of records is considered as two independent ground motions and scaled to the $MCE_R$ target spectrum using the amplitude scaling approach in ASCE 7-16 [10]. To obtain acceptable results such as realistic scaling factors at the higher modes of the 2D modeled structures, each component of a pair of ground motion is scaled

individually to achieve the minimum mean squared error of the difference between the $MCE_R$ target spectrum and the record response spectrum over a period range between $0.2T$ and $2T$, where $T$ corresponds to the fundamental period of the system. Fig. 2-4 shows the median spectrum of the 44 scaled ground motions matched with the $MCE_R$ spectrum for the 6-story SCBFs. In this case, $T$ is the fundamental period of the chevron system for the lower limit of the scaling range and that of the TSX system for the upper limit. This approach results in a common set of scaling factors for structures with the same number of stories but different bracing configurations for the SCBFs. Similarly, a common set of scaling factors is used for the 4-ELF and 4-RSA SMFs, while the 8-, 12-, and 20-RSA SMFs have unique sets of scaling factors. To obtain the scaling factors under the DE level, the corresponding $MCE_R$ scaling factors are multiplied by 2/3.

## 2.4. FLOOR ACCELERATION DEMANDS

### *2.4.1. PFA/PGA Ratio*

This section aims to provide an improved estimate of the PFA/PGA ratio in code-compliant structures. At this stage, response history analyses of the archetype structural models are performed using the ground motion suite scaled to the DE and $MCE_R$ levels to produce floor absolute acceleration histories. The PFA/PGA ratio is determined along the normalized height, $z/h$, i.e., the ratio of the floor elevation to the total height of the building.

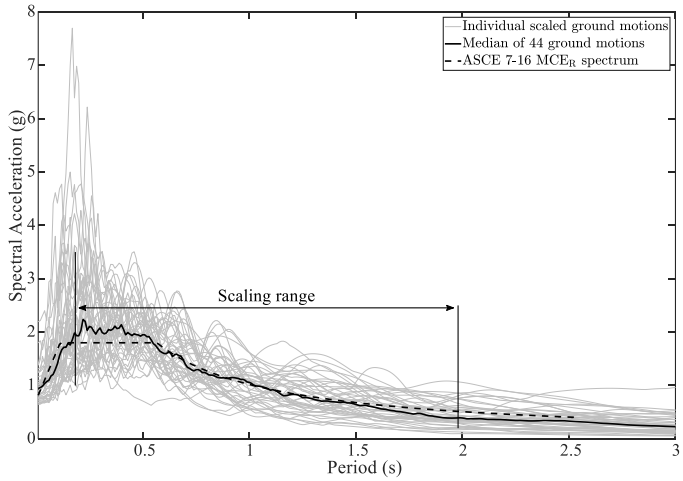


***Fig. 2-4. Acceleration response spectra of the $MCE_R$-scaled ground motions for the 6-story SCBFs (5% damping)***

Fig. 2-5 shows the median and 84$^{th}$ percentile values (84 PCTL) of the PFA/PGA ratio at each floor of the SCBF configuration under the DE and $MCE_R$ levels. The profiles of peak story drift ratio (PSDR) are also presented to link the discussion on acceleration demands to the extent of inelastic behavior, which is in many cases easier to discern in PSDR profiles. The vertical dashed lines in the PSDR profiles show the drift ratio limit. The symbol 'r' in the PSDR plots stands for roof level. Fig. 2-6 shows the corresponding distributions for the SMF systems. Although the study presents limited results under the $MCE_R$ level (Section 6.1), mainly to gain insight into the effects of stronger inelastic action on the PFA/PGA distributions, the focus is largely on the seismic demands on NSCs at the DE level. As can be seen in the figures, the PSDR increases when the ground motion intensity is increased, while the PFA/PGA ratio generally decreases. This occurs because, while $PGA_{MCE_R}/PGA_{DE}$ =1.5, the level of increased inelastic response in going from DE to $MCE_R$ results in saturation of PFA; therefore, the $PFA_{MCE_R}/PFA_{DE}$ ratio is smaller than 1.5. For instance, considering the median of the data points for the SCBFs, the lowest PFA/PGA value of the 6-chevron system occurs on the 6$^{th}$ floor, and it decreases by a factor of about 2/3 going from DE to $MCE_R$. As an example of the SMF behavior, the maximum decrease in PFA/PGA ratio for the design 12-RSA occurs on the 12$^{th}$ floor by 15% from lower to higher intensity.

Comparing between low- and high-rise buildings tends to suggest a more marked reduction of PFA/PGA up the height of tall buildings. Accordingly, high-rise structures are more influenced by structural inelastic behavior. This nonlinearity related behavior was also noted by Taghavi and Miranda [22]. One possible explanation for the overall decreasing trend of the PFA/PGA ratio with building height is PFA saturation, which generally happens in the top floors, while the lower floors experience an increasing trend in acceleration response. Another explanation is the higher mode effects, which induce large shear demands on the top floors and initiate early buckling in the braces, resulting in lower acceleration demands in the upper floors relative to the PGA.

Comparing the analysis results with the ASCE 7-16 formula, it can be seen that the ASCE 7-16 formula is overconservative at the top floors. On the other hand, in some

cases, the PFA/PGA ratio in the lower floors exceeds the ASCE 7-16 value at the DE level, while the number of the data points for which this occurs reduces at the $MCE_R$ level. This is because the level of inelastic action in the structures at the higher ground motion intensity level results in PFA saturation and smaller PFA/PGA ratios under the $MCE_R$ level compared to the DE level. Due to the greater inelastic action activated in the modeled buildings, the reduction in the PFA/PGA ratio in this study is more pronounced compared to previous studies [14, 25].

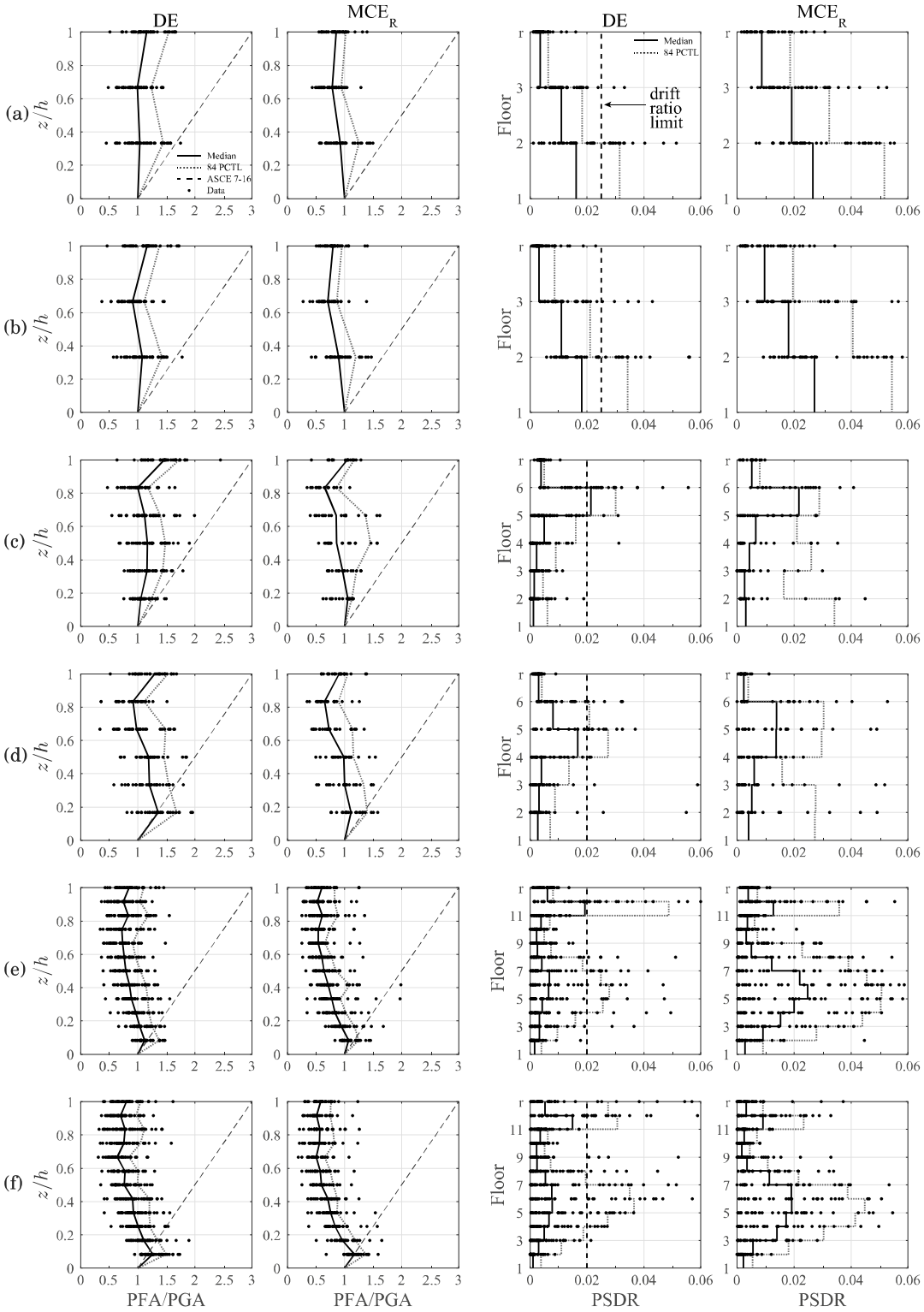


***Fig. 2-5. Distributions of PFA/PGA and peak story drift ratio of the SCBF systems (a) 3-chevron (b) 3-TSX (c) 6-chevron (d) 6-TSX (e) 12-chevron (f) 12-TSX***

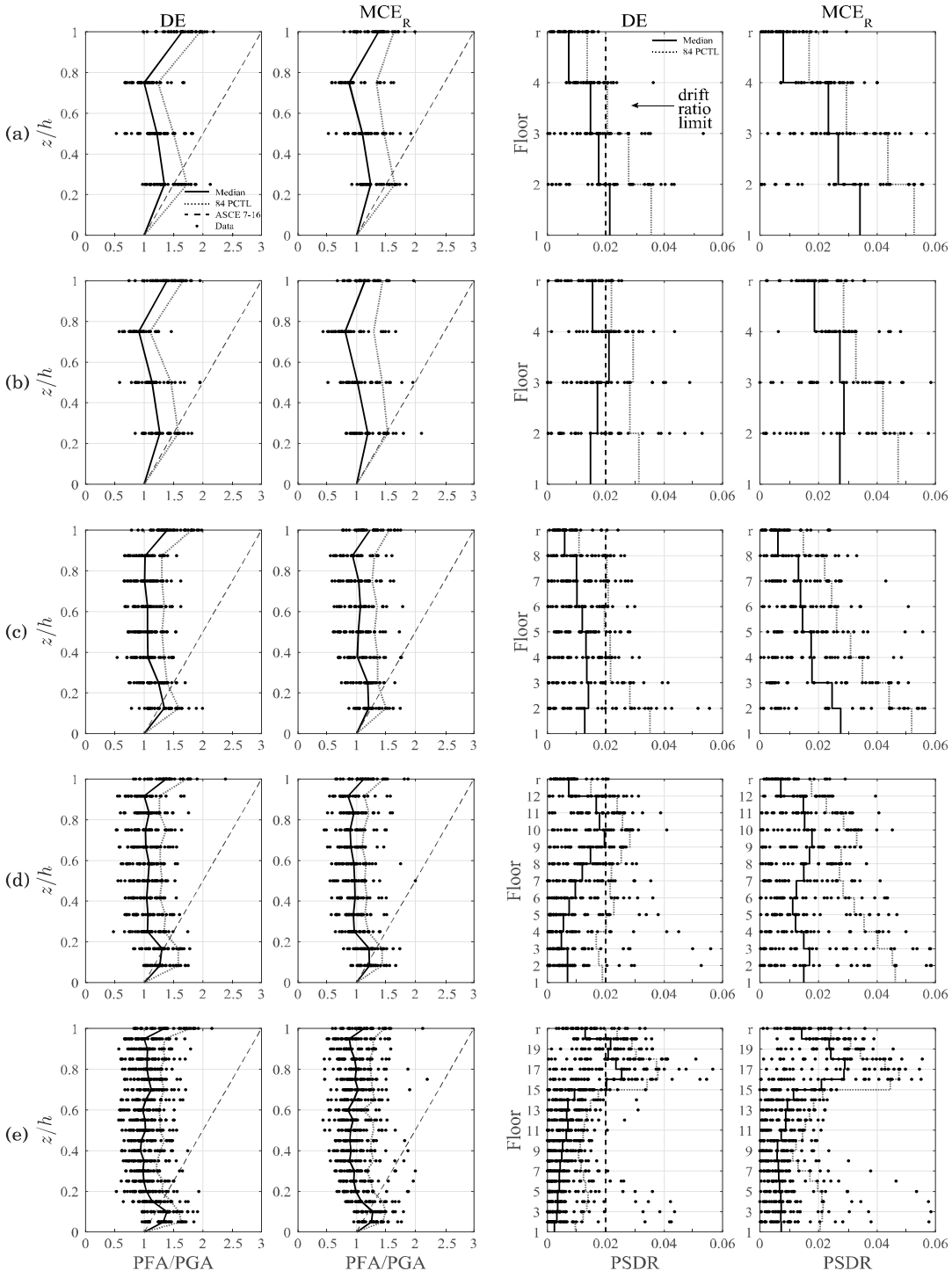


***Fig. 2-6. Distributions of PFA/PGA and peak story drift ratio of the SMF systems (a) 4-ELF (b) 4-RSA (c) 8-RSA (d) 12-RSA (e) 20-RSA***

The unsymmetrical behavior of the SCBF braces in tension and compression, including buckling under compression that results in strength deterioration, makes the prediction of the nonlinear behavior quite complicated. The distribution of acceleration

over the height varies according to the location of concentrated nonlinearity associated with this complex behavior of the braces. For example, as can be seen in the profiles of PFA/PGA ratio in Fig. 2-5, the lowest values of PFA/PGA are observed in the fifth and sixth floors of the 6-TSX structure at the $MCE_R$ level, which is consistent with the PSDR profile, which exhibits its largest values in the fourth and fifth floors. In the case of the chevron configuration of the 6-story SCBF, the lowest PFA/PGA occurs on the sixth floor, which is due to the drift concentration on the fifth floor. A similar trend is observed for the 12-chevron system, in which the largest story drifts and the lowest PFA/PGA values could be attributed to the nonlinearity of the floors under the DE and $MCE_R$ demands.

In the moment frame buildings, the formation of the plastic hinges initiates in beams and at the bottom of the columns on the first floor. Increasing the intensity level from DE to $MCE_R$, the plastic hinges in the beams distribute along the height of the structure. It can be seen in Fig. 2-6 that the 4-RSA system (flexible system) shows a more uniform distribution of the PSDR up the height of the building compared to the 4-ELF (stiff system). For the other SMFs, a general trend of smaller PFA/PGA values above floors that experience larger story drifts is observed. This is similar to what was seen for the SCBFs, though not as pronounced.

### *2.4.2. Fourier Amplitude Spectra of Floor Accelerations*

The effect of higher modes on the absolute accelerations of floors with localized nonlinearity is examined next through Fourier amplitude spectra (FAS). Fig. 2-7 shows three representative examples of the computed FAS corresponding to DE-level shaking. Fig. 2-7(a) shows the FAS of the fourth floor of the 6-TSX due to the Coolwater record, fourth floor of the 12-chevron structure under Imperial Valley earthquake, Delta record and $11^{th}$ floor of the 12-TSX structure under Imperial Valley earthquake, El Centro Array #11 record. Also shown is the FAS of the ground motion scaled to the DE level. The vertical lines indicate the structure's first three natural frequencies. The first peak, at around 1.01 Hz (0.99 s) corresponds to the first mode of response, while the peaks at around 2.7 Hz (0.37 s) and 3.57 Hz (0.28 s) are associated with the second and third modes of vibration, respectively. The ground motion has considerable energy content around its first mode frequency. However, as a consequence of nonlinearity the fourth

floor Fourier amplitude spectrum reduces around the first mode and increases around the higher modes, especially the second mode. When the excitation level is reduced to 0.1 DE, producing only elastic response in the structure, the Fourier amplitude shows a larger peak around the first modal period compared to the second modal period. Figs. 7 (b) and (c) show the fourth floor FAS of the 12-chevron system and the $11^{th}$ floor FAS of the 12-TSX system due to the El Centro Array #11 record, 1979 Imperial Valley earthquake. According to the distribution of the PSDR in Figs 5 and 6, these floors show one of the largest drifts along the height of the selected buildings. This observation implies that the building nonlinearity can increase the relative contribution of the higher modes, which significantly affects the seismic response of the buildings.

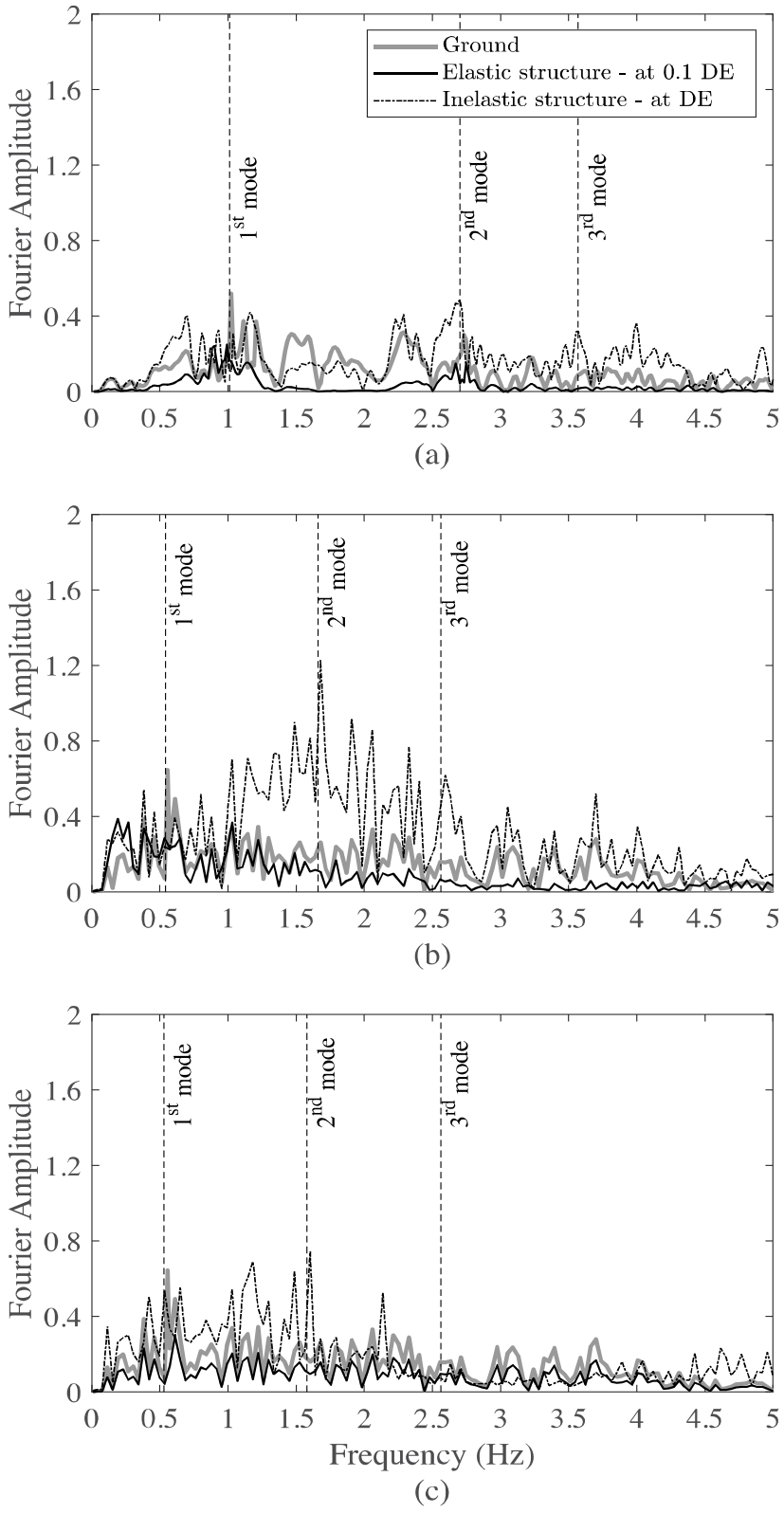


***Fig. 2-7. Fourier spectra of the (a) fourth floor of the 6-TSX structure, 1992 Landers earthquake, Coolwater record (b) fourth floor of the 12-chevron structure, Imperial Valley earthquake, Delta record (c) 11$^{th}$ floor of the 12-TSX structure, Imperial Valley earthquake, El Centro Array #11 record (DE level)***

## 2.5. MODIFIED EQUATION FOR THE PFA/PGA RATIO

A key consideration toward computing the induced seismic forces on attached NSCs involves estimating the acceleration at their attachment points. The ASCE 7-16 approach for NSCs requires that the horizontal seismic design force on the component's center of mass is computed from the PFA, modified by factors to take into account the component's importance, dynamic amplification, and response modification which could be attributed to the energy dissipation capability of the component and its attachments [10]. The PFA is assumed to be equal to the PGA times the height factor, 1 + 2 *z*/*h*. As such, the horizontal seismic design force, $F_p$, is computed from [10]

$$\frac{F_p}{W_p} = \frac{0.4 S_{DS} I_p}{R_p} a_p \left(1 + 2\frac{z}{h}\right) \tag{2-1}$$

where $W_p$ is the weight of the NSC, $S_{DS}$ is the short period design spectral acceleration, $a_p$ is the NSC amplification factor which varies from 1.0 to 2.5, $R_p$ is the NSC response modification factor which varies from 1 to 12, and $I_p$ is the NSC importance factor which varies from 1 to 1.5.

In the corresponding formulation from Eurocode 8 [35], the PFA/PGA is combined with the NSC amplification through the following equation:

$$S_a = a_g S \left( \frac{3(1+\frac{z}{h})}{1+(1-\frac{T_p}{T_n})^2} - 0.5 \right) \tag{2-2}$$

where $a_g$ is the peak ground acceleration at the DE level, $S$ is a soil factor (1.0 for rock sites), $T_p$ and $T_n$ are the fundamental vibration periods of the NSC and building, respectively [35].

The PFA/PGA ratio proposed by ATC-120 [36] is calculated based on the fundamental period of the building, from:

$$\frac{PFA}{PGA} = 1 + a_1\left(\frac{z}{h}\right) + a_2\left(\frac{z}{h}\right)^{10} \tag{2-3}$$

where $a_1 = 1/T_{aBldg} \le 2.5$, $a_2 = [1-(0.4/T_{aBldg})^2] > 0$, and $T_{aBldg}$ is the fundamental period of the building determined according to Equation 12.8-7 in ASCE 7-16. To account for the reduction in floor acceleration due to building nonlinearity, the PFA/PGA ratio given by Eq. (2-3) is divided by a constant, the building ductility reduction factor, $R_{\mu bldg}$, which is computed from $(1.1R/\Omega_0)^{0.5}$, where $R$ and $\Omega_0$ are the response modification factor and overstrength factor of the seismic force resisting system, as given in ASCE 7-16, Table 12.2-1. For SCBFs and SMFs, the resulting $R_{\mu bldg}$ values are 1.82 and 1.71, respectively.

Demands on NSCs in ASCE 7-16 and ATC-120 are based on the DE level. While the ATC-120 project considered expanding the evaluation of NSCs to include $MCE_R$ level shaking, it was ultimately decided to limit the evaluation to the DE because of the cost of the additional analysis and insufficient information about the performance of the NSCs under $MCE_R$-level shaking [37]. Thus, although so far, the present paper has considered demands at both the DE and $MCE_R$ to gain insight into the effect of stronger shaking, the evaluation from here on focuses on demands at the DE level only, so as to frame the discussion in the context of the state of the art.

Fig. 2-8 illustrates the PFA/PGA data points for each SCBF and SMF archetype, as well as a curve that corresponds to a surface fitted to the median of the data points for that type of LFRS at the DE level. The PFA/PGA expressions for SCBFs and SMFs are respectively given by:

$$\frac{PFA}{PGA} = 1 + 1.45(1 + 0.41T_a)\sqrt{\frac{z}{h}}\left[\left(\frac{z}{h} - 0.67\right)^2 - 0.011T_a^4\right] \qquad (2\text{-}4)$$

$$\frac{PFA}{PGA} = 1 + 18.6(1 - 0.17T_a)\sqrt{\frac{z}{h}}\left[\left(\frac{z}{h} - 0.63\right)^2 + 0.053\right]^2 \qquad (2\text{-}5)$$

where $T_a$ is the fundamental period of the buildings determined from eigenvalue analysis. The coefficients of Eqs. (2-4) and (2-5) are obtained using bivariate nonlinear least squares regression in Mathematica [54]. As such, Eq. (2-4) is valid only for SCBFs with $0.53\text{ s} < T_a < 1.95\text{ s}$, and Eq. (2-5) is valid only for SMFs with $1.26\text{ s} < T_a < 4.45\text{ s}$. The formulas have been evaluated to have an acceptable model error and to be homoscedastic.

The results of this study point toward a different relationship for PFA/PGA than those in ASCE 7-16 (i.e., Eq. (2-1)) and ATC-120 (Eq. (2-3)). It should be noted that the regression formula avoids the drawback of having steps between different period ranges [e.g., 14]. Fig. 2-8 also compares the results of this study with the recommendations for the PFA/PGA ratio presented in ASCE 7-16 and ATC-120. Yielding of the braces in the SCBFs and the spread of the plastic hinges in the SMFs limit the transmitted accelerations along the height of the buildings, making the PFA/PGA ratio suggested by ATC-120 overconservative in the top floors. Although the ATC-120 formula is less conservative in comparison to the linear relationship in ASCE 7-16, it still overestimates the PFA/PGA ratio at the top floors of stiff structures. This overestimation by the ATC-120 equation is mainly due to the constant value of $R_{\mu bldg}$ along the height of the buildings. On the other hand, ATC-120 underestimates the PFA/PGA ratio in the lower floors, especially in the high-rise systems.

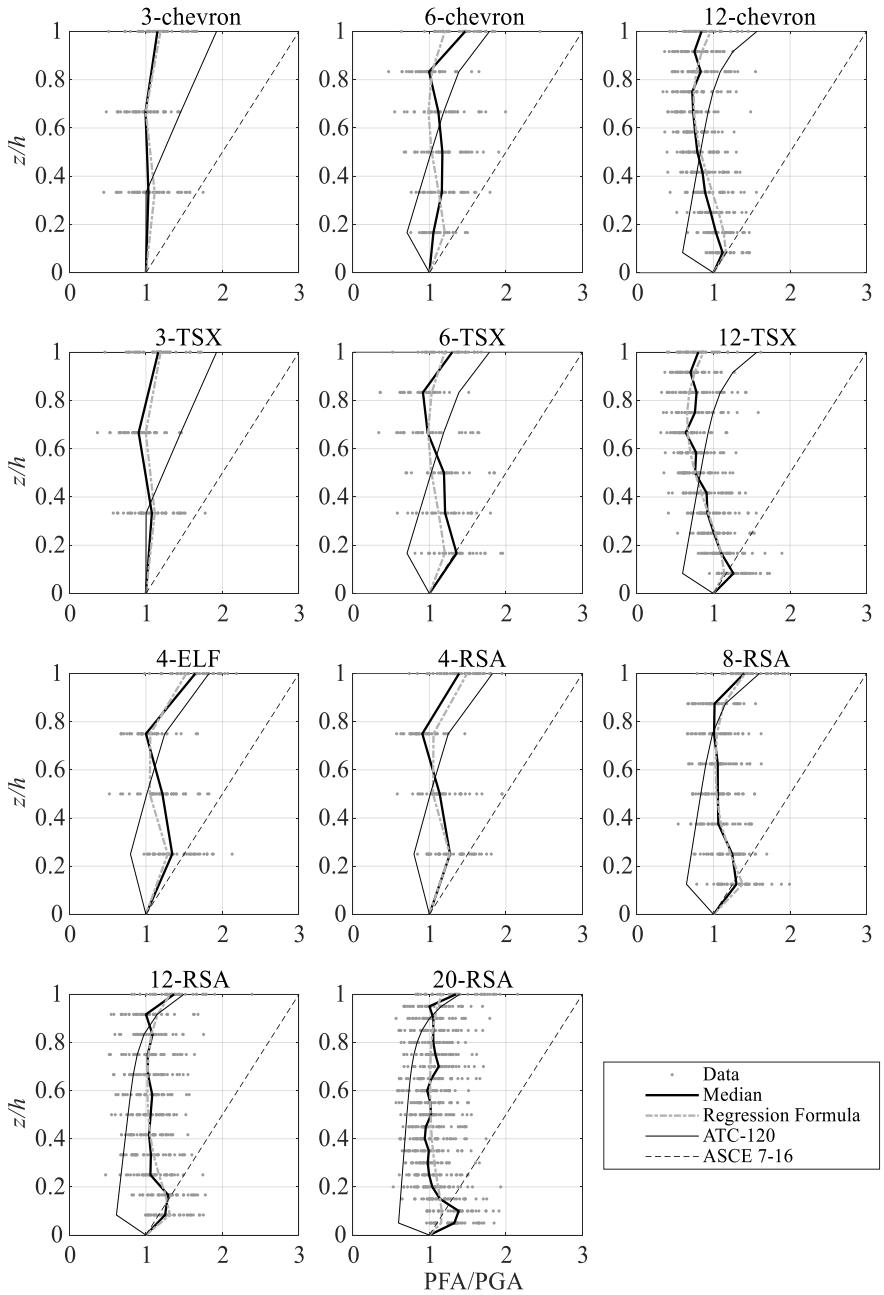


***Fig. 2-8. Profile of PFA/PGA over building height for seismic design of acceleration-sensitive NSC (DE level)***

## 2.6. FLOOR RESPONSE SPECTRA

In this section, the floor absolute acceleration histories computed from the analyses of the OpenSees models are used to develop acceleration floor response spectra. A reliable estimate of PCA is critical, as it is used to quantify the seismic design force on NSCs. In the ASCE 7-16 design force formula for NSCs (Eq. (2-1)), the component response modification factor, $R_p$, is used to consider the effect of NSC inelastic response. This

study focuses on elastic NSCs (i.e., $R_p = 1$), while the effect of NSC nonlinearity will be investigated in a future study. This section reviews the median elastic FRS corresponding to the 44 ground motions scaled to the DE level. As can be seen in Fig. 2-4, most of the FEMA P695 ground motions have large spectral accelerations at the higher-mode periods of the structures, which can significantly affect demands on acceleration-sensitive flexible NSCs as most of them have fundamental periods that lie in the short-period range (e.g., < 0.3 s [10]).

Figs. 2-9 and 2-10 show the 5% damped elastic FRS for the SCBF and SMF systems, respectively. A value of 5% damping is used to comply with the standard value in codes. The median ground response spectra are also included in the figures to help ascertain how the spectral shape changes over the height of the building. The first few structural periods are shown in Figs. 2-9 and 2-10 using vertical dashed lines, with the exception of the first period of the 20-RSA archetype, which is larger than the upper range of the plotted floor spectra. As can be seen in the figures, the floor spectra generally exhibit spikes when the NSCs are in tune with the modal periods of the primary structure, especially for low-rise SCBFs and SMFs. Also notable is that, because of the smaller fundamental periods of the SCBF systems than the SMFs, their spikes are closer to the natural periods of most common NSCs. The ASCE 7-16 standard considers the maximum values of the PFA/PGA ratio and NSC amplification factor as 3 and 2.5, respectively. Accordingly, the maximum possible PCA at the roof level is 7.5 PGA. Since the design PGA is $0.4S_{DS}$ = 0.4 g in this study, the PCA is 7.5 × 0.4 g = 3 g, which is shown with a horizontal dashed line in the figures. From the computed FRS, it can be concluded that ASCE 7-16 greatly overestimates the peak component acceleration for the NSCs tuned with the first mode of the buildings. For the NSCs tuned with the higher modes of the buildings, ASCE 7-16 is conservative for all 5% damped NSCs mounted on the roof level of the SCBFs and most of the SMFs. The most notable exception is short SMFs, such as 4-ELF, which shows that the maximum PCA is underestimated by the ASCE 7-16 by 23%. Furthermore, it can be seen in the figures that the maximum PCA suggested by ASCE 7-16 is close to 3 g for tall SMF buildings, which implies an acceptable prediction by the code.

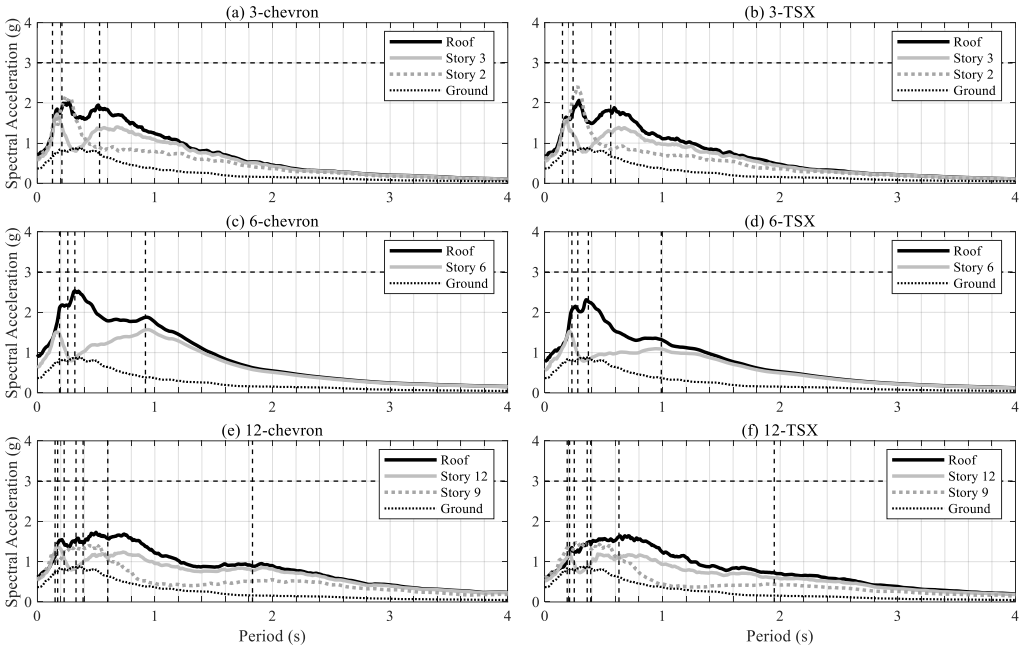


***Fig. 2-9. Median floor response spectra for SCBF archetype buildings under DE level (5% damping), (a) 3-chevron (b) 3-TSX (c) 6-chevron (d) 6-TSX (e) 12-chevron (f) 12-TSX, vertical dashed lines show the first few structural periods***

The effect of PFA saturation on the FRS can be observed in Figs. 9 and 10. The figures show that the peaks of the floor spectra near the first structural period increase up the height of the structures. This suggests that attached NSCs in this period range (which are less common) will experience demands that follow an increasing trend with height, as is suggested by the increasing PFA/PGA ratio in ASCE 7-16 [10]. However, the floor spectral accelerations exhibit a trough between the peaks associated with the higher-mode periods for the floors that exhibit large inelastic response.

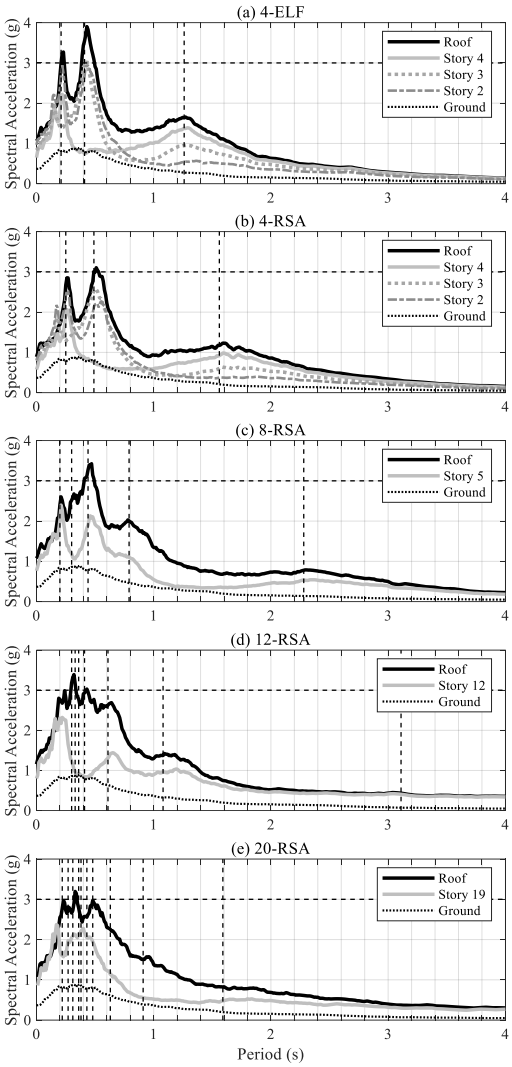


***Fig. 2-10. Median floor response spectra for SMF archetype buildings under DE level (5% damping), (a) 4-ELF (b) 4-RSA (c) 8-RSA (d) 12-RSA (e) 20-RSA, vertical dashed lines show the first few structural periods***

For instance, in the 6-story SCBFs, the FRS for the 6$^{th}$ floor drops near the second- and third-mode periods, while it increases around the fourth-mode period. A similar behavior is observed in the spectra of the 3$^{rd}$ floors in 3-story SCBF structures, in which the spectra decrease between the first and second modes and then increase between the second and third modes. As can be seen in Fig. 2-5, this reduction in the FRS of the 3$^{rd}$ floor can be related to the distribution of PFA/PGA for the SCBFs. It is seen in Fig. 2-5 that the 3$^{rd}$ and 6$^{th}$ floors are the ones that experience the lowest PFA/PGA ratios in the 3-story and 6-story SCBF structures, respectively. In the 12-story SCBFs, the most marked drop occurs around the fourth and fifth modal periods in the FRS of the 12$^{th}$ floor for the 12-chevron system. The 11$^{th}$ floor experiences the

largest PSDR, which results in nearly the smallest PFA/PGA ratio at the 12$^{th}$ floor. As an example of the SMF structures, the 5$^{th}$ floor spectrum of the 8-RSA drops around the fourth mode period due to acceleration saturation. A similar trend is observable for the 12-RSA in which the 12$^{th}$ floor spectrum shows a small dip around the fourth and fifth modal periods, and for the 20-RSA with localized nonlinearity on the 19$^{th}$ floor, which results in a reduction around the small modal periods. At these modal periods, the floor spectral acceleration becomes similar to the ground spectral acceleration due to acceleration saturation.

In addition, it can be seen that the difference between the ground spectra and the FRS becomes larger up the height of the building. This effect is present but less pronounced in the SCBFs. Moreover, as previously explained by Sullivan et al. [27], increasing nonlinearity results in a broadening of the peaks over a wider range of periods in the FRS. As such, because of the spread of spikes in the FRS due to nonlinear action in tall SCBF and SMF buildings, a reduction in the FRS is less visible compared to mid-rise and low-rise buildings.

It can also be seen that the shape of the FRS clearly changes along the height of the buildings. For example, an increase in the height of the NSC location in the building results in a greater rate of increase for the floor spectral amplitude associated with the first modal period than for the higher modes. Moreover, at the fundamental periods of the buildings, the difference between the median ground acceleration spectrum and the floor spectra becomes larger over the height. However, due to acceleration saturation, this increase is not clearly observable around the higher modes of the buildings, especially for the taller SCBF systems. It can be seen from the comparison of two configurations of the SCBF that, due to the larger stiffness of the chevron systems, larger spectral acceleration is experienced by the NSCs tuned to the fundamental periods of this system than the TSX system. The same is observed when comparing the 4-ELF with larger stiffness than the 4-RSA system.

Although a viscous damping ratio of 5% has typically been considered for NSCs, which was the basis for using that value in this study, the limited information in the literature suggests that values in the 1-3% range might be more appropriate for typical NSCs [55]. FRS for 2% viscous damping were generated as part of this study

but are not shown here because of space constraints. The 2% FRS exhibit very similar shapes to the 5% FRS, but with larger amplitudes.

### 2.7. COMPONENT AMPLIFICATION FACTOR

The value of the component amplification factor, $a_p$, varies from 1.0 to 2.5 in ASCE 7-16. The suggested values depend on the ratio of the period of the NSC ($T_p$) to the fundamental period of the supporting structure ($T_1$). Since the dynamic properties of the structure may not be known at the time the NSCs are designed, ASCE 7-16 recommends that a value of 2.5, i.e., the maximum, be assigned to NSCs that are generally classified as flexible [10].

Fig. 2-11 shows the median of the PCA/PFA with respect to $T_p / T_r$ for all floors of selected low-rise buildings (3-TSX SCBF and 4-ELF SMF) and for some of the lower, middle and top floors of selected tall structures (12-chevron SCBF and 12-RSA SMF), at the DE level. $T_r$ is the resonant period, defined as *the period*[1] producing the largest value in the roof FRS, which is near $T_2$ for the 3-TSX, 4-ELF and 12-chevron and $T_7$ for the 12-RSA. Vertical lines show the effective $T_p / T_r$ ratio for $T_p$ < 0.3 s, covering most NSCs in a building [10]. The trends shown here are representative of all archetype structures evaluated in this investigation. The $a_p$ value suggested by Singh et al. [56] and adopted in ASCE 7-16 is also shown in the figures. As can be seen in the figures, in the range of $0 < T_p / T_r < 0.5$ and $T_p / T_r > 2.0$, the ASCE 7-16 value for $a_p$ is equal to 1.0. The component amplification factor is considered to be constant over a wide period range of NSCs in ASCE 7-16, but Fig. 2-11 shows that the median PCA/PFA for the 3-TSX structure exceeds the code suggested maximum value of 2.5 for a period range of $T_p / T_r < 0.5$. As can be seen in the figure, the component amplification factor can also be less than one, which depends on the fundamental period and level of the nonlinearity of the frames. This deamplification was previously noted by Medina et al. [18] in a study on elastic and inelastic moment frames.

[1] Correction: “the period” should read “the structural period closet to the NSC period”

Additionally, Fig. 2-11 demonstrates that the amplification factors of NSCs depend not only on the $T_p / T_r$ ratio, but also on the location of the NSC and the distribution of nonlinearity in the structure. According to Figs. 5 and 6, the nonlinear behavior results in the maximum value of the PSDR profile being in the floor where nonlinear behavior concentrates, and the minimum PFA/PGA ratio occurring above this floor.

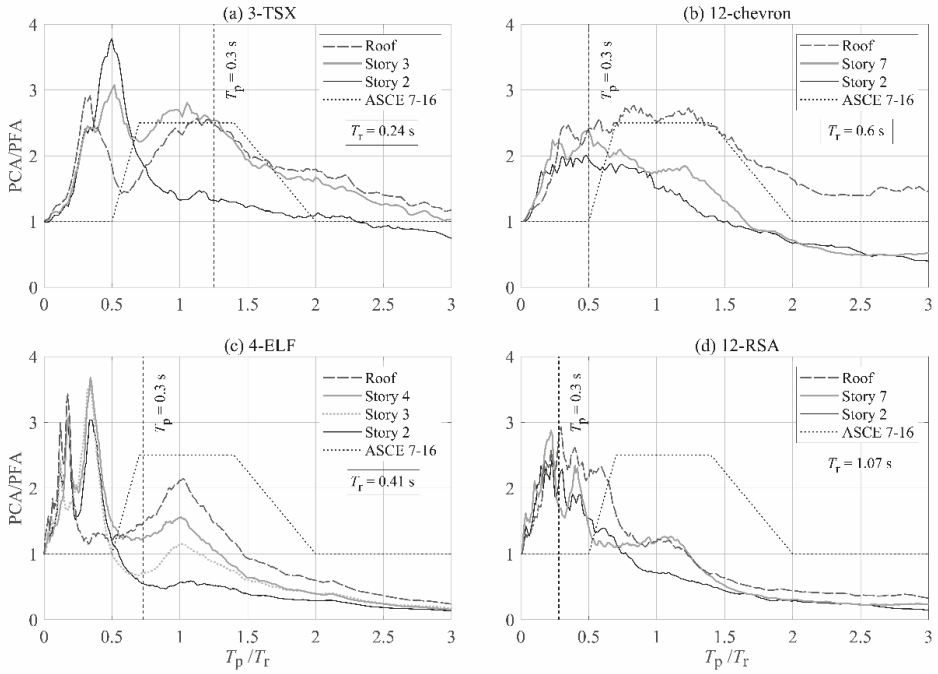


***2-11. Median of PCA/PFA under DE level, 5% component damping ratio, (a) 3-TSX .Fig (b) 12-chevron (c) 4-ELF (d) 12-RSA***

Fig. 2-12 compares PCA/PFA up the height of the different archetype SCBF and SMF buildings, for $T_p = T_1$ and $T_p = T_2$. The maximum value of 2.5 per ASCE 7-16 is also shown. It can be concluded from the figure that a PCA/PFA ratio of greater than 2.5 that has been reported for elastic 5% damped NSCs in previous studies [14, 18, 27, 28] is generally conservative at the first mode periods for structures with inelastic behavior, especially for the SMF systems. However, results are close to the value of 2.5 per ASCE 7-16 for the first modal period of the low- and mid-rise SCBF archetype buildings. Considering the NSCs tuned with the second modal period of the buildings, the PCA/PFA exceeds 3 in the lower floors of the short structures. Therefore, the NSC amplification factor should be evaluated depending on both the first and second modal

periods. It can be also seen that increasing the number of stories results in a reduction in the NSC amplification factor.

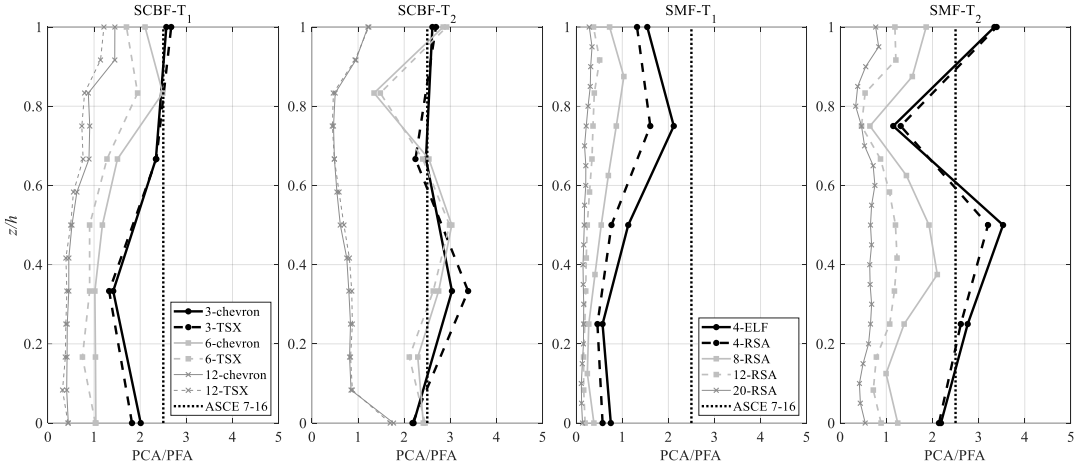


***Fig. 2-12. Effect of the modal period on the component amplification factor***

The design force, $F_p$, proposed by ATC-120 is given by

$$\frac{F_p}{W_p} = PGA \times \left[ \frac{\frac{PFA}{PGA}}{R_{\mu Bldg}} \right] \times \left[ \frac{\frac{PCA}{PFA}}{R_{pocomp}} \right] \times I_p \qquad (2\text{-}6)$$

where $W_p$ and $I_p$ are the weight and importance factor of the NSC, respectively. $R_{pocomp}$ is the inherent component reverse strength margin factor with a placeholder value of 1.3 [36]. The PCA/PFA values are given in Table 4-2 in ATC-120 [36].

Next, the paper focuses on developing a formula for the NSC amplification factor. FRS are generated for NSCs located at every floor of the SCBF and SMF archetype buildings under the 44 ground motions. Then, for each building, a median curve of the NSC amplification factor in terms of component-to-building period ratio is obtained. Fig. 2-13 shows the median of maximum NSC amplification factor, which occurs at different floor levels of the SCBF and SMF buildings. Although using the fundamental period of the building, $T_a$, in the period ratio would be practical, plotting the PCA/PFA curves in terms of $T_p / T_a$ produces widely scattered curves across the normalized period range (not shown herein due to space limitations), and a formula based on this period ratio would be both complex and unreliable. Therefore, a resonant period, $T_r$ is used in the period ratio of the proposed NSC amplification factor formula.

Eq. (2-7) presents the equation of the best conservative fitted curve for NSC amplification factor while the constants of the formula are evaluated conducting least square regression analysis of the median curve. It should be noted that engineering judgement is used to achieve a conservative estimation of the fitted curve. Due to the similarity in the shape of the fitted curves for both SCBF and SMF structures, the same formula has been selected for both LFRS. As shown, the proposed equation provides an acceptable prediction of median NSC amplification across the normalized period ratio from 0 to 3. Eq. (2-7) is valid only for SCBFs with $0.53\ \text{s} < T_a < 1.95\ \text{s}$ for SMFs with $1.26\ \text{s} < T_a < 4.45\ \text{s}$.

$$a_P = 1 + \frac{12\left(\frac{T_P}{T_r}\right)}{\left(\frac{T_P}{T_r}\right)^{3.8} + 3.5} \tag{2-7}$$

The maximum value of the seismic design force normalized by $PGA \times W_p$ is calculated using Eqs. (2-4 to 2-7) for the elastic NSCs, and results are presented in Table 2-3. The effect of building nonlinearity has been included in the PFA/PGA ratio from Eqs. (2-4) and (2-5); therefore, $R_{\mu bldg}$ is considered to be 1.0 in the seismic design force of the present study. The normalized design forces recommended by the ASCE 7-16 and Eurocode 8 are also included in Table 2-3. According to Eq (13.3-2) in ASCE 7-16, the upper limit recommended for the normalized seismic design force is 4.0. The PCA/PGA ratio recommended by the Eurocode 8 varies from 2.5 at the ground to 5.5 at roof level.

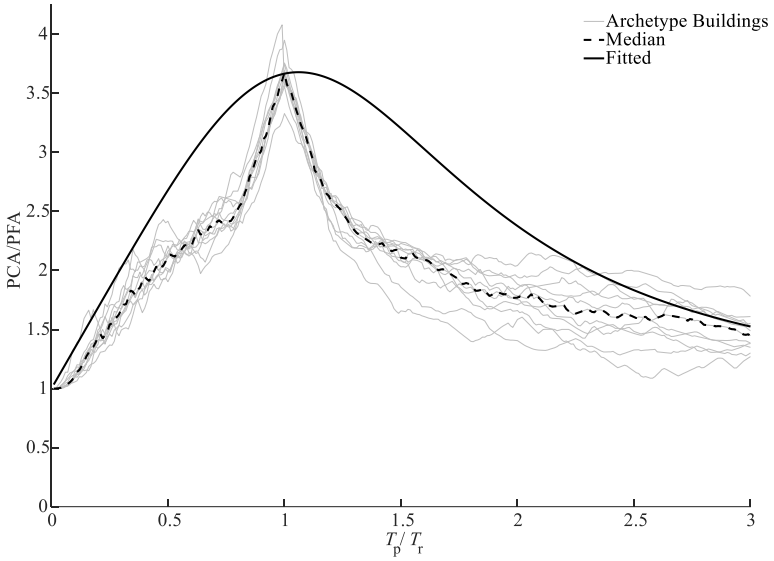


***Fig. 2-13. Maximum PCA/PFA curves of the 11 archetype buildings together with the median of all buildings and a regression formula***

The normalized force calculated based on the recommendation of ATC-120 using Eq. (2-6) is also included in Table 2-3. The maximum PCA/PFA ratio proposed by ATC-120 for elastic components mounted on the ground and elevated floors are 2.5 and 4, respectively. It can be concluded from the table that the recommended design formula by ATC-120 is still conservative for the SCBF archetypes, with maximum difference of 33% with the results of this study. However, the ATC-120 underestimates the normalized design force with the maximum difference of 9% for high-rise SMFs. The ASCE 7-16 underestimates the seismic design force, especially in the SCBF archetypes. Moreover, the results show that the difference between the maximum design force ratio recommended by Eurocode 8 and the corresponding ratio obtained in this study is greater for the SCBF systems than for the SMFs, with maximum difference of 42%.

***Table 2-3 Maximum seismic design force of NSCs***

| $\frac{F_p}{PGA \times W_p}$ | ASCE 7-16 | Eurocode 8 | ATC-120 | Regression Formula |
|---|---|---|---|---|
| 3-chevron | 4.0 | 5.5 | 5.9 | 4.4 |
| 3-TSX | 4.0 | 5.5 | 5.9 | 4.4 |
| 6-chevron | 4.0 | 5.5 | 6.5 | 4.4 |
| 6-TSX | 4.0 | 5.5 | 6.5 | 4.4 |
| 12-chevron | 4.0 | 5.5 | 4.8 | 3.6 |
| 12-TSX | 4.0 | 5.5 | 4.8 | 3.2 |
| 4-ELF | 4.0 | 5.5 | 5.6 | 5.6 |
| 4-RSA | 4.0 | 5.5 | 5.6 | 5.5 |
| 8-RSA | 4.0 | 5.5 | 4.9 | 5.2 |
| 12-RSA | 4.0 | 5.5 | 4.5 | 4.9 |
| 20-RSA | 4.0 | 5.5 | 4.2 | 4.3 |

## 2.8. CONCLUSIONS

This study evaluated demands on acceleration-sensitive NSCs in archetype steel buildings with SCBFs and SMFs ranging from 3 to 20 stories. In contrast to past studies that relied on data from instrumented buildings subjected to significantly weaker shaking than the DE level, the present study quantified the inelastic behavior of the buildings. The floor motions were then used to evaluate the demands on elastic NSCs through floor response spectra. The provisions of ASCE 7-16 and recommendations of ATC-120 for NSCs were evaluated and new equations were provided for estimating PFA/PGA and PCA/PFA based on regression of the data generated from the analyses. The main conclusions of the study are as follows:

- The ATC-120 project used data from instrumented buildings subjected to significantly weaker shaking than the DE level and considered a constant factor ($R_{\mu bldg}$) along the height to account for the inelasticity behavior of the buildings, while the PFA/PGA ratio quantified in this study incorporates the distribution on inelasticity in the structure. The results of the present study showed that the use of the ATC-120-recommended constant $R_{\mu bldg}$ factor resulted in underestimation of accelerations in lower floors. An equation for the PFA/PGA ratio which accounts for the dynamic characteristics of the buildings was presented.
- An additional specific finding is associated with ASCE 7-16, which uses a constant value for ap regardless of the location of the NSC in the building and the NSC fundamental period. Although it was concluded that ap should be evaluated considering both the first and second periods of the structures, the NSC amplification was proposed based on the resonant period. The

concentration of nonlinearity affects the distribution of acceleration over the height, with a pronounced effect in the high-rise structures.

- The seismic design force of the NSC, obtained using the PFA/PGA ratio and NSC amplification factor quantified in this study, was compared with the design force recommended by Eurocode 8 and ATC-120. The results showed that the design force equation recommended by ATC-120 was conservative for the SCBF archetypes, with differences of up to 33%. In contrast, the ATC-120 seismic design force underpredicted the demands in the SMFs, with a maximum difference of 9%. Moreover, the maximum and minimum differences between the design force ratio recommended by Eurocode 8 and this study are observed for the high-rise SCBFs and low-rise SMFs, respectively.

Soil-structure interaction, which typically reduces the viscous damping ratio of high-rise buildings and increases the damping ratio of low- and mid-rise buildings [51], may be considered as a relevant parameter in future studies. In addition, future research is needed to quantify the effects of vertical floor excitation, torsion, and floor diaphragm rigidity.

- **ACKNOWLEDGMENTS**

Financial support for this work was provided by the Natural Sciences and Engineering Research Council of Canada.

### 2.9. REFERENCES

[1] Miranda E, Aslani H, Taghavi S. Assessment of Seismic Performance in Terms of Economic Losses. In: Proceedings of the International Workshop on Performance-Based Seismic Design Concepts and Implementation. Richmond, CA; 2004:149-160.

[2] Aslani H, Miranda E. Probabilistic Earthquake Loss Estimation and Loss Disaggregation in Buildings. Report No. 157. John A. Blume Earthquake Engineering Center, Department of Civil Engineering. Stanford University, California. 2005.

[3] Ramirez CM, Liel AB, Mitrani-Reiser J, Haselton CB, Spear AD, Steiner J, Deierlein GG ME. Expected earthquake damage and repair costs in reinforced concrete frame buildings. Earthq Eng Struct Dyn. 2012;41:1455-1475. https://doi.org/10.1002/eqe.2216.

[4] Ramirez CM, Miranda E. Building-Specific Loss Estimation Methods & Tools for Simplified Performance-Based Earthquake Engineering. Report No. 171.

John A. Blume Earthquake Engineering Center, Department of Civil Engineering. Stanford University, California. 2009.
[5] Tagahvi S, Miranda E. Response Assessment of Nonstructural Building Elements. PEER Report 2003/05. Pacific Earthquake Engineering Research Center, University of California, Berkeley. 2003.
[6] Filiatrault A, Uang C-M, Folz B, Christopoulos C, Gatto K. Reconnaissance Report of the February 28, 2001 Nisqually (Seattle-Olympia) Earthquake. Report No. SSRP-2001/02. La Jolla, California; 2001.
[7] Fierro EA, Miranda E, Perry CL. Behavior of Nonstructural Components in Recent Earthquakes. In: Architectural Engineering Conference (AEI) 2011. Oakland, California: American Society of Civil Engineers; 2011:369-377. https://doi.org/10.1061/41168(399)44.
[8] Miranda E, Mosqueda G, Retamales R, Pekcan G. Performance of Nonstructural Components during the 27 February 2010 Chile Earthquake. Earthq Spectra. 2012;28:453-471. https://doi.org/10.1193/1.4000032.
[9] Filiatrault A, Sullivan T. Performance-based seismic design of nonstructural building components: The next frontier of earthquake engineering. Earthq Eng Eng Vib. 2014; 13:17-46. https://doi.org/10.1007/s11803-014-0238-9.
[10] ASCE 7-16. Minimum Design Loads for Buildings and Other Structures. Reston, VA; 2016. https://doi.org/10.1061/9780784414248.
[11] Anajafi H, Medina RA. Evaluation of ASCE 7 equations for designing acceleration-sensitive nonstructural components using data from instrumented buildings. Earthq Eng Struct Dyn. 2018;47(4):1075-1094. https://doi.org/10.1002/eqe.3057.
[12] Singh MP, Moreschi LM, Suárez LE, Matheu EE. Seismic Design Forces. I: Rigid Nonstructural Components. J Struct Eng. 2006;132(10):1524-1532. https://doi.org/10.1061/(ASCE)0733-9445(2006)132:10(1524).
[13] Singh MP, Moreschi LM, Suárez LE, Matheu EE. Seismic Design Forces. II: Flexible Nonstructural Components. J Struct Eng. 2006;132(10):1533-1542. https://doi.org/10.1061/(ASCE)0733-9445(2006)132:10(1533).
[14] Fathali S, Lizundia B. Evaluation of current seismic design equations for nonstructural components in tall buildings using strong motion records. Struct Des Tall Spec Build. 2011;20:30-46. https://doi.org/10.1002/tal.736.
[15] ASCE 7-10. Minimum Design Loads for Buildings and Other Structures. Reston, VA; 2010. https://doi.org/10.1061/9780784412916.
[16] Anajafi H, Medina RA. Lessons Learned from Evaluating the Responses of Instrumented Buildings in the United States: The Effects of Supporting Building Characteristics on Floor Response Spectra. Earthq Spectra. 2019;35(1):159-191. https://doi.org/10.1193/081017eqs159m.
[17] Kazantzi AK, Vamvatsikos D, Miranda E. Evaluation of Seismic Acceleration Demands on Building Nonstructural Elements. J Struct Eng. 2020;146(7):1-15. https://doi.org/10.1061/(ASCE)st.1943-541x.0002676.
[18] Medina RA, Sankaranarayanan R, Kingston KM. Floor response spectra for light components mounted on regular moment-resisting frame structures. Eng Struct. 2006;28(14):1927-1940. https://doi.org/10.1016/j.engstruct.2006.03.022.
[19] D'Angela D, Magliulo G, Coenza E. Seismic damage assessment of unanchored nonstructural components taking into account the building

response. 2021; Struct Saf. 93: 102-126. https://doi.org/10.1016/j.strusafe.2021.102126.
[20] Flores FX, Lopez-Garcia D, Charney FA (2015): Assessment of floor accelerations in special steel moment frames. Journal of Constructional Steel Research, 106, 154-165. https://doi.org/10.1016/j.jcsr.2014.12.006.
[21] Ray-Chaudhuri S, Villaverde R. Effect of Building Nonlinearity on Seismic Response of Nonstructural Components: A Parametric Study. J Struct Eng. 2008;134(4):661-670. https://doi.org/10.1061/(ASCE)0733-9445(2008)134:4(661).
[22] Taghavi S, Miranda E. Probabilistic Seismic Assessment of Floor Acceleration Demands in Multi-Story Buildings. Technical Report 162. The John A. Blume Earthquake Engineering Center, Stanford University, Stanford, CA, 2006.
[23] Wieser J, Pekcan G, Zaghi AE, Itani A, Maragakis M. Floor Accelerations in Yielding Special Moment Resisting Frame Structures. Earthq Spectra. 2013;29(3):987-1002. https://doi.org/10.1193/1.4000167.
[24] Flores FX, Astudillo BX, Pozo S. Effective Modeling of Special Steel Moment Frames for the Evaluation of Seismically Induced Floor Accelerations. J Struct Eng. 2021;147(1): Pages 04020311. https://doi.org/10.1061/(ASCE)st.1943-541x.0002851.
[25] Ray-Chaudhuri S, Hutchinson TC. Effect of nonlinearity of frame buildings on peak horizontal floor acceleration. J Earthq Eng. 2011;15(1):124-142. https://doi.org/10.1080/13632461003668046.
[26] International Code Council. International Building Code. Country Club Hills, IL. 2003.
[27] Sullivan TJ, Calvi PM, Nascimbene R. Towards improved floor spectra estimates for seismic design. Earthq Struct. 2013;4(1):109-132. https://doi.org/10.12989/eas.2013.4.1.109.
[28] Haymes K, Sullivan T, Chandramohan R. A practice-oriented method for estimating elastic floor response spectra. Bulletin of the New Zealand Society for Earthquake Engineering. 2020;53(3):116-136. https://doi.org/10.5459/bnzsee.53.3.116-136.
[29] Vukobratovic V, Fajfar P. A method for the direct determination of approximate floor response spectra for SDOF inelastic structures. Bull Earthquake Eng. 2015; 13:1405-24. https://doi.org/10.1007/s10518-014-9667-0.
[30] Kazantzi A, Vamvatsikos D, Miranda E. The effect of damping on floor spectral accelerations as inferred from instrumented buildings. Bull Earthq Eng. 2020; (18):2149-2164. https://doi.org/10.1007/s10518-019-00781-3.
[31] Merino RJ, Perrone D, Filiatrault A. Consistent floor response spectra for performance-based seismic design of nonstructural elements. Earthq Eng Struct Dyn. 2019;49(3):261-284. https://doi.org/10.1002/eqe.3236.
[32] Alonso-Rodríguez A, Miranda E. Dynamic behavior of buildings with non-uniform stiffness along their height assessed through coupled flexural and shear beams. Bull Earthq Eng. 2016;14(12):3463-3483.
[33] Salari N, Mohsenzadeh V, Konstantinidis D, Wiebe L. Acceleration demands on nonstructural components in special concentrically braced frame structures. In: 12th Canadian Conference on Earthquake Engineering. Quebec City, Canada; 2019:1-8.

[34] Petrone C, Magliulo G, Manfredi G. Floor response spectra in RC frame structures designed according to Eurocode 8. Bull Earthq Eng. 2016;14(3):747-767.
[35] CEN (2004b) Eurocode 8: design of structures for earthquake resistance—part 1: general rules, seismic actions and rules for buildings. EN 1998-1. Brussels, Belgium.
[36] NIST. Recommendations for Improved Seismic Performance of Nonstructural Components. NIST GCR 18-917-43; 2018. https://doi.org/10.6028/nist.gcr.18-917-43.
[37] NIST. Evaluation of the FEMA P-695 Methodology for Quantification of Building Seismic Performance Factors. NIST GCR 10-917-8; 2010.
[38] FEMA P695. Quantification of Building Seismic Performance Factors. Washington, D. C.; 2009.
[39] American Institute of Steel Construction. Seismic Provisions for Structural Steel Buildings. Chicago, Illinois; 2016.
[40] American Institute of Steel Construction. Specification for Structural Steel Buildings. Chicago, Illinois; 2016.
[41] Mazzoni S, McKenna F, Scott MH, Fenves GL. Open System for Earthquake Engineering Simulation (OpenSEES). Pacific Earthquake Engineering Research Center. 2006.
[42] Karamanci E, Lignos DG. Computational Approach for Collapse Assessment of Concentrically Braced Frames in Seismic Regions. J Struct Eng. 2014;140(8). https://doi.org/10.1061/(ASCE)st.1943-541x.0001011.
[43] Lignos D, Krawinkler H. Sidesway Collapse of Deteriorating Structural Systems under Seismic Excitations. Report No. TR-172. John A. Blume Earthquake Engineering Center, Department of Civil Engineering. Stanford University, California. 2009.
[44] Lignos DG, Krawinkler H. Deterioration Modeling of Steel Components in Support of Collapse Prediction of Steel Moment Frames under Earthquake Loading. J Struct Eng. 2011;137(11):1291-1302. https://doi.org/10.1061/(ASCE)st.1943-541x.0000376.
[45] Ibarra LF, Medina RA, Krawinkler H. Hysteretic models that incorporate strength and stiffness deterioration. Earthq Eng Struct Dyn. 2005;34(12):1489-1511. https://doi.org/10.1002/eqe.495.
[46] Gupta A, Krawinkler H. Seismic Demands for the Performance Evaluation of Steel Moment Resisting Frame Structures. Report No. 132. John A. Blume Earthquake Engineering Center, Department of Civil Engineering. Stanford University, California. 1999.
[47] ATC 72-1. Modeling and Acceptance Criteria for Seismic Design and Analysis of Tall Buildings. Redwood City, California; 2010.
[48] Hsiao P, Lehman DE, Roeder CW. Evaluation of the response modification coefficient and collapse potential of special concentrically braced frames. Earthq Eng Struct Dyn. 2013;42:1547-1564. https://doi.org/10.1002/eqe.2286.
[49] Mohsenzadeh V, Wiebe L. Effect of beam-column connection fixity and gravity framing on the seismic collapse risk of special concentrically braced frames. Soil Dyn Earthq Eng. 2018;115:685-697. https://doi.org/10.1016/j.soildyn.2018.09.035.
[50] Singh A, Ang AHS. Stochastic prediction of maximum seismic response of

light secondary systems. Nucl Eng Des. 1974; 29:218–30. http://www.lib.ncsu.edu/resolver/1840.20/28754.

[51] Cruz C, Miranda E. Evaluation of soil-structure interaction effects on the damping ratios of buildings subjected to earthquakes. Soil Dyn Earthq Eng. 2017;100:183-195. https://doi.org/10.1016/j.soildyn.2017.05.034.

[52] Uriz P, Mahin S. Toward Earthquake-Resistant Design of Concentrically Braced Steel-Frame Structures, Pacific Earthquake Engineering Research Center. 2008.

[53] Lee C, Jeon S, Kim J, Uang C. Effects of Panel Zone Strength and Beam Web Connection Method on Seismic Performance of Reduced Beam Section Steel Moment Connections. J Struct Eng. 2006;131(12):1854-1865. https://doi.org/10.1061/(ASCE)0733-9445(2005)131:12(1854).

[54] Wolfram Research, Inc., Version 12.1, Mathematica. 2020.

[55] Kazantzi A, Vamvatsikos D, Miranda E. Effect of Yielding on the Seismic Demands of Nonstructural Elements. In: 16th European Conference on Earthquake Engineering. 2018.

[56] Singh MP, Suarez LE, Matheau EE, Maldonado GO. Simplified Procedures for Seismic Design of Nonstructural Components and Assessment of Current Code Provisions (NCEER-93-0013). 1993.

# Chapter 3. Seismic Demands on Inelastic Nonstructural Components in Steel Buildings

Manuscript submitted to *Journal of Structural Engineering*

Neda Salari, M.ASCE[1], Dimitrios Konstantinidis, M.ASCE[2]

## Abstract

This paper presents an extensive numerical investigation of the acceleration demands on inelastic nonstructural components (NSCs) mounted on code-compliant archetype buildings with Special Concentrically Braced Frames (SCBF) or Special Moment resisting Frames (SMF), ranging from three to twenty stories. In contrast to recent studies, which have used floor motions recorded in instrumented buildings during generally weak to moderate earthquakes, in this study the demands on the inelastic NSCs are assessed using floor motions obtained from nonlinear response history analyses of the buildings under design-earthquake level excitation. The effects of the dynamic characteristics of the supporting structure and the location, target ductility, and inherent (viscous) damping ratio of the NSCs on their acceleration demands are quantified. The component amplification factor of inelastic NSCs is quantified, observed trends are discussed, and a simplified formula to estimate the component amplification factor is presented. The results of this study are compared with the code requirements in ASCE 7-22, which is largely based on the recommendations of the Applied Technology Council 120 project (ATC-120), and notable differences are observed especially for NSCs supported above grade plane. In addition, the paper presents a formula for damping modification factor for inelastic NSCs mounted at the roof level of the archetype buildings. Finally, a comparison is presented between the NSC seismic force computed in this study and that obtained based on the two possible

[1] Ph.D. Candidate, Dept. of Civil Engineering, McMaster University, 1280 Main Street West, Hamilton, ON L8S 4L8; E-mail: salaritn@mcmaster.ca

[2] Associate Professor, Dept. of Civil and Environmental Engineering, University of California, Berkeley, CA 94720-1710; ORCID: https://orcid.org/0000-0001-5924-8682 (corresponding author). Email: konstantinidis@berkeley.edu

design procedures in ASCE 7-22. For in-resonance NSCs supported above grade, it is observed that ASCE 7-22 mostly underpredicts the ratio of peak component acceleration (PCA) to peak floor acceleration (PFA), which also results in generally underpredicting the horizontal seismic force on acceleration-sensitive nonstructural components.

**Keywords***:* ASCE 7-22, ATC-120, Nonstructural components, Component ductility, Component amplification factor, Component damping ratio

### 3.1. Introduction

Damage to nonstructural components (NSCs) during earthquakes results in substantial economic losses, disruption of building operations, and delays in post-disaster recovery (Filiatrault et al. 2001; Filiatrault et al. 2002; Taghavi and Miranda 2003). Past investigations have shown that the acceleration demands on elastic NSCs in existing standards are generally conservative, especially for inelastic buildings with long fundamental periods (Fathali and Lizundia 2011; Ray-Chaudhuri and Hutchinson 2011).

Although considerable efforts have been spent on improving the simplified design approach for attached NSCs, only a few studies have actually considered the nonlinearity of NSC in evaluating their seismic performance (Villaverde 2006; Ray-Chaudhuri and Villaverde 2008; Vukobratović and Fajfar 2012, 2017; Miranda et al. 2018a; Anajafi et al. 2020; Kazantzi et al. 2020b,c). However, the results of these studies were based on either *generic* models with no strength and stiffness degradation or recorded data from instrumented buildings subjected to ground motions that were significantly weaker than the design level earthquakes and could not elicit inelastic behavior in the structures (Anajafi and Medina 2018; Miranda et al. 2018a; Anajafi et al. 2020; Kazantzi et al. 2020b,c). Anajafi et al. (2020) quantified the effect of NSC inelasticity by evaluating their response reduction factor and inelastic displacement ratio. Results showed that the amplitude of the response reduction factor and the displacement ratio vary with the ratio of the NSC period to the structural period, NSC damping ratio, and level of nonlinearity in the NSC. A study by Miranda et al. (2018a), which used floor motion data from instrumented buildings, noted that while the elastic NSC tuned to the fundamental period of the building experienced peak component

accelerations (PCA) 7.5 times larger than the peak floor acceleration (PFA), the amplification factor PCA/PFA for inelastic NSCs with the ductility of 2.0 was only about 1.5, rendering the maximum value of 2.5 in ASCE 7-16 (ASCE 2016) conservative. Kazantzi et al. (2020b) proposed simplified equations for estimating the NSC amplification factor for inelastic NSCs based on analysis of the instrumented building data. Kazantzi et al. (2020c) proposed an approximate strength-reduction factor for inelastic NSCs. They concluded that the strength-reduction factor obtained from floor accelerations is notably different from that obtained from recorded ground motions on rock or firm soil.

A few studies have evaluated floor response spectra (FRS) for inelastic NSCs using acceleration responses of instrumented buildings and numerical building models (Viti et al. 1981; Chaudhuri and Villaverde 2008; Vukobratović and Fajfar 2017; Kazantzi et al. 2018). Vukobratović and Fajfar (2017) considered displacement ductility levels of 1.0 and 1.5 with a viscous damping ratio of 1% to 7%. The authors showed that NSC inelasticity can result in a remarkable decrease in the FRS (excluding the rigid NSCs) for both elastic and inelastic structures. Kazantzi et al. (2018) generated FRS for inelastic NSCs using the floor acceleration responses of instrumented buildings. They showed that the inelastic behavior of the NSC can result in a reduction in their seismic demands.

In a recent study, the authors evaluated the seismic demands on acceleration-sensitive *elastic* NSCs attached to code-compliant archetype structures (Salari et al. 2022). The study compared the results for PFA/PGA (where PGA = peak ground acceleration) and PCA/PFA for elastic NSCs with the demands computed based on the provisions of ASCE 7-16 (ASCE 2016) and the recommendations of the Applied Technology Council 120 project (ATC-120) presented in the NIST GCR-18-917-43 report (NIST 2018), which was the basis for changes introduced in ASCE 7-22 (ASCE 2022). The results showed that the PFA/PGA and the PCA/PFA for elastic NSCs as required by ASCE 7-16 and ASCE 7-22 are conservative when the structures are subjected to design earthquake (DE) level shaking.

This paper quantifies the effects of structural and nonstructural response nonlinearities on the seismic response of NSCs located in eleven code-designed special concentrically braced frame (SCBF) and special moment frame (SMF) archetype

buildings. The study follows a decoupled (cascading) analysis approach using the floor acceleration responses from Salari et al. (2022) as input to analyze the response of the inelastic NSCs. These floor motions correspond to structures responding in the inelastic range, whereas in previous studies that considered data from instrumented buildings, the intensity level of the ground motions was not large enough to elicit inelastic response in the buildings (Anajafi and Medina 2018). The paper compares the component amplification factor, PCA/PFA, obtained by nonlinear response history analysis (NLRHA) of the inelastic NSCs, with the values of the ratio $[C_{AR} / R_{po}]$ in the ASCE 7-22 formula for the horizontal seismic design force on a NSC, $F_p$, given by

$$F_p = 0.4 S_{DS} I_p W_p \left[ \frac{H_f}{R_\mu} \right] \left[ \frac{C_{AR}}{R_{po}} \right] \qquad (3\text{-}1)$$

where $S_{DS}$ = the design-earthquake spectral acceleration at short periods, $I_p$ = the NSC's importance factor, $W_p$ = the NSC's operating weight, $H_f$ = a factor for force (or acceleration) amplification as a function of the height where the NSC is supported in the structure, $R_\mu$ = a structure ductility reduction factor, $C_{AR}$ = a component resonance ductility factor that converts the peak floor acceleration into the peak component acceleration, and $R_{po}$ = a component strength factor. The term $0.4 S_{DS}$ in Eq. (1) represents the PGA, while the terms $[H_f / R_\mu]$ and $[C_{AR} / R_{po}]$ represent PFA/PGA and PCA/PFA, respectively. Eq. (3-1) can be used even in the absence of detailed information about the structure, but when a nonlinear structural model is available, ASCE 7-22 offers an alternative formula that uses the mean peak floor acceleration $a_i$ (obtained by NLRHA of the structural model for a DE ground motion suite) in lieu of $0.4 S_{DS} [H_f / R_\mu]$ in Eq. (3-1) to compute the seismic design force. In this study, for the purposes of modeling a NSC, all sources of nonlinearity in the NSC and its mounting fixtures are lumped together, allowing a bilinear SDOF oscillator to represent the NSC, as in most past studies on the subject. Absolute acceleration FRS are generated for specific NSC target ductility levels and inherent NSC damping ratios between 1.25 to 6.0 and 1% to 7%, respectively. The study evaluates the effect of parameters that control the inelastic FRS, including modal periods of the structure and the location, target

ductility, and damping ratio of the NSC. A damping modification factor for inelastic NSCs with different target ductility levels is presented, as are design-oriented approximate formulas for the PCA/PFA factor based on the NLRHA results. The approximate-formula predictions are compared to the $[C_{AR} / R_{po}]$ values in ASCE 7-22 (ASCE 2022). Lastly, the seismic design forces predicted by the approximate equations are compared with the seismic design forces predicted by ATC-120. Also compared are the seismic design forces obtained by NLRHA of the inelastic NSCs and by the ASCE 7-22 formula based on $a_i$ instead of $0.4S_{DS}[H_f / R_\mu]$. The comparison is made at both the grade and above-grade planes. The comparisons mentioned here have not been the subject of previous studies.

## 3.2. Analysis Methods

### *3.2.1. Summary of Building Designs, Structural Modeling, and Ground Motions*

This section gives a general overview for the benefit of the reader, while specific details on the building designs, techniques employed in the OpenSees (2006) modeling, and the ground motion suite used can be found in Salari et al. (2022).

A total of eleven archetype buildings were considered, six with SCBFs and five with SMFs. The SCBFs included 3-, 6-, and 12-story designs, with either chevron or Two-story X (TSX) configurations. The SMFs included 4- (two designs), 8-, 12-, and 20-story designs. The labeling scheme used to later refer to the SCBFs includes the number of stories and the SCBF configuration, i.e., 3-chevron, 3-TSX, 6-chevron, 6-TSX, 12-chevron, and 12-TSX. As shown in Fig. 1, the buildings have a rectangular plan with one bay of SCBF in each direction for 3- and 6-story buildings and two bays of SCBFs for the 12-story building. Fig. 2 illustrates the plan and elevation view of the SMFs. An Equivalent Lateral Force (ELF) procedure and a Response Spectrum Analysis (RSA) procedure were used to design the 4-story SMFs, while the remaining SMFs were designed using the RSA approach only. Because the ELF method results in unrealistically large section members for taller SMF structures, high-rise SMFs designed with ELF method are ignored. Therefore, the SMFs are labeled 4-ELF, 4-RSA, 8-RSA, 12-RSA, and 20-RSA. The plans and elevations of the SCBF and SMF buildings are the same as the frames presented in NIST GCR 10-917-8 report (NIST

2010). The buildings were assumed to be located in San Francisco (site coordinates: 37.783°N, 122.392°W), on Site Class D soil, and designed for office occupancy (Risk Category II) and Seismic Design Category D, following ASCE 7-22, ANSI/AISC 341-16 (AISC 2016a), and ANSI/AISC 360-16 (AISC 2016b) provisions. The corresponding mapped spectral accelerations at 0.2 s and 1 s were $S_{DS}$ = 1.0 g and $S_{D1}$ = 0.6 g, respectively. For the column, beam, and brace sections used in the SCBF and SMF designs, the reader is referred to Salari et al. (2022), where detailed information about the developed 2D models of the buildings in OpenSees (OpenSees 2006) can also be found. Table 3-1 lists the modal periods of the buildings.

Nonlinear response history analyses of these models were carried out using the FEMA P695 (FEMA 2009) suite of 22 far-field ground motions, each having two orthogonal horizontal components. Because the structural models in this study are 2D, each orthogonal component was considered as an independent excitation, resulting in a total of 44 ground motion records, and scaled to the risk-targeted maximum considered earthquake ($MCE_R$) spectrum using the approach described in ASCE 7-22 (ASCE 2022). Further details are presented in Salari et al. (2022). The corresponding $MCE_R$ scale factors were multiplied by a factor of 2/3 to obtain the scale factors at the DE level.

### *3.2.2. Modeling of Inelastic NSCs*

The response history analyses of the OpenSees structural models produced absolute acceleration response histories at the different floor levels, which were subsequently used as the input acceleration for the nonlinear SDOFs representing the NSCs. In this context, the dynamic interaction between the supporting structure and the NSCs was neglected, which has been shown to be valid when the masses of the NSCs are small compared to the mass of the supporting structure (Singh and Ang 1974; Taghavi and Miranda 2006). The NSCs were modeled as elastic-perfectly-plastic SDOF systems. A finite post-yield stiffness could be chosen (for instance, 2 to 3% to represent anchorage material yielding), as mentioned earlier; however, since the exact value of post-yield stiffness would depend on the particular component and its various possible sources of nonlinearity, the post-yield stiffness was generically chosen to be zero. Constant-ductility FRS for various values of inherent (viscous) damping ratio, $\beta_{comp}$,

and varying target ductility values, $\mu_{comp}$, were finally generated using an iterative procedure (Chopra 2016). Because of the cost of additional analysis and lack of information about the performance of the NSCs under $MCE_R$-level shaking (NIST 2018), acceleration demands on NSCs in ASCE 7-22 are based on the DE level. Similarly, the evaluation here focuses on demands at the DE level only.

### 3.3. Floor Response Spectra for Inelastic NSC

To highlight the effect of $\mu_{comp}$ on the peak NSC accelerations, $\mu_{comp}$ values of 1.5 and 2.0 are considered in this section. Effects of other ductility levels, namely 1.75, 4.0, and 6.0, will be studied later in the paper.

Although the ATC-120 and ASCE 7-22 project used the traditional assumption of $\beta_{comp}$ = 5%, smaller values have been reported in experimental studies (Archila et al. 2012; Astroza et al. 2015). Watkins et al. (2009) evaluated the damping ratio of many floor- and wall-mounted mechanical and electrical components, and an average damping ratio of 2.1% was estimated from the results of hammer testing. Thus, even though 5% has been traditionally used for the NSCs, the present study uses a 2% inherent damping ratio for NSCs as the default value. Nonetheless, different values of damping ratio ranging from 1 to 7% are considered in the section

#### *3.3.1. Effect of NSC Damping Ratio on the Roof Response Spectra.*

Figs. 3-3 and 3-4 show median acceleration response spectra of nonlinear NSCs mounted on selected floors of the SCBF and SMF structures. The median ground spectra of the 44 ground motions are included in Figs. 3-3 and 3-4 for comparison. The vertical dashed lines indicate the first few structural periods. Note that for the 12-RSA and 20-RSA structures, the fundamental periods, which are greater than 3 s, are not shown. The figures also show horizontal lines corresponding to the maximum possible PCA at the roof level based on ASCE 7-22. Therefore, the results of this study are compared to the maximum possible code values. Since the design PGA, which is $0.4S_{DS}$, is equal to 0.4 g in the present study, the maximum value of PCA at the roof is $\text{PCA} = 0.4\text{g} \times [H_f / R_\mu] \times [C_{AR} / R_{po}]$. Table 2 shows the parameters used to calculate the maximum PCA values, corresponding to the horizontal lines. The maximum PCA is obtained by considering the maximum value of the height factor, $H_f$, calculated at the

roof level using Eq. (13.3-4) in ASCE 7-22, which requires the fundamental period of the structure, $T_a$. The latter is determined using Eq. (12.8-8) in ASCE 7-22. The structure ductility reduction factor is computed using $R_\mu = [1.1R/(I_e\Omega_0)]^{1/2} \geq 1.3$, where values for the response modification coefficient, $R$, and overstrength factor, $\Omega_0$, are obtained from Table 12.2-1 in ASCE 7-22. An importance factor, $I_e$, of 1 is used. The NSC resonance ductility factor, $C_{AR}$, is considered for NSCs that are likely to be in resonance, and quantified in Table C13.3-1 in ASCE 7-22 [alt. Table 4-2 in NIST GCR-18-917-43]; i.e., $C_{AR}$ = 2.2 and 1.4 for $\mu_{comp}$ = 1.5 and $\mu_{comp}$ = 2.0, respectively. An elastic-perfectly-plastic system is used to model the NSC; therefore, the over-strength reduction factor, $R_{po}$, is considered to be 1.0.

For most of the floors, a peak is not observed in the FRS near the fundamental period of the structure. However, peaks emerge at higher periods, except for the high-rise SCBFs, in which structural nonlinearity results in a broadening of the peaks over a wider range of periods. Period elongation due to structural nonlinear response results in the peaks of the FRS shifting slightly to the right of the vertical lines.

It is apparent from the figures that an increase in NSC ductility from 1.5 to 2.0 results in a greater reduction in the largest peaks when the NSCs are mounted on flexible systems (the SMFs) than on stiff systems (the SCBFs). For instance, the maximum floor spectral acceleration for the 12-TSX structure drops from 2.4 g for a component with $\mu_{comp}$ = 1.5 to about 1.8 g for $\mu_{comp}$ = 2.0. The same demand parameter for the 12-RSA structure drops from 3.0 g for $\mu_{comp}$ = 1.5, to 2.0 g for $\mu_{comp}$ = 2.0. Moreover, increasing the flexibility of the structures in the SMFs results in a larger reduction in the spectral acceleration of the largest peak when the NSC experiences higher levels of ductility. For example, the spectral acceleration of the largest peak for NSC with $\mu_{comp}$ = 1.5 reduces by 15% from 4-ELF to the more flexible system (4-RSA), while $\mu_{comp}$ = 2.0 results in a larger reduction, of the order of 19%, in the spectral acceleration of the largest peak.

A comparison of the maximum spectral acceleration for NSCs with $\mu_{comp}$ = 1.5 mounted on the 12-chevron and 12-TSX structures shows that the FRS peaks that concentrate around the higher modes of the structures exceed 1.6 g and 2.3 g, respectively. These are smaller than the corresponding value for the flexible frame (12-RSA), which is close to 3 g. In addition, increasing the target ductility level results in a

smaller relative difference in the maximum PCA of the stiff systems (SCBF) compared to the flexible systems (SMF).

As can be seen in the figures, the maximum spectral acceleration of the NSCs with $\mu_{comp}$ = 1.5 increases by around 3% from the 3-chevron to the 3-TSX structure, while the difference between the 12-chevron and 12-TSX building exceeds 45%, which is likely related to higher mode effects in the high-rise buildings.

Next, the maximum PCA values per ASCE 7-22 (at the roof level), represented using horizontal lines in Figs. 3-3 and 3-4, are compared against the values computed in this study for NSCs mounted on the roof level. As can be seen, when the NSC is in resonance with the first structural mode, the code value significantly overestimates the maximum PCA in all cases. For NSCs with lower periods (i.e., in resonance with the higher structural modes), which is the case for most NSCs, the code value either roughly equal or underestimates the computed PCA values, depending on the height and the type of the seismic-force resisting system (SFRS). For SCBF structures with 3 or 12 stories, good agreement is observed between the code prediction and the computed PCA values at the roof level. However, the code predictions underestimate the PCAs computed for NSCs mounted on the roof of the 6-story SCBFs. For SMF structures (Fig. 3-4), the code prediction always underestimates the computed PCA. Furthermore, it can be seen that demands on very flexible or vibration-isolated components with large periods follow the trend in ASCE 7-22, i.e., an increasing acceleration up the height of the building.

Comparison of the FRS in Figs. 3-3 and 3-4 shows that the largest peaks expand over a wider range of periods in the SCBFs than in the SMFs. This capping-and-spreading effect is associated with the yielding of the braces. The nonlinearity of the structural components influences a wider period range of the FRS (Sullivan et al. 2013; Buccella et al. 2021). It should be noted that the higher mode spectral accelerations are amplified in the floors experiencing inelastic action. For instance, in the 3-story SCBFs, the response spectrum for the 3$^{rd}$ floor decreases around the first and second modes, while it increases around the 3$^{rd}$ mode. It can be seen that the 4$^{th}$ floor spectrum of the 4-story SMF structures drops around the second mode, which is due to the acceleration saturation that occurs in the PFA/PGA profile (Salari et al. 2022).

Finally, it is observed that the floor spectral shapes vary along the height of the buildings. For example, as the elevation of the NSC increases, the spectral acceleration corresponding to the first structural period increases at a greater rate than the values related to the higher modes. Considering the first structural period, the spectral acceleration at lower floors decreases as the target ductility level increases. However, there is a lesser reduction or even an unexpected increase around the higher modes. As previously mentioned, in some cases, a reversal trend with a drop in spectral acceleration is observed at higher structural modes. Furthermore, the difference between the peak value of the median ground spectrum and the peak of floor spectra increases up the building, particularly in the first period.

### 3.4. Effect of NSC Ductility on the Component Amplification Factor

Fig. 3-5 illustrates two representative examples of the effect of NSC ductility on the component amplification factor, PCA/PFA, for 2%-damped components mounted on the roof of the 6-TSX and 8-RSA structures. The horizontal axis plots the period of the NSC, $T_p$, normalized by the resonant period of the buildings, $T_r$, which is defined herein as the structural period closest to the peak of the FRS (Salari et al. 2022). Based on dominant peaks of the roof spectra (see Figs. 3 and 4), the resonant periods are those of the second and third modes for 6-TSX and 8-RSA, respectively. As can be seen, even small ductility levels, such as 1.5 or 2.0, result in a considerable reduction in PCA/PFA for NSCs with periods tuned to the resonant period of the structure. For example, $\mu_{comp}$ = 1.5 reduces PCA/PFA from 4.2 to 2.6 compared to the elastic case, at the resonant period of the 6-TSX building. A similar reduction is observed for the 8-RSA structure, in which the PCA/PFA decreases from 4.8 to 2.7. It can be concluded that increasing the ductility level of the NSC from 1.0 (elastic case) to 1.5 is more effective in reducing the NSC acceleration demands in the SMF structure than in the SCBF structure.

Fig. 3-6 shows the ratio of roof-mounted component amplification factor for ductility level $\mu_{comp}$, denoted as $(\text{PCA/PFA})_{\mu_{comp}}$, to the component amplification factor of an elastic component, i.e., $(\text{PCA/PFA})_{\mu_{comp}=1}$, as a function of $\mu_{comp}$. The responses correspond to a component with period $T_p$ equal to the resonant period of select archetype buildings. The figure illustrates how this ratio decreases as the target ductility level increases. As can be seen, the reduction rate is greater for components in the SMFs

compared to the SCBFs. For example, the maximum reduction in the ratio of the component amplification factor from the elastic component to $\mu_{comp}$ = 2.0 is observed for the 8-RSA building with an approximate value of 62%, while the minimum reduction is observed for the 12-TSX with the approximate value of 33%.

### 3.5. Effect of NSC Damping Ratio on the Roof Response Spectra

As mentioned above, recent experimental studies have reported lower values than 5% for the NSC inherent damping ratio (Archila et al. 2012; Astroza et al. 2015). This section aims to quantify the effect of inherent damping ratio of the NSCs, $\beta_{comp}$, on the NSC force demand. Figs. 3-7 and 3-8 illustrate the normalized PCA, defined here as the ratio of PCA for NSCs with different damping values and the PCA of 2%-damped NSCs. Results are shown for the 4-RSA, 6-chevron, 8-RSA, and 12-TSX structures, representing different heights of the SCBF and SMF structures. As in Figs. 3-3 and 3-4, the vertical dashed lines indicate modal periods of the structure. Fig. 3-7 shows results for NSCs with $\mu_{comp}$ = 1.5 mounted at the roof level, while Fig. 3-8 shows the same for $\mu_{comp}$ = 2.0. Results show that increasing $\beta_{comp}$ from 1 to 7% for $\mu_{comp}$ = 1.5 and 2.0 appreciably reduces the normalized PCA, especially for NSCs with periods near the modal periods of the buildings. The largest reduction of 40% is associated with the NSC with $\mu_{comp}$ = 1.5 tuned with the third mode of the 4-RSA building. For NSCs away from the resonant periods, increasing $\beta_{comp}$ results in a notably smaller reduction of the normalized PCA compared to the in-tune cases. For NSCs with $\mu_{comp}$ = 2.0, increasing $\beta_{comp}$ from 1 to 7% reduces the PCA by as much as 30% for the 4-RSA building.

There are two damping mechanisms acting in the component to control the normalized PCA: that associated with inelastic action and that with inherent viscous damping. As the inelastic action increases ($\mu_{comp}$ = 1.5 to 2.0), the relative effect of the viscous damping becomes smaller in reducing the response. This shift in the dominant damping source is also observed in Figs. 3-7 and 3-8. As can be seen, there is a smaller separation among the normalized PCA curves for $\mu_{comp}$ = 2.0 compared to $\mu_{comp}$ = 1.5. Fig. 9 shows the trend of reduction in maximum PCA (over all $T_p$ periods considered) with $\beta_{comp}$ ranging from 1 to 7% for $\mu_{comp}$ = 1.5 and 2.0. As can be seen, increasing $\mu_{comp}$ from 1.5 to 2.0 not only reduces the PCA values but also makes the response curves flatter, suggesting a reduced sensitivity to the NSC viscous damping for all considered

buildings. When increasing $\beta_{comp}$ from 1 to 7%, the maximum reduction of 65% is observed for the 4-RSA building for NSCs with $\mu_{comp}$ =1.5, while the minimum reduction of 40% is observed for the NSC with $\mu_{comp}$ =1.5 attached to the high-rise SCBF. The reduction is less pronounced for the higher level of ductility of $\mu_{comp}$ =2.0 compared to $\mu_{comp}$ =1.5.

### 3.6. Damping Modification Factor Formula

Recognizing the significant effects of inherent damping on the NSC response, this section focuses on providing guidance that could inform future code development aiming to account for NSC damping values other than 5%. Since most previous investigations evaluating the DMF mainly focused on elastic NSCs (Anajafi and Medina 2019b; Kazantzi et al. 2020a), there is a need to evaluate the DMF for inelastic NSCs. A damping modification factor (DMF) can be used to estimate the PCA on a NSC with arbitrary inherent damping ratio $\beta_{comp}$ based on the PCA of a NSC with $\beta_{comp}$ = 5%, as follows:

$$\mathrm{PCA}_{\beta_{comp}} = \mathrm{DMF} \times \mathrm{PCA}_{\beta_{comp}=5\%} \tag{3-2}$$

where the PCA values correspond to inelastic NSCs having the same target ductility.

Various DMF expressions are available in the literature and even design/evaluation standards for structures. For instance, ASCE/SEI 41-17 (2017) provides the following formula for elastic ground-motion response spectra:

$$\mathrm{DMF} = \frac{5.6 - \ln(100\beta)}{4.0} \tag{3-3}$$

where $\beta$ = the effective viscous damping ratio of the structure. Since ground motions generally have broadband spectra, Eq. (3-3) is inappropriate for floor motion spectra, which have semi-narrowband characteristics (Anajafi and Medina 2019b). Anajafi and Medina (2019b) proposed a modified form of the DMF expression in ASCE/SEI 41 to be applied for elastic NSCs mounted on short to midrise steel moment-resisting frames and reinforced concrete shear wall buildings. In the present study, results for NSC ductility of 1.5 and 2.0 and NSC damping ratio of 1, 2, and 7% are considered toward developing a practical DMF expression. The median curve of the DMF is obtained for each SCBF and SMF building under the 44 motions. The shapes of the median curves

suggest a fitted DMF that is linear in $T_p / T_r$ for $T_p / T_r \le 0.5$, quadratic over $0.5 < T_p / T_r \le 1.5$, and constant for $T_p / T_r > 1.5$; specifically,

$$\text{DMF} = \begin{cases} \left[0.5\alpha + \beta + 2(\gamma - 1)\right]\dfrac{T_p}{T_r} + 1, & 0 \le \dfrac{T_p}{T_r} \le 0.5 \\ \alpha\left(\dfrac{T_p}{T_r}\right)^2 + \beta\dfrac{T_p}{T_r} + \gamma, & 0.5 < \dfrac{T_p}{T_r} \le 1.5 \\ 2.25\alpha + 1.5\beta + \gamma, & \dfrac{T_p}{T_r} > 1.5 \end{cases} \quad (3\text{-}4)$$

where continuity is enforced at the transitions. Table 3-2 presents the regression coefficients $\alpha$, $\beta$, and $\gamma$ obtained using least squares for the inelastic NSCs attached to all archetype buildings considered. Note that the shapes of the fitted curves for the SCBF and SMF structures were similar, so a common DMF formula was proposed for the two SFRS. Fig. 10 shows the median of the DMF for the NSC mounted on the roof level of all archetype buildings considered in this study. It should be noted that the DMF for the inelastic NSC with $\beta_{comp}$ = 7% can be approximated by 1.0, and the corresponding graphs are not shown for the sake of clarity. As can be seen in the figure, increasing the ductility from 1.5 to 2.0 results in smaller DMF values for damping ratios lower than 5% and larger values for damping ratios greater than 5%. The maximum predicted DMF for ductility of 1.5 is 1.30 and 1.18 for 1% and 2% damping, respectively. For the ductility of 2.0, the values are 1.15 and 1.10 for damping of 1% and 2%, respectively.

### 3.7. Component Amplification Factor Formula for NSCs Mounted on SCBF and SMF Buildings

Based on the numerical results of this study, this section presents an expression for the component amplification factor of inelastic NSCs attached to the code-based designed buildings responding in their inelastic range. To be able to draw comparisons of the amplification factor obtained in this study with those in ATC-120 and ASCE 7-22, the analyses are repeated for 5%-damped NSCs. Fig. 3-11 shows the median curves of the PCA/PFA for 5%-damped NSC with $\mu_{comp}$ = 1.25, 1.5, 1.75, 2.0, 4.0, and 6.0 mounted on the roof level of the archetype buildings. Although using the fundamental period of

the building, $T_a$, would be practical, plotting the PCA/PFA curves in terms of $T_p / T_a$ generates widely spread curves across the normalized period range (not shown herein due to space limitations), and a formula based on this period ratio would be both complicated and unreliable. Therefore, a resonant period, $T_r$, is used in the period ratio of the component amplification factor formula. Values of the resonant period $T_r$ of each archetype, along with the corresponding mode number, are listed in Table 3-1. It should be noted that a conservative estimation of the NSC amplification factor could be obtained by using an appropriate structural period. Therefore, the proposed formula can be used for practical applications without a need to generate the FRS. Eq. (3-5) presents a formula for PCA/PFA of 5%-damped NSCs. Engineering judgment is used to achieve the best conservative estimate of the fitted curve.

$$\text{PCA/PFA} = \begin{cases} 1 + a\left(\dfrac{T_p}{T_r}\right)^2, & \dfrac{T_p}{T_r} < 1 \\ 1 + a + b\left\{\exp\left[c\left(\dfrac{T_p}{T_r} - 1\right)\right] - 1\right\}, & \dfrac{T_p}{T_r} \geq 1 \end{cases} \tag{3-5}$$

where *a*, *b*, and *c* are parameters that depend on the component ductility $\mu_{comp}$ and given by Eqs. (3-6-a) and (3-6-b) for the SCBF and SMF systems, respectively:

$$\left.\begin{aligned} a &= 3.2853\left(\mu_{comp}\right)^{-1.604} \\ b &= 2.5786\left(\mu_{comp}\right)^{-0.742} \\ c &= 0.0557\left(\mu_{comp}\right)^3 - 0.7239\left(\mu_{comp}\right)^2 + 2.8964\left(\mu_{comp}\right) - 4.1685 \end{aligned}\right\} \text{ for SCBFs} \tag{3-6-a}$$

$$\left.\begin{aligned} a &= 3.1981\left(\mu_{comp}\right)^{-1.611} \\ b &= 2.0676\left(\mu_{comp}\right)^{-0.722} \\ c &= 0.093\left(\mu_{comp}\right)^3 - 1.1265\left(\mu_{comp}\right)^2 + 4.1608\left(\mu_{comp}\right) - 5.2999 \end{aligned}\right\} \text{ for SMFs} \tag{3-6-b}$$

The parameter values in Eqs. (3-6-a) and (3-6-b) were estimated by nonlinear least square regression analysis. Eq. (3-5) together with (3-6-a) or (3-6-b) provides an acceptable estimate of the median computed amplification factor for NSC with $\mu_{comp}$ < 6.0. The corresponding PCA/PFA curves for $\mu_{comp}$ = 1.25, 1.5, 1.75, 2.0, 4.0, and 6.0 are shown in Fig. 3-11 (a) and (b). However, because the resulting curves for the two

systems are similar, the parameters *a*, *b*, and *c* can alternatively be estimated by combining the SCBF and SMF data, which provides common values:

$$\left.\begin{aligned} a &= 3.1711\left(\mu_{\text{comp}}\right)^{-1.583} \\ b &= 1.9598\left(\mu_{\text{comp}}\right)^{-0.634} \\ c &= 0.0939\left(\mu_{\text{comp}}\right)^{3} - 1.2112\left(\mu_{\text{comp}}\right)^{2} + 4.8998\left(\mu_{\text{comp}}\right) - 6.8827 \end{aligned}\right\} \text{ for combined SCBF and SMFs}$$

(3-6-c)

The NSC amplification factor values per ASCE 7-22/ ATC-120 are shown in Fig. 3-12, for NSCs that are "more likely" in resonance with the building. Note that while ASCE 7-22 uses $C_{\text{AR}}$ to represent PCA/PFA for different NSCs, the dependence of $C_{\text{AR}}$ on NSC ductility, $\mu_{\text{comp}}$, is meant to be the same in the two documents. That dependence is shown in Table 3-4, which has been adapted from Table C13.3-1 in ASCE 7-22 (ASCE 2022) and Table 4-2 in NIST GCR 18-917-43 (NIST 2018) and is presented here for convenience. As can be seen in Fig. 3-12, the differences between the NSC amplification factor values in the ASCE 7-22/ATC-120 and this study are large for the NSC "supported above grade plane" (ASCE 2022) but small for NSCs "supported at grade plane". It should be mentioned that the amplification factor for the NSCs "supported at grade plane" is obtained by applying the scaled ground motions to the NSCs. Considering the above grade plane results (Fig. 3-12b) for $\mu_{\text{comp}}$ = 1.25, 1.5, and 2.0 (not 4.0 because ATC-120 recommended a constant PCA/PFA of 1.4 for $\mu_{\text{comp}} \geq 2.0$), the relative difference between the PCA/PFA values in this study and in ASCE 7-22 increases as the NSC target ductility increases from $\mu_{\text{comp}}$ = 1.25 to $\mu_{\text{comp}}$ = 2.0. However, this trend cannot be reported for the NSCs supported on the grade plane (Fig. 3-12a), for which the relative difference fluctuates as the target ductility increases.

## 3.8. Comparison of NSC Seismic Design Force Values Based on Different Methods

Fig. 3-13(a) illustrates a comparison between the NSC seismic design force at the roof level as computed by ATC-120 using NLRHA, $F_{\text{p}}^{\text{NLRHA}}$, for a typical example building (NIST 2018, Figure 4-42) and as computed using the ATC-120-proposed NSC design

formula, $F_{\mathrm{p}}^{\text{ATC-120}}$. The results are presented as a ratio on the vertical axis, with the horizontal line at $F_{\mathrm{p}}^{\text{NLRHA}} / F_{\mathrm{p}}^{\text{ATC-120}} = 1$ separating safe and unsafe predictions. As elsewhere in this work, the horizontal axis is in terms of $T_{\mathrm{p}} / T_{\mathrm{r}}$. According to ATC-120, such plots are derived for various archetype buildings and story levels in order to assure the adequacy of the proposed design force in different conditions. The acceptance criteria considered by ATC-120 (NIST 2018) is based on a maximum failure probability of 10%. For computing this probability, ATC-120 estimates the ratio between the number of failing NSCs to the total quantity of NSCs. The failing NSCs are also considered to have periods falling inside the failure interval around the resonant period. It can be seen from Fig. 3-13(a) that, for NSCs with periods near the resonant structural period, the chances of failure are high, while there is an appreciable margin of safety for NSCs with periods away from resonance. This suggests that the failure risk of NSCs designed based on the ATC-120 recommendations is markedly nonuniform over the period range.

Fig. 3-13(b) presents a similar comparison, but here $F_{\mathrm{p}}^{\text{NLRHA}}$ corresponds to the NSC force obtained by averaging the NLRHA results of the archetype buildings considered in this study and the denominator is the force computed using the approximate PCA/PFA formula in this study, i.e., Eq. (3-5). In addition to separating safe and unsafe regions, the horizontal lines at $F_{\mathrm{p}}^{\text{NLRHA}} / F_{\mathrm{p}}^{\text{ATC-120}} = 1$ or $F_{\mathrm{p}}^{\text{NLRHA}} / F_{\mathrm{p}}^{\text{Eq. (5)}} = 1$ represent when the design force values (per ATC-120 or per Eq. (5)) are equal to the forces computed by NLRHA. Thus, considering the NLRHA values to be the benchmark, the distance between a data point and the horizontal line indicates the estimation error in the design force. The $F_{\mathrm{p}}^{\text{NLRHA}} / F_{\mathrm{p}}^{\text{Eq. (5)}}$ curve in Fig. 3-13(b) attains notably smaller values near resonance compared to the $F_{\mathrm{p}}^{\text{NLRHA}} / F_{\mathrm{p}}^{\text{ATC-120}}$ curve in Fig. 3-13(a), and it remains close to unity uniformly over the period range, which suggests both a small prediction error and a fairly uniform level of failure risk (alt. safety margin). The maximum distance between the $F_{\mathrm{p}}^{\text{NLRHA}} / F_{\mathrm{p}}^{\text{Eq. (5)}}$ curve and the horizontal line at one is 0.05, indicating that this study's prediction formula has a maximum error of 5%. In contrast, Fig. 3-13(a) shows that the estimation error of the

ATC-120 formula is not uniform over the period range and attains values as large as 50% at the tails.

As mentioned in the Introduction section, in lieu of using Eq. (1) to compute the horizontal NSC seismic design force, $F_p$, ASCE 7-22 offers a formula that can be used when floor accelerations for the supporting structure have been computed by NLRHA, but the dynamic properties of the NSC have not been explicitly modeled in the NLRHA (ASCE 7-22):

$$F_p = I_p W_p a_i \left[ \frac{C_{AR}}{R_{po}} \right] \tag{3-7}$$

where $a_i$ = the mean PFA for the DE-level motion suite. Figs. 3-14 and 3-15 show a comparison of the normalized seismic design force, $F_p / (I_p W_p)$, obtained by different methods for inelastic NSCs supported at grade plane (ground level) and at the roof level, respectively. An in-resonance condition is assumed for all cases. The figures plot the normalized force obtained using the ASCE 7-22 (equivalent) "static" design force [Eq. (1)] and ASCE 7-22 "NLRHA" [Eq. (7)] formulas. The $a_i$ factor is computed based on the PFA values reported by Salari et al. (2022) [see Eqs. (3-4) and (3-5) therein, which correspond to SCBFs and SMFs, respectively]. The figures also show the NSC force computed based on the response history analysis results of this study. In Fig. 3-14, for the NSCs at grade plane, $F_p / (I_p W_p)$ values that correspond to "This study" are the computed PCA of the NSCs when subjected to the scaled ground motions. In Fig. 3-15, for NSCs at the roof level, $F_p / (I_p W_p)$ is computed using

$$F_p / (I_p W_p) = \mathrm{PGA} \left[ \frac{\mathrm{PFA}}{\mathrm{PGA}} \right] \left[ \frac{\mathrm{PCA}}{\mathrm{PFA}} \right] \tag{3-8}$$

where the values for PFA/PGA are also as proposed by Salari et al. (2022) [Eqs. (3-4) and (3-5) therein], while the values for PCA/PFA are those proposed in the present study for above grade plane (i.e., Eqs. (3-5) and (3-6-c)).

It should be noted that the reason why there are different graphs for different archetypes in Fig. 3-14, even though the NSCs are supported at grade plane, is because the ground motion suite was scaled with different factors for the archetypes, based on their fundamental periods. As can be seen, the NSC seismic design force at grade plane

by ASCE 7-22's NLRHA method is roughly 50% larger than by the static method. Since the $F_p / (I_p W_p)$ values for the two ASCE 7 methods are computed using the same $C_{AR}$ value, the differences arise because of the input base acceleration, which at grade plane corresponds to the PGA; for the "static" procedure, that is $0.4S_{DS}$ = 0.4g, while for the NLRHA, it is the actual PGA of the ground motion (approx. 0.6g). The ASCE 7 NLRHA method provides conservative values compared to the results of this study in every case, though with varying degree of conservatism: in some cases as much as double, while in others negligible. In contrast, the values of this study and those by the ASCE 7 static procedure are generally close to each other, with only a few exceptions of the ASCE 7 formula underpredicting the demands. The largest differences between the static values and those of this study arise at the ground level of the low- and mid-rise SMF archetypes.

For NSCs mounted at the roof level, Fig. 3-15 shows that the ASCE 7 static procedure provides larger values than the ASCE 7 NLRHA method in every SCBF archetype and for all values of NSC ductility. The seismic force values of this study [per Eq. (3-7)] for the SCBF archetypes are either roughly the same or larger than the ASCE 7-22 static values, with the relative difference growing larger in going from $\mu_{comp}$ = 1.25, to 1.5, to 2.0. For $\mu_{comp}$ = 4.0, however, the trend reverses, and the ASCE 7-22 static values are larger than those of this study. This reversal in the trend is only because the same value of $C_{AR}$ is used for any value of $\mu_{comp}$ greater or equal to 2 (see Table 4). The figure also shows that the results of this study for SCBFs are larger than the ASCE 7 NLRHA values in every case, except for $\mu_{comp}$ = 4.0 for the above reason.

In comparing the two ASCE 7 procedures for the SMF archetype, the trend is reversed from that observed for SCBFs, i.e., the NLRHA formula values are larger than the static formula values in all cases. The values of this study are larger than both the ASCE 7-22 static and NLRHA values, with the relative difference increasing with component ductility up to 2; for $\mu_{comp}$ = 4.0, the results of this study are slightly larger than the ASCE 7-22 static values but slightly smaller than the NLRHA ones.

In closing, it is interesting to note the way in which ASCE 7-22 estimates PFA (i.e., $\text{PFA} = 0.4S_{DS}(H_f / R_\mu)$) affects the comparison of the NSC seismic forces. As seen in Fig. 3-12, the PCA/PFA values of this study exceed those of ASCE 7-22 static. The

relative differences in $F_p / (I_p W_p)$ between these two methods decreases compared to the differences in PCA/PFA values because the ASCE 7-22 static procedure overestimates the PFA compared to the NLRHA. In contrast, the relative differences in $F_p / (I_p W_p)$ values between this study and ASCE 7-22 static increases in the case of SMFs because, for these archetypes, the ASCE 7-22 procedure underestimates the PFAs.

### 3.9. Conclusions

This study investigated the acceleration demands on nonlinear nonstructural components in Concentrically Braced Frame and Special Moment Frame buildings. Nonlinear response history analyses were conducted using floor motions obtained from a previous study by the authors. The study quantifies the effect of nonlinearity in both structural and structural components. The effect of location, ductility level and damping ratio of the component were evaluated.

The following highlight the main conclusions of the study:

- Even low ductility levels, such as 1.25 ,1.5 and 2.0, result in a considerable reduction in amplification factor PCA/PFA of the NSCs mounted on systems with periods tuned to the modal periods of the primary structure. Results indicate that increasing the NSC ductility level from 1.0 to 6.0 results in a larger reduction in PCA/PFA value at the resonant period of the flexible structures (SMFs) compared to the stiff structures (SCBFs).
- The 5%-damped NSC amplification factor (PCA/PFA) obtained in this study is compared to the recommended values by the ATC-120 and ASCE 7-22. As the ductility in the NSC increases, the difference between the PCA/PFA recommended by ATC-120 and ASCE 7-22 with the corresponding values computed in this study becomes smaller for the NSCs attached to the ground level. An equation for the NSC amplification factor in terms of the normalized period is proposed.
- Comparing the ratio of NSC amplification factor at the roof level for different ductility levels to the component amplification factor of an elastic component at the period of resonance shows a reduction in the ratio of the component amplification factor from the elastic component to $\mu_{comp}$ = 2.0. This reduction is

observed with a maximum value of 62% for the 8-RSA and minimum value of 33% for 12-TSX buildings.

- The results indicate that increasing the $\beta_{comp}$ from 1 to 7% reduces the PCA, especially when the period of the NSC approaches resonance with the modal periods of the buildings. An expression for the damping modification factor for NSC is proposed for $\mu_{comp}$ = 1.5 and 2.0.
- The values of the seismic design force as predicted in this study deviate from NLRHA results by less than 10%, while the deviation is larger than 50% for ATC-120 predictions.
- For NSCs mounted at grade plane, and for the ground motion suite considered, the values of the NSC seismic force computed in this study and those by the ASCE 7 static procedure are generally close to each other, while the ASCE 7 NLRHA procedure provides conservative values compared to the results of this study.
- For NSCs mounted at the roof level of the SCBF archetypes, the NSC seismic force value computed in this study is generally equal or larger than the ASCE 7-22 static values and always larger than the ASCE 7-22 NLRHA method. For NSCs mounted at the roof-level of SMFs, the seismic force values of this study are larger than the ASCE 7 static and NLRHA values. The relative difference between the values of this study and the two ASCE procedures grow larger with increasing NSC ductility.

### 3.10. References

Anajafi H, Medina RA. (2018). "Evaluation of ASCE 7 equations for designing acceleration-sensitive nonstructural components using data from instrumented buildings." *Earthquake Engineering and Structural Dynamics*, 47(4),1075-1094.

Anajafi H, Medina RA. (2019a). "Lessons Learned from Evaluating the Responses of Instrumented Buildings in the United States: The Effects of Supporting Building Characteristics on Floor Response Spectra." *Earthquake Spectra*, 35(1),159-191.

Anajafi H, Medina RA. (2019b). "Damping modification factor for elastic floor spectra." *Bulletin of Earthquake Engineering*, 17(11),6079-6108.

Anajafi H, Medina RA, Santini E. (2020). "Inelastic floor spectra for designing anchored acceleration-sensitive nonstructural components." *Bulletin of Earthquake Engineering*, 18(5),2115-2147.

Archila M, Ventura C, Figueira A, Yang Y. (2012). "Model Testing of Non-structural

Components for Seismic Risk Assessment." Conference Proceedings of the Society for Experimental Mechanics Series. In: *Topics on the Dynamics of Civil Structures.* (1), 239-246.

ASCE/SEI 41-13. (2014). "Seismic evaluation and retrofit of existing buildings." Reston, VA.

ASCE 7-16. (2016). "*Minimum Design Loads for Buildings and Other Structures*." Reston, VA.

ASCE 7-22. (2022). "*Minimum Design Loads and Associated Criteria for Buildings and Other Structures*." Reston, VA.

Astroza R, Pantoli E, Restrepo JI, Conte JP. (2015). "Experimental Evaluation of the Seismic Response of a Rooftop-Mounted Cooling Tower." *Earthquake Spectra*, 31(3),1567-1589.

Buccella N, Wiebe L, Konstantinidis D, & Steele T. (2021). "Demands on nonstructural components in buildings with controlled rocking braced frames." *Earthquake Engineering & Structural Dynamics*, 50(4), 1063-1082.

Chopra AK (2016). *Dynamics of Structures: Theory and Applications to Earthquake Engineering*. 5th ed. Pearson.

Cruz C, Miranda E. (2018). "First Mode Damping Ratios Inferred From the Seismic Response of Buildings." In: *Eleventh U.S. National Conference on Earthquake Engineering*. Los Angeles, California.

Derrick A. Watkins, Chiu L, Tara C. Hutchinson, Hoehler MS. (2009). "Survey and Characterization of Floor and Wall Mounted Mechanical and Electrical Equipment in Buildings." *Report No. SSRP–2009/11*. La Jolla, California.

FEMA P695. (2009). "*Quantification of Building Seismic Performance Factors*." Federal Emergency Management Agency. Washington, D. C.

Fathali S, Lizundia B. (2011). "Evaluation of current seismic design equations for nonstructural components in tall buildings using strong motion records." The *Structural Design of Tall and Special Buildings*. 20,30-46.

Filiatrault A, Uang C-M, Folz B, Christopoulos C, Gatto K. (2001). "Reconnaissance Report of the February 28 , 2001 Nisqually." *Report No. SSRP-2001/02*. La Jolla, California.

Filiatrault A, Christopoulos C, Stearns C. (2002). "Guidelines, Specifications, and Seismic Performance Characterization of Nonstructural Building Components and Equipment." PEER Report 2002/05. *Pacific Earthquake Engineering Research Center*, University of California, Berkeley.

Filiatrault A, Sullivan T. (2014). "Performance-based seismic design of nonstructural building components: The next frontier of earthquake engineering." *Earthquake Engineering and Engineering Vibration*. 13,17-46.

Kazantzi A, Vamvatsikos D, Miranda E. (2018). "Effect of Yielding on the Seismic Demands of Nonstructural Elements." In: *16th European Conference on Earthquake Engineering*. Thessaloniki, Greece.

Kazantzi A, Vamvatsikos D, Miranda E. (2020a). "The effect of damping on floor spectral accelerations as inferred from instrumented buildings." *Bulletin of Earthquake Engineering*, (18),2149-2164.

Kazantzi AK, Vamvatsikos D, Miranda E. (2020b). "Evaluation of Seismic Acceleration Demands on Building Nonstructural Elements." *Journal of Structural Engineering*, 146(7),1-15.

Kazantzi A, Miranda E, Vamvatsikos D. (2020c). "Strength-reduction factors for the

design of light nonstructural elements in buildings." *Earthquake Engineering and Structural Dynamics*, 49(13),1329-1343.

MATLAB. (2018). 9.7.0.1190202 (R2019b). Natick, Massachusetts: The MathWorks Inc.

McKenna F, Scott M. H, Fenves G. L. (2010). "Nonlinear finite-element analysis software architecture using object composition." *Journal of Computing in Civil Engineering*, 24(1),95-107.

Medina R, Krawinkler H. (2003). "Seismic Demands for Nondeteriorating Frame Structures and Their Dependence on Ground Motions." *John A. Blume Earthquake Engineering Center*. Report No. 144.

Medina RA, Sankaranarayanan R, Kingston KM. (2006). "Floor response spectra for light components mounted on regular moment-resisting frame structures." *Engineering Structures*, 28(14),1927-1940.

Miranda E. (1993). Site-dependent strength-reduction factors. Journal of Structural Engineering, 119(12), 3503-3519.

Miranda E, Kazantzi A, Vamvatsikos D. (2018a). "New approach to the design of acceleration-sensitive non-structural elements in buildings." In: *16th European Conference on Earthquake Engineering*. Thessaloniki, Greece.

Miranda E, Kazantzi, AK, Vamvatsikos D (2018b) Towards a new approach to design acceleration-sensitive non-structural components. In: Proceedings of the 11th national conference in earthquake engineering, Earthquake Engineering Research Institute

NIST. NIST GCR 10-917-8. (2010). "Evaluation of the FEMA P-695 Methodology for Quantification of Building Seismic Performance Factors."

NIST. NIST GCR 18-917-43. (2018). "Recommendations for Improved Seismic Performance of Nonstructural Components."

Ray-Chaudhuri S, Hutchinson TC. (2011). "Effect of nonlinearity of frame buildings on peak horizontal floor acceleration." *Journal of Earthquake Engineering*, 15(1),124-142.

Ray-Chaudhuri S, Villaverde R. (2008). "Effect of Building Nonlinearity on Seismic Response of Nonstructural Components: A Parametric Study." *Journal of Structural Engineering*, 134(4),661-670.

Salari N, Konstantinidis D, Mohsenzadeh V, Wiebe L. (2022). "Demands on Acceleration-sensitive Nonstructural Components in Special Concentrically Braced Frames and Special Moment Frames." *Engineering Structures*, 260, 114031.

Sankaranarayanan R, Medina R. (2007). "Acceleration response modification factors for nonstructural components attached to inelastic moment-resisting frame structures." *Earthquake Engineering and Structural Dynamics*, 36,2189-2210.

Singh A, Ang AHS. (1974). "Stochastic prediction of maximum seismic response of light secondary systems." *Nuclear Engineering and Design*, 29,218–30.

Sullivan TJ, Calvi PM, Nascimbene R. (2013). "Towards improved floor spectra estimates for seismic design." *Earthquake and Structures*, 4(1),109-132.

Taghavi S, Miranda E. (2006). "Probabilistic Seismic Assessment of Floor Acceleration Demands in Multi-Story Buildings." Technical Report 162. *The John A. Blume Earthquake Engineering Center*, Stanford University, Stanford, CA.

Tagahvi S, Miranda E. (2003). "Response Assessment of Nonstructural Building Elements." PEER Report 2003/05. *Pacific Earthquake Engineering Research*

*Center*, University of California, Berkeley.

Villaverde R. (1997). "Seismic Design of Secondary Structures: State of the Art." *Journal of Structural Enginering*, (123),1011-1019.

Villaverde, R. (2006). "Simple method to estimate the seismic nonlinear response of nonstructural components in buildings. *Engineering Structures*, 28(8), 1209-1221.

Viti G, Olivieri M, Travi S (1981). "Development of non-linear floor response spectra." *Nuclear Engineering and Design*, 64(1),33–38

Vukobratovic V, Fajfar P. (2012). "A Method for Direct Determination of Inelastic Floor Response Spectra." In: *15th World Conference on Earthquake Engineering*. Lisbon, Portugal.

Vukobratović V, Fajfar P (2017). "Code-oriented floor acceleration spectra for building structures." *Bulletin of Earthquake Engineering*, 15(7),3013–3026.

Wieser J, Pekcan G, Zaghi AE, Itani A, Maragakis M. (2013). "Floor Accelerations in Yielding Special Moment Resisting Frame Structures." *Earthquake Spectr*a. 29(3),987-1002.

# TABLES

***Table 3-1. Modal and resonant periods of the buildings with SCBF and SMF seismic force resisting systems (SFRS)***

| SFRS | Design configuration | $T_1$ (s) | $T_2$ (s) | $T_3$ (s) | $T_r$ (s) [mode number] |
|---|---|---|---|---|---|
| SCBF | 3-chevron | 0.53 | 0.21 | 0.13 | 0.21 [2] |
| | 3-TSX | 0.56 | 0.24 | 0.15 | 0.24 [2] |
| | 6-chevron | 0.92 | 0.32 | 0.26 | 0.32 [2] |
| | 6-TSX | 0.99 | 0.37 | 0.28 | 0.37 [2] |
| | 12-chevron | 1.83 | 0.60 | 0.39 | 0.32 [4] |
| | 12-TSX | 1.95 | 0.63 | 0.39 | 0.22 [5] |
| SMF | 4-ELF | 1.26 | 0.41 | 0.21 | 0.21 [3] |
| | 4-RSA | 1.56 | 0.49 | 0.25 | 0.25 [3] |
| | 8-RSA | 2.28 | 0.79 | 0.43 | 0.43 [3] |
| | 12-RSA | 3.11 | 1.08 | 0.61 | 0.30 [6] |
| | 20-RSA | 4.45 | 1.59 | 0.91 | 0.24 [8] |

***Table 3-2. Parameters used to calculate the maximum PCA based on Eq. (5) and as required per ASCE 7-22 (Horizontal lines in Figs. 3 and 4)***

| | | | | | $\mu_{comp}$ =1.5 | $\mu_{comp}$ =2.0 |
|---|---|---|---|---|---|---|
| Archetype | Height (m) | $T_a$ (s) | $H_f$ | $R_\mu$ | PCA (g) | PCA (g) |
| 3-chevron | 13.71 | 0.35 | 3.88 | 1.81 | 1.88 | 1.20 |
| 3-TSX | 13.71 | 0.35 | 3.88 | 1.81 | 1.88 | 1.20 |
| 6-chevron | 27.42 | 0.58 | 3.24 | 1.81 | 1.58 | 1.00 |
| 6-TSX | 27.42 | 0.58 | 3.24 | 1.81 | 1.58 | 1.00 |
| 12-chevron | 54.84 | 0.98 | 2.85 | 1.81 | 1.39 | 0.88 |
| 12-TSX | 54.84 | 0.98 | 2.85 | 1.81 | 1.39 | 0.88 |
| 4-ELF | 16.60 | 0.69 | 3.12 | 1.71 | 1.60 | 1.02 |
| 4-RSA | 16.60 | 0.69 | 3.12 | 1.71 | 1.60 | 1.02 |
| 8-RSA | 32.60 | 1.18 | 2.73 | 1.71 | 1.41 | 0.90 |
| 12-RSA | 48.60 | 1.62 | 2.56 | 1.71 | 1.32 | 0.84 |
| 20-RSA | 80.60 | 2.43 | 2.39 | 1.71 | 1.23 | 0.78 |

***Table 3-3. Regression coefficient values of the proposed DMF formula [Eq. (4)]***

| $\mu_{comp}$ | $\beta_{comp}$ | $\alpha$ | $\beta$ | $\gamma$ |
|---|---|---|---|---|
| 1.5 | 1% | -0.42 | 0.83 | 0.92 |
| | 2% | -0.23 | 0.47 | 0.96 |
| 2.0 | 1% | -0.16 | 0.32 | 1.0 |
| | 2% | -0.1 | 0.22 | 1.0 |

***Table 3-4. Component ductility categories (adapted from ASCE/SEI 7-22, Table C13.3-1)***

| Ductility Category | Component Ductility, $\mu_{comp}$ | PCA/PFA ($C_{AR}$) Supported At Grade Plane | PCA/PFA ($C_{AR}$) Supported Above Grade Plane |
|---|---|---|---|
| Elastic | 1 | 2.5 | 4.0 |
| Low | 1.25 | 2.0 | 2.8 |
| Moderate | 1.5 | 1.8 | 2.2 |
| High | ≥2.0 | 1.4 | 1.4 |

## FIGURES

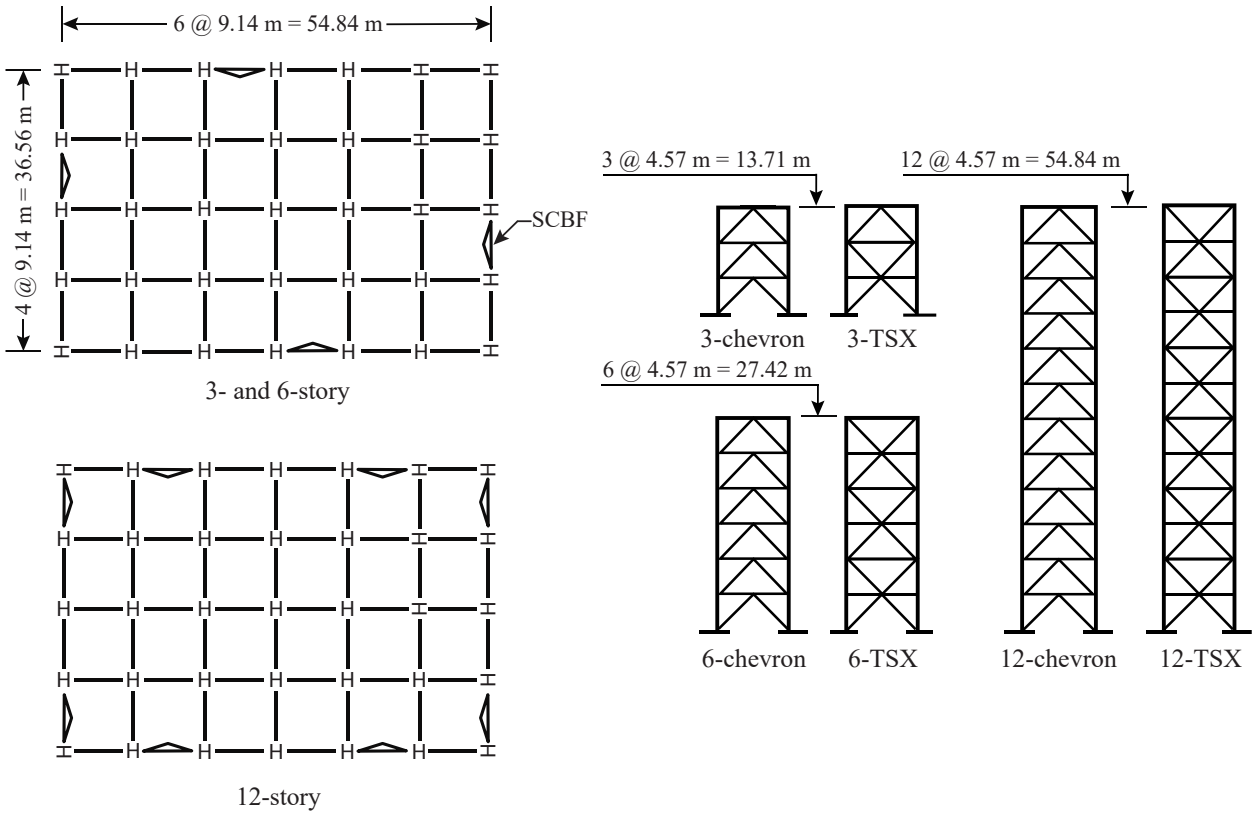


***Fig. 3-1. Plan and elevation views of the SCBF buildings***

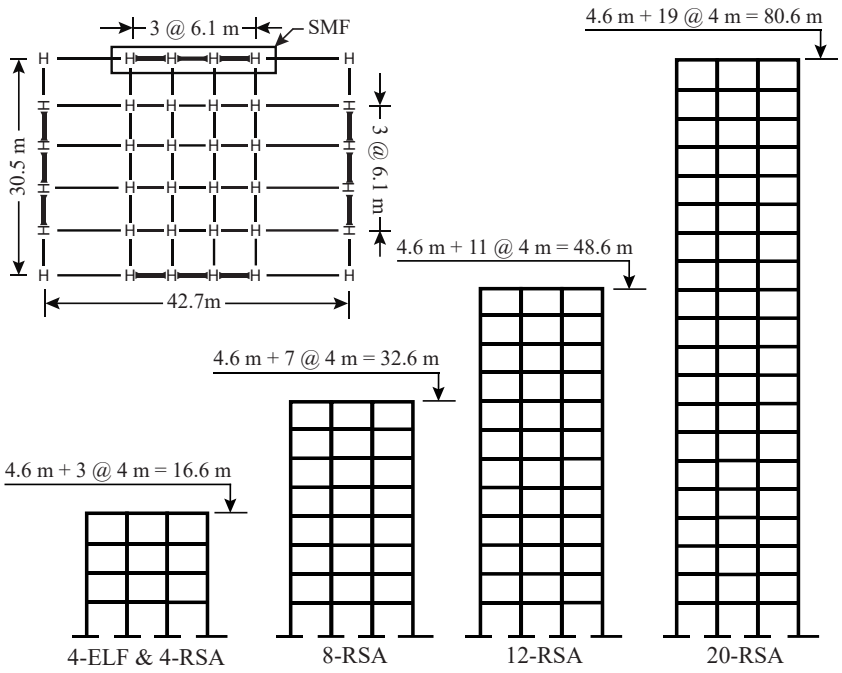


***Fig. 3-2. Plan and elevation views of the SMF buildings***

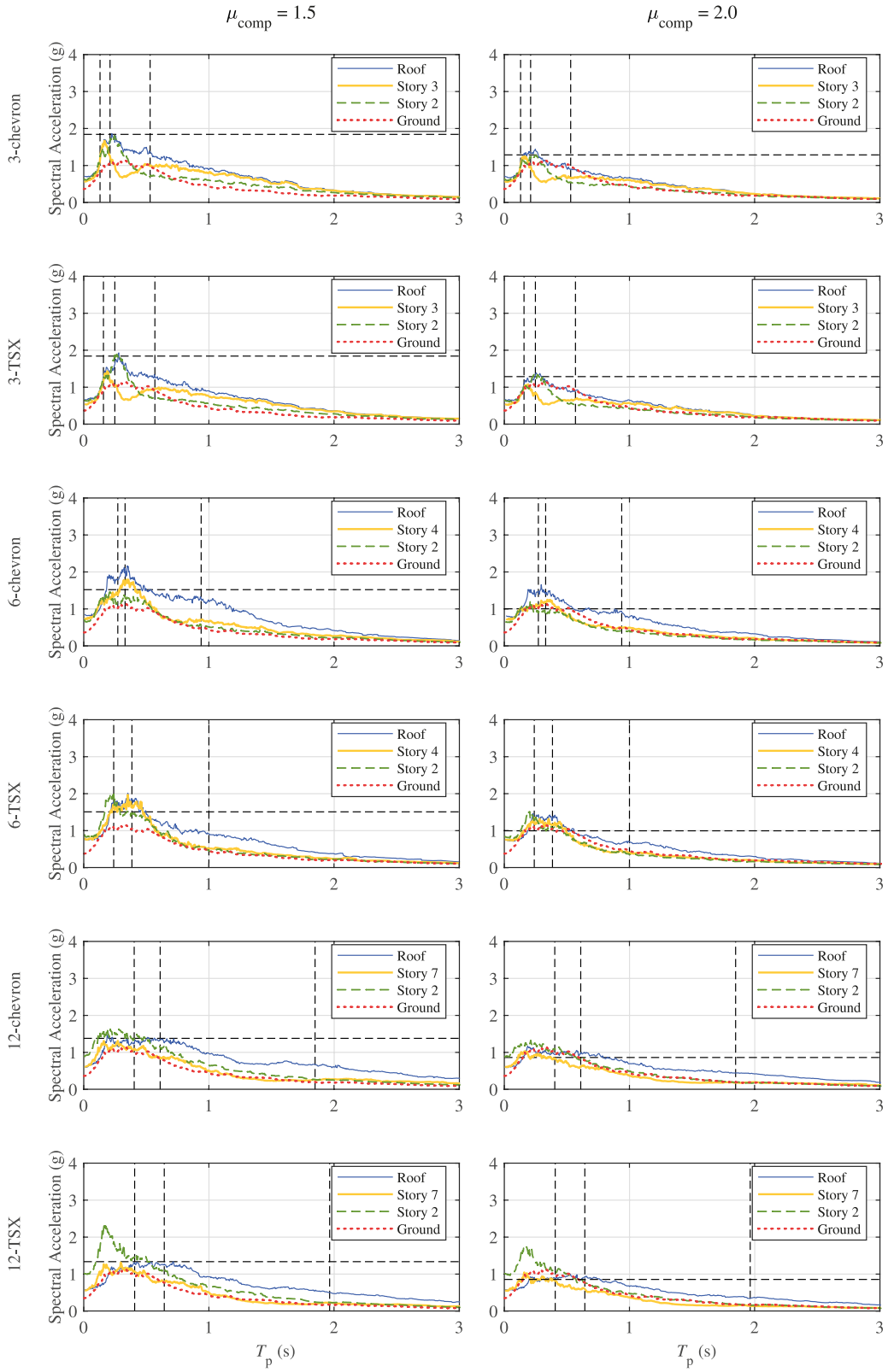


***Fig. 3-3. Constant-ductility floor response spectra for NSCs mounted on the SCBF structures (βcomp = 2%)***

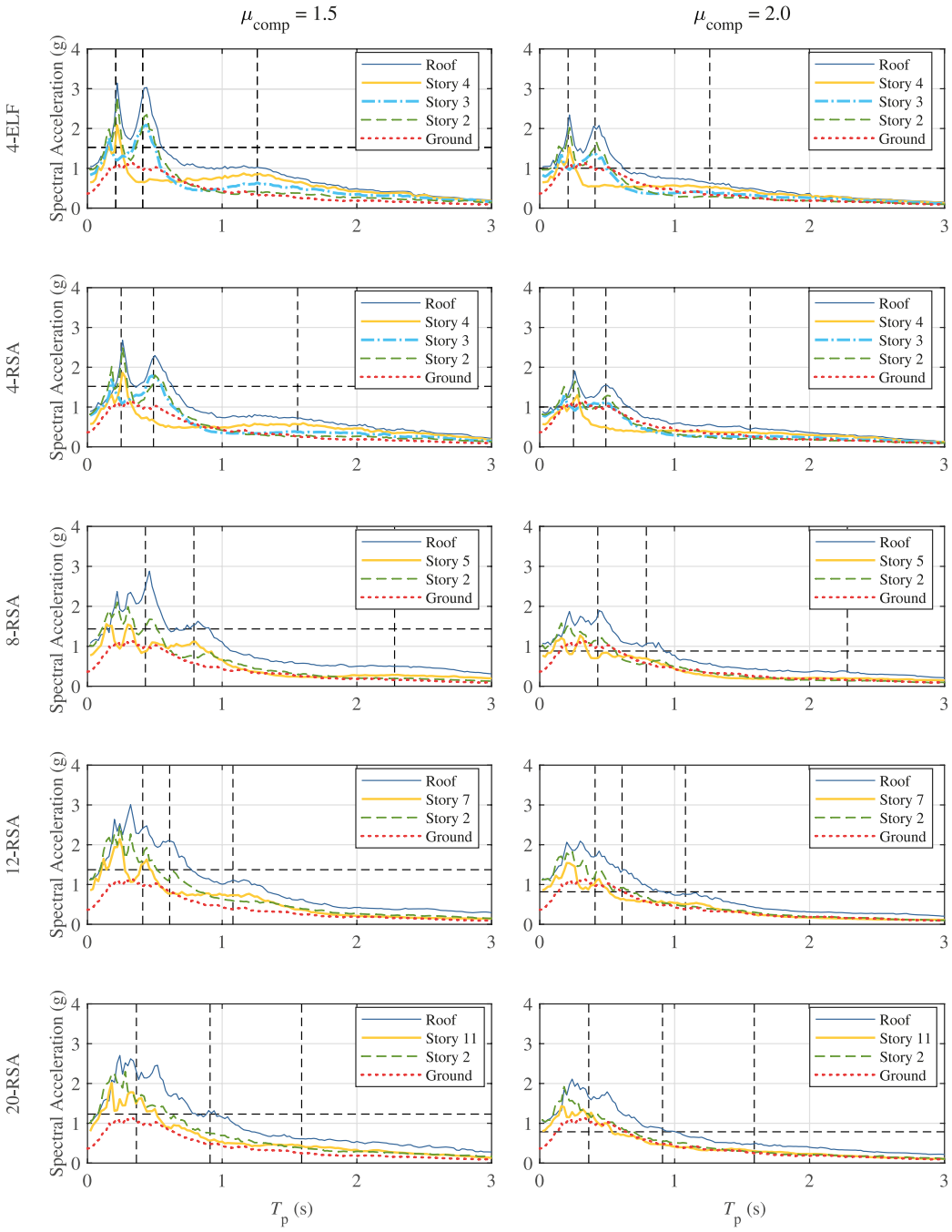


***Fig. 3-4. Constant-ductility floor response spectra for NSCs mounted on the SMF structures ($\beta_{comp}$ = 2%)***

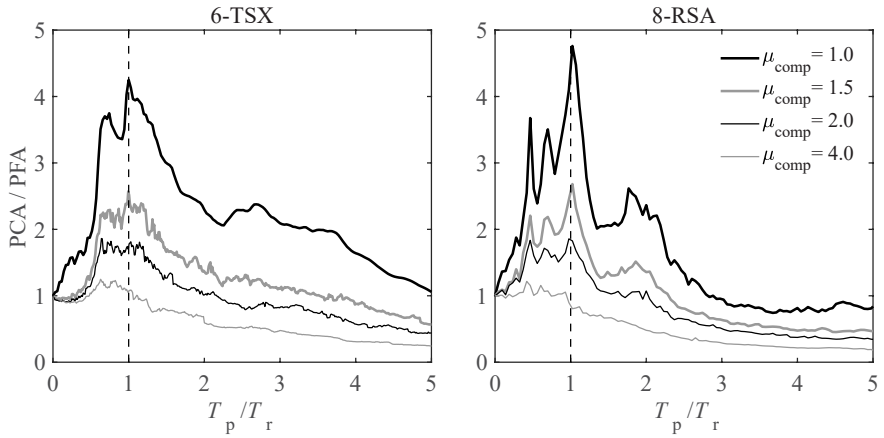


***Fig. 3-5. Component amplification factor spectra for NSCs mounted at the roof levels of 6-TSX and 8-RSA ($\beta_{comp}$ = 2%)***

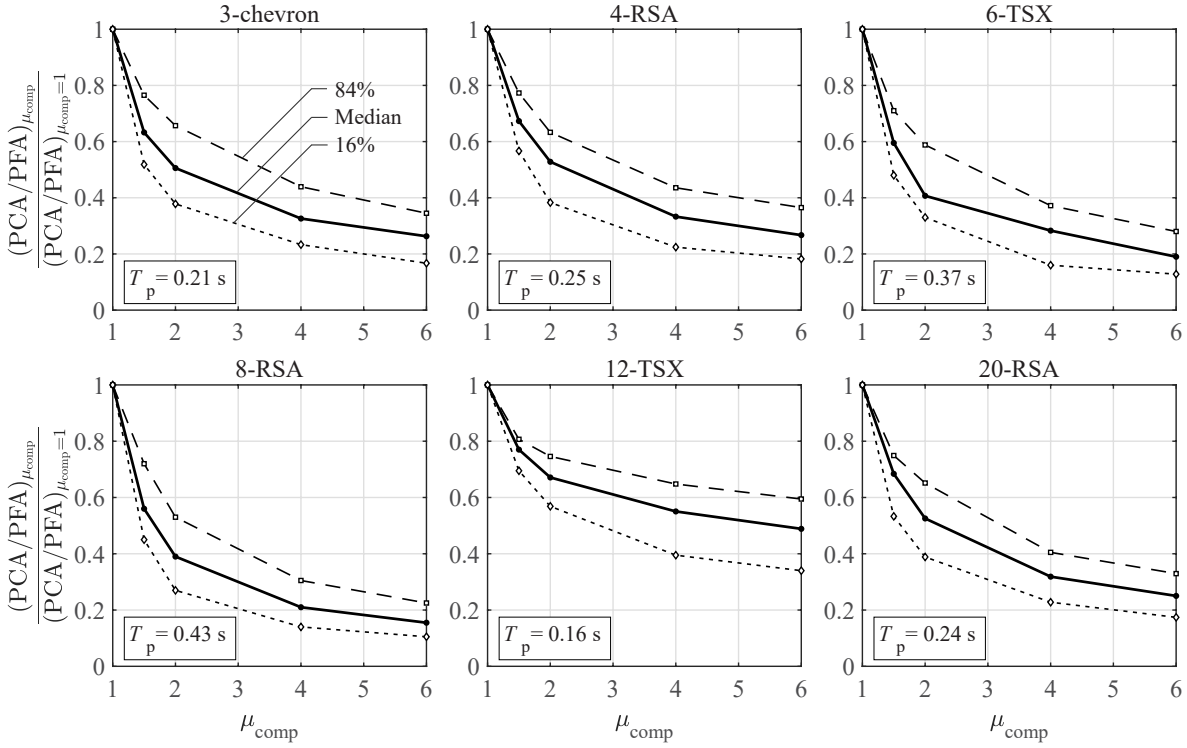


***Fig. 3-6. Component amplification factor as a function of target ductility for NSC mounted at the roof level ($\beta_{comp}$ = 2%)***

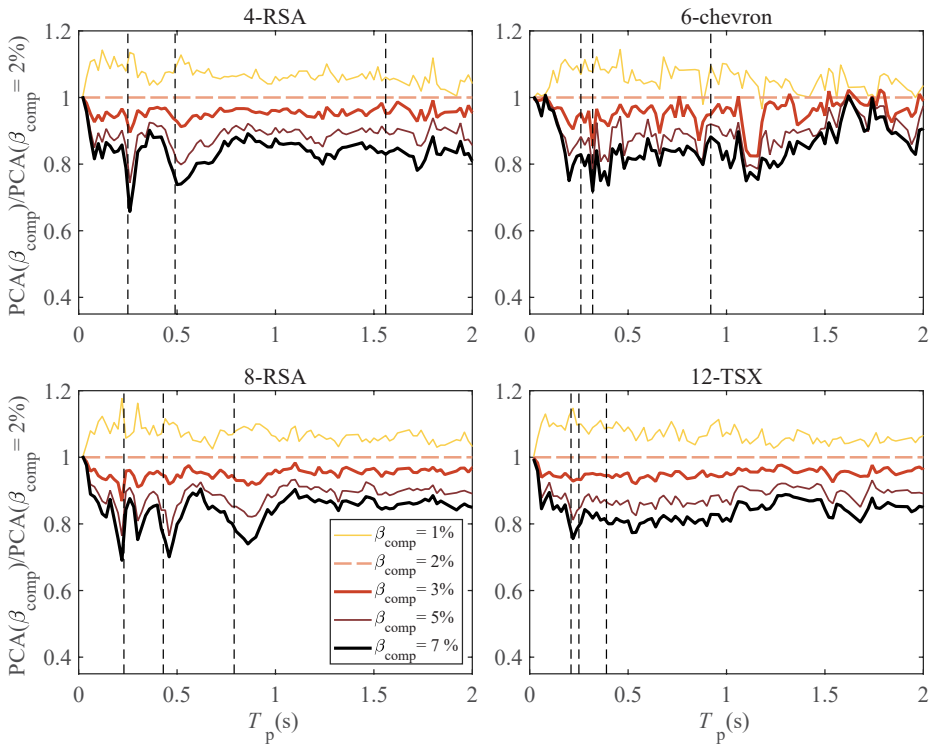


***Fig. 3-7. Effect of NSC damping ratio on roof-level response spectra ($\mu_{comp}$ = 1.5)***

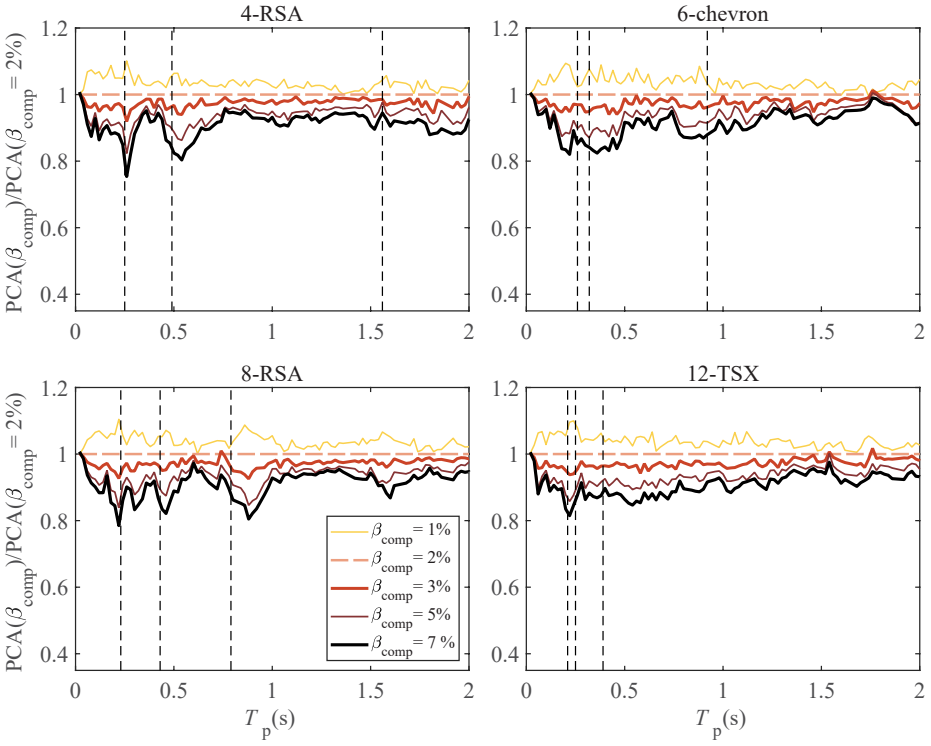


***Fig. 3-8. Effect of NSC damping ratio on roof-level response spectra ($\mu_{comp}$ = 2.0)***

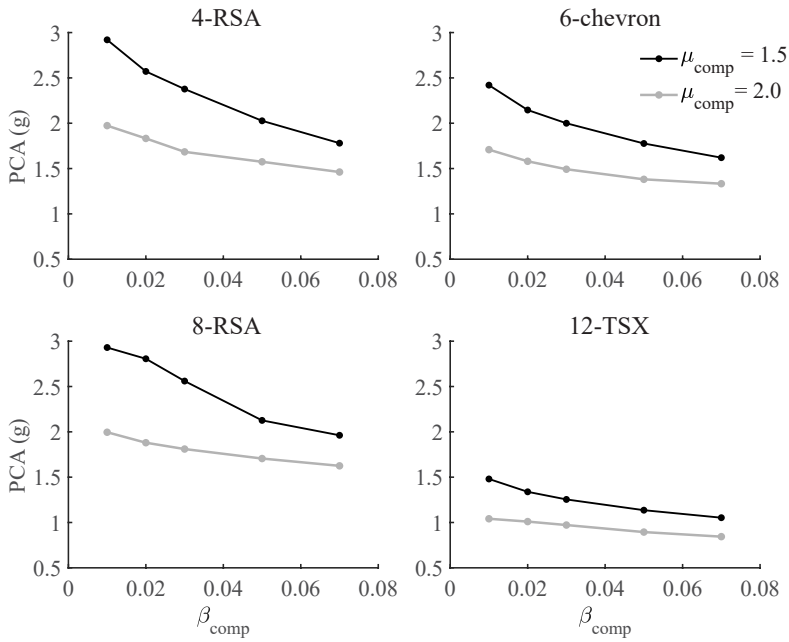


***Fig. 3-9. Effect of ductility level on PCA reduction from $\beta_{comp}$=1% to $\beta_{comp}$=7%***

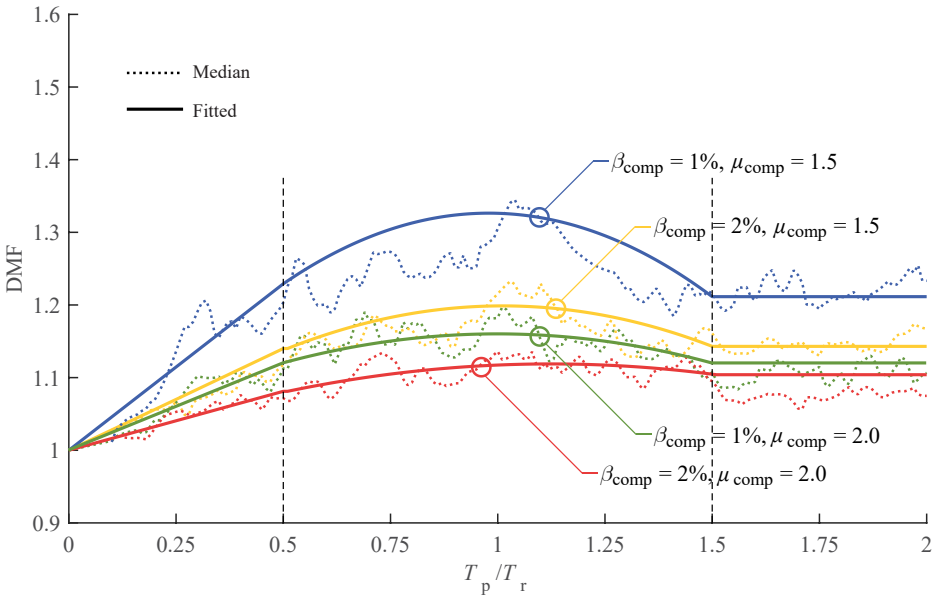


***Fig. 3-10. Damping modification factor (DMF) at the roof level***

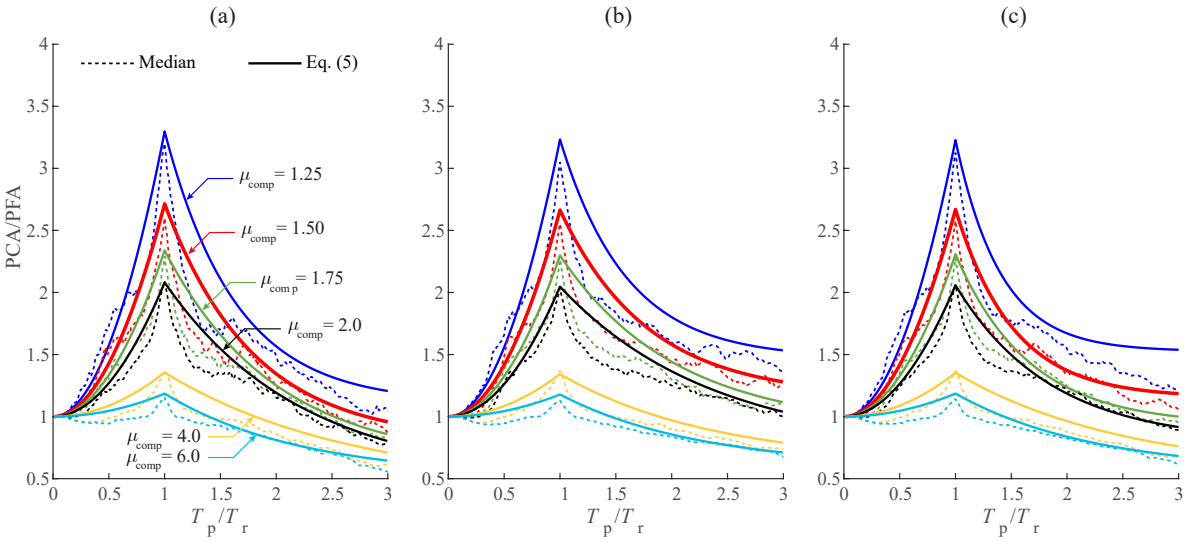


***Fig. 3-3. Median component amplification factor PCA/PFA ($\beta_{comp}$ = 5%) as a function of the ratio of component period to resonant structural period, $T_p / T_r$: (a) SCBF (b) SMF (c) Combined***

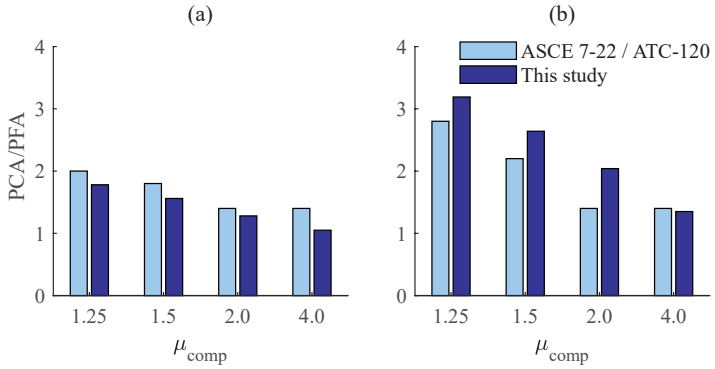


***Fig. 3-12. Comparison of the component amplification factor ($\beta_{comp}$ = 5%) for in-resonance NSCs in ASCE 7-22/ATC-120, and this study for NSC (a) supported at grade plane (b) supported above grade plane***

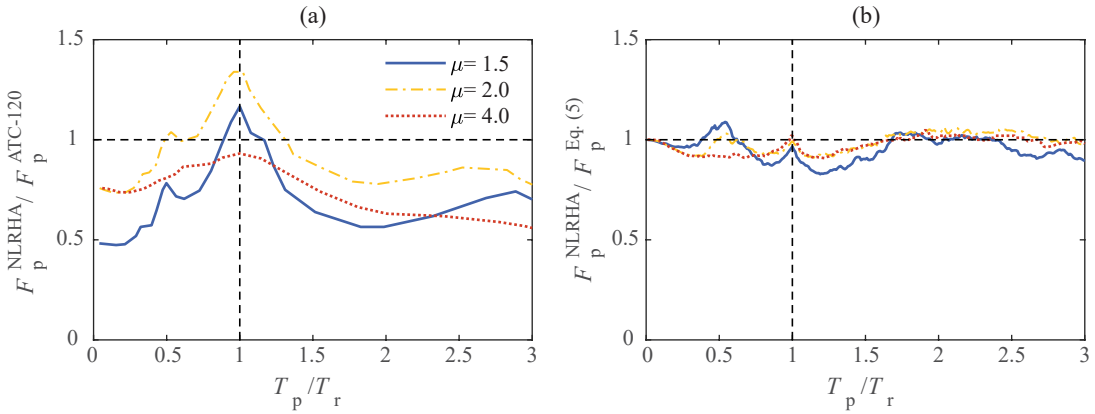


***Fig. 3-4. Deviation of seismic design force predicted by: (a) the ATC-120 formula [adapted from Figure 4-42 in (NIST 2018)], and (b) this study's prediction formula, from the seismic design force values computed by NLRHA***

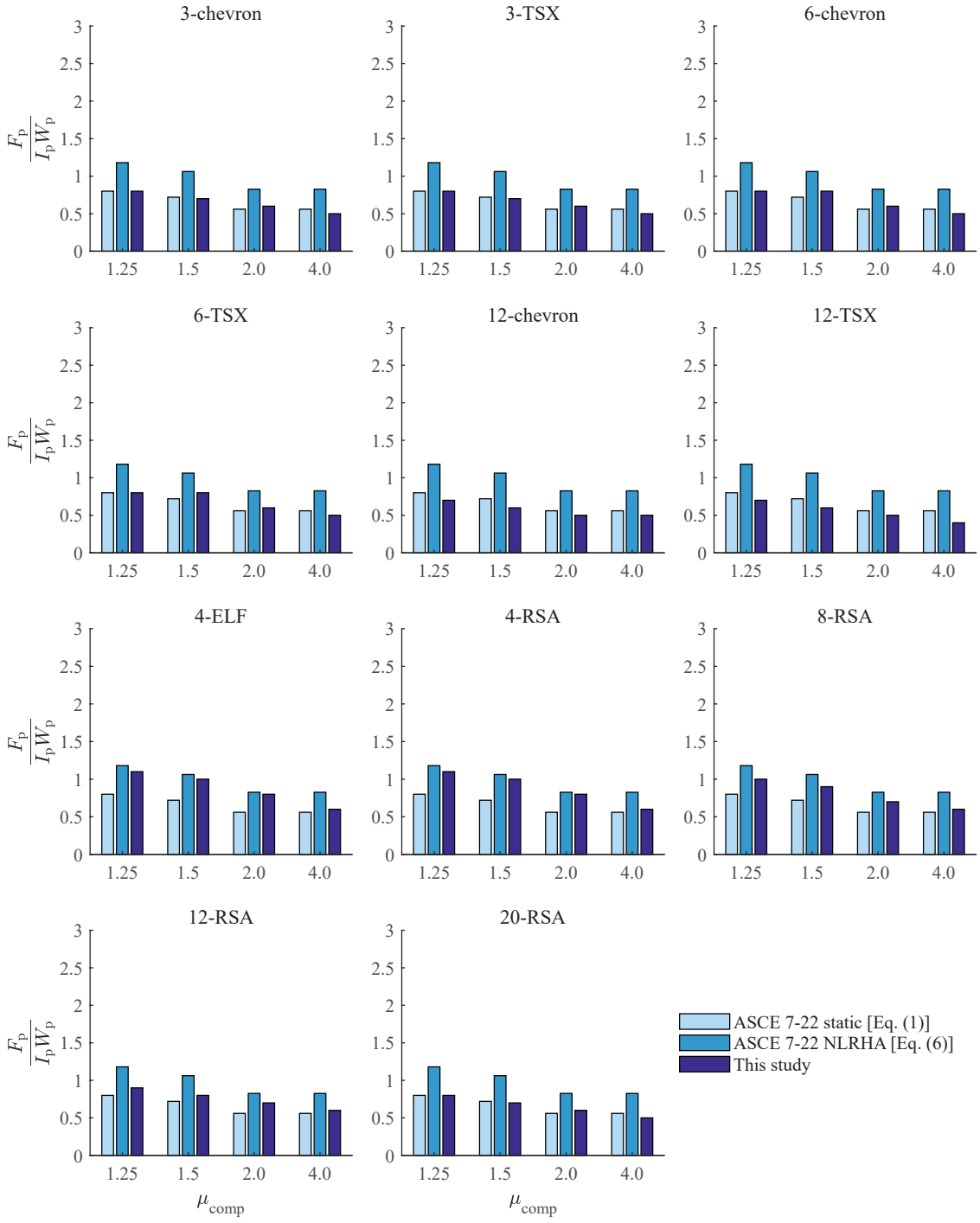


***Fig. 3-5. Comparison of the normalized design force for NSCs supported at grade plane***

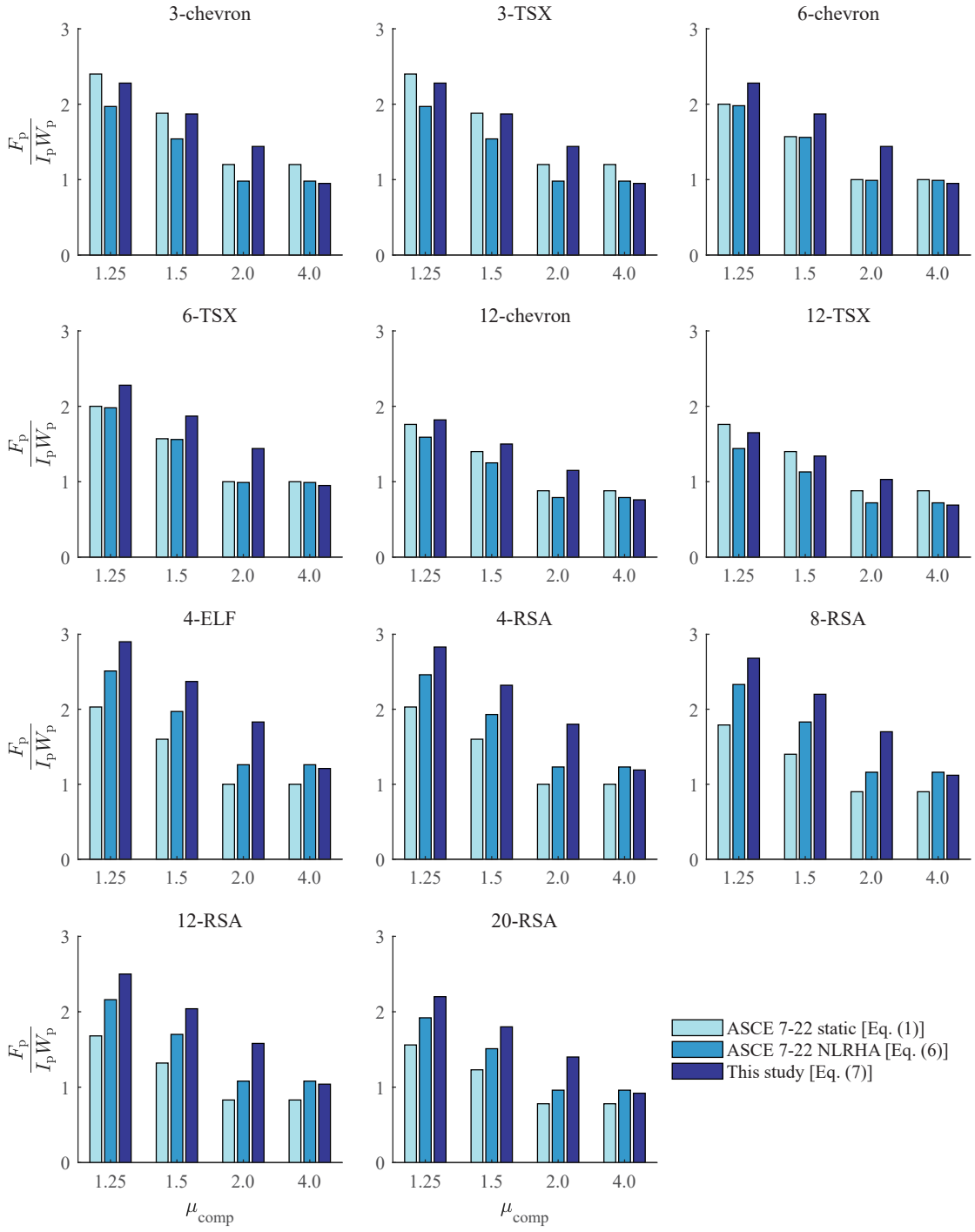


***Fig. 3-6. Comparison of the normalized design force for NSCs supported at the roof level***

# Chapter 4. Simplified Seismic Nonstructural Loss-Based Design of Special Concentric Braced Frames

Manuscript ready to submit to *Engineering Structures*

Neda Salari, Dimitrios Konstantinidis, Lydell Wiebe, Michael Tait

## Abstract

Performance-based design methods provide accurate procedures for evaluating buildings with respect to design goals. However, they are expensive in terms of time and computation cost. In this study, a simplified design procedure is proposed for special concentrically braced frames (SCBFs) based on probabilistic seismic repair cost and downtime losses. The proposed design method relies on spectra that present the relation between three parameters: static yielding base shear ($C_y$), maximum interstory drift (MID), and the mentioned seismic loss terms. These spectra allow selection of the appropriate design $C_y$ for reaching target MIDs or losses associated with acceptable exceedance probabilities. These parameters connect the practical design procedures to the complicated risk-based performance goals. After establishing the concepts of the proposed methodology, its development and application are illustrated for 3, 6, and 12-story SCBFs with chevron and two-story-X configurations. For this purpose, incremental dynamic analysis (IDA) and pushover are performed and the results are used within the FEMA P58's seismic loss estimation procedure. Focusing on nonstructural components and comparatively assessing the IDA and pushover-based results, only the latter is found to be consistent with the underlying static linear designs represented by the $C_y$ parameter. That is, the inability of the $C_y$ parameter to account for inelastic cyclic behavior prevents it from mutually predicting accurate IDA-derived losses. The design spectra are finally employed for the design of an example SCBF structure and the initial predictions of the losses are compared with actual values computed by analyzing the designed structure. A set of user-friendly MATLAB tools are also provided to enhance the implementation of the developed design procedure.

## Keywords

Performance-based seismic design, simplified design procedure, seismic nonstructural losses, special concentrically braced frame, maximum interstory drift, design base shear, seismic loss spectra

### 4.1. Introduction

Seismic loss is one of the key decision variables being addressed by the most recent performance evaluation guidelines such as FEMA P58 (FEMA-P58, 2018). Such evaluation guidelines form the building block of performance-based seismic design (PBSD) methods that aim to rationally balance the earthquake-induced losses with the construction costs. While the framework for quantifying seismic losses, such as repair cost, repair time, and casualties, is well addressed, its utilization in routine design entails considerable challenges. Addressing these challenges and enhancing the loss-based design process can be considered to allow broader utilization of the guidelines by the engineering community. This idea has been followed by several recent studies including (Katsanos & Vamvatsikos, 2017; Vamvatsikos & Aschheim, 2016; Vamvatsikos, Kazantzi, & Aschheim, 2016). According to the FEMA P58 guideline, a Monte-Carlo approach should be followed for combining the uncertainties associated with various aspects of the loss estimation procedure. Propagating these uncertainties to estimate the probability of exceeding various loss thresholds is the main focus of this guideline. However, as also mentioned in other guidelines such as FEMA-445 (FEMA, 2006), the complexity and costs of the loss evaluation procedures hinder performing adequate design iterations that are required for a safe yet economical design. It should be noted that the performance estimation procedure of FEMA P58 should be accompanied with design adjustments and evaluation repetitions until a satisfactory performance is achieved via a minimal construction cost. Performing these adjustments is not, however, straightforward due to the fact that under earthquake loading, there is a non-invertible relation between the seismic intensity and structural responses (Katsanos & Vamvatsikos, 2017). In other words, it is difficult to accurately predict the design adjustments required for satisfying the economic and performance criteria. Despite the recent advancements in optimization methods in automating design iterations (Fragiadakis & Papadrakakis, 2008; Franchin & Pinto, 2012; Lazar & Dolsek, 2012;

Mackie & Stojadinović, 2007; Steneker, Filiatrault, Wiebe, & Konstantinidis, 2020), orchestrating the optimization engines with the performance evaluation procedures is a sophisticated procedure which might be out of reach for engineering practice. Furthermore, the high costs associated with the evaluation iterations even limit the applications of automated optimization programs (Vamvatsikos & Aschheim, 2016).

Some of the potential approaches for solving these restrictions were addressed by early developers of PBSD, such as Cornell and Krawinkler (Cornell & Krawinkler, 2000). While some of these methods were used for the design of buildings and bridges whose importance justified the utilization of complex methods (Fragiadakis & Papadrakakis, 2008; Krawinkler, Zareian, Medina, & Ibarra, 2006; Mackie & Stojadinović, 2007), they were too costly for common design practitioners (Liao, 2010). Later attempts were thus made by other researchers to address these restrictions. A short review of these studies is presented in the next paragraphs.

Various attempts were made to simplify PBSD, even before a complete definition was provided for it. These include development of direct displacement-based design (DDBD) methods (Aschheim, 2002; Calvi & Kingsley, 1995; Kowalsky, Priestley, & Macrae, 1995; Moehle, 1992; Panagiotakos & Fardis, 1999). These methods quantified the structural performance in terms of the maximum earthquake-induced lateral displacement and relied on single degree of freedom (SDOF) systems that represented the characteristics of the main structure. The maximum elastic or inelastic displacement spectra of the SDOF system for different vibration periods were used for estimating the design yielding base shear coefficient, $C_y$, corresponding to a target maximum displacement demand under the considered ground motion level (Chopra & Goel, 2001). Although DDBD methods provided a rather direct address of the performance objective (displacement), they needed special considerations to address effects such as higher vibration modes and hysteretic response complexity of the structural systems (Vamvatsikos et al., 2016). These methods also lacked the ability to address more advanced performance objectives such as the structural or nonstructural damage level and the probabilistic seismic losses (Vafaee & Saffari, 2017).

Vamvatsikos and Aschheim (Vamvatsikos & Aschheim, 2016) introduced the concept of yield frequency spectra (YFS) that allowed designers to obtain the design $C_y$ through a more direct procedure compared to the DDBD approach. The YFS method

also included probabilistic aspects of the performance objective and targeted multiple ductility demand levels and the acceptable exceedance probabilities selected for them. Vamvatsikos and Aschheim (Vamvatsikos & Aschheim, 2016) demonstrated the application of the YFS method in the design of an 8-story reinforced concrete structure by targeting the Eurocode's allowable drift.

In addition to the practical aspects of various PBSD methodologies, selection of the target performance measures is also associated with important economic and social impacts. From the resilience point of view, the time and cost required to return the structures back to their operational stage after a damaging seismic event, need to be minimized. These concerns and the interests of stakeholders have led to the development of loss-based PBSD methods such as the FEMA P58 (FEMA-P58, 2018). This guideline currently addresses the casualties, the repair cost, and the repair time corresponding to damage to the structural and nonstructural components of buildings. This methodology relies on fragility data expressing the vulnerability of the building and its components to various structural response parameters. Many structural components have been tested for obtaining these data., In the case of drift-sensitive nonstructural components (NSCs), only judgment-based fragility data have been proposed by FEMA P58 (FEMA-P58, 2018). Some experimental and analytical studies have focused on acceleration-sensitive NSCs (Anajafi & Medina, 2018; Anajafi, Medina, & Santini-Bell, 2020; Filiatrault, Perrone, Merino, & Calvi, 2021; Salari, Konstantinidis, Mohsenzadeh, & Wiebe, 2022). But, their results are commonly presented as the acceleration spectra predicting the maximum seismic force imposed on NSCs during an earthquake. These data may be useful for the prescriptive force-based design of NSCs, as addressed in guidelines such as ASCE 7-22 (ASCE-7, 2022). However, they do not predict the NSC damage as it is done by the fragility data required in the PBSD procedure. On the other hand, NSCs form 50-90% of the value of typical buildings (Miranda & Taghavi, 2003) depending on the occupancy type and the equipment technology. Thus, the development of the fragility data required for NSC loss estimation forms major concerns of the current stage of PBSD development. While providing these missing data are beyond the scope of the current study, improving the functionality of NSC-targeted PBSD methods is to be addressed in this article. This is pursued by proposing a simplified design approach that relies on the prediction of loss

probability curves for NSCs mounted on special concentrically braced frames (SCBFs). The selection of the SCBF structural system is aligned with the previous studies by the authors (Salari et al., 2022) on the seismic demands of NSCs mounted on these structures.

The PBSD methodology proposed in the current study follows DDBD and YFS methods to represent the lateral strength using static yielding base shear coefficient ($C_y$=$V_y$/$W$, where $V_y$ and $W$ are the yielding base shear and the seismic weight of the building, respectively). In addition to the yield strength, nonlinear dynamic characteristics of a designed structure, and the associated record-to-record uncertainties are also represented. For this purpose, the mean annual frequency of exceedance (MAFE) for the nonlinear maximum interstory drift (MID) response of the structures is used. This was also done by Vamvatsikos and Aschheim (Vamvatsikos & Aschheim, 2016) who developed the MAEF spectra for various MID levels and a set of selected $C_y$ values. The current study aims to augment this approach by introducing the seismic losses associated with this characteristic information.

In this study, a simplified NSC loss-based design procedure is proposed and implemented for SCBFs with chevron and two-story-X (TSX) braces. This procedure relies on developed spectra that plot the MAFE for various levels of NSC losses and MID demands, denoted by $\lambda_L$ and $\lambda_{MID}$, respectively. Considering the NSC losses is the main improvement provided by this procedure in the method used by Vamvatsikos and Aschheim (Vamvatsikos & Aschheim, 2016). In general, the developed design spectra need to be applicable for structures with various site locations, performance groups, and geometries. However, providing a complete answer to this requirement is beyond the scope of this article and is only pursued by considering 3-12-story office buildings employing SCBFs. In addition, among the wide range of NSCs commonly used in office buildings, only those included in FEMA P58 (FEMA-P58, 2018) guideline are considered and divided into "seismic" and "non-seismic" categories, with respect to their response to the lateral drift. The plan area and site seismicity level parameters are also considered as design variables. In addition, for design map development, the two alternative demand estimation procedures proposed by FEMA P58 (FEMA-P58, 2018), which are based on static pushover (SPO) and IDA methods, are comparatively studied. The final part of the study provides an example application of the developed design

tools. Using this design application, the design-stage loss predictions are evaluated against the accurate final computations to assess the success of the design procedure in reaching the target performance.

### 4.2. Methodology

As mentioned in the previous section, this study focuses on proposing a simplified NSC-loss based PBSD procedure. Concentrating on the NSCs and neglecting the structural losses are based on the following reasons:

I. The costs associated with the nonstructural assets are of a more dominant order for office and healthcare buildings due to the presence of technological facilities. Even for residential buildings, the NSC costs can form a comparable share of the total cost (Miranda & Taghavi, 2003).

II. As described later, the loss values have a linear relation with the plan area and the number of NSCs contained in. This relation allows interpolation of the loss spectra of building plans with any arbitrary areas using the spectra obtained for a given plan area. On the other hand, the number and sizes of the structural members have a much more complicated relationship with the building geometry. Thus, the inclusion of the structural members would lead to a loss-area relation that could not be properly assumed or predicted for the design of arbitrary geometries.

III. The design spectra have to be used for selecting the structural members that are expected to differ from those assumed during the development procedure of the spectra. This is in contrary to the NSCs which are not expected to change during the design procedure. Thus, including the losses associated with the structural members could definitely deviate the actual losses from those estimated in the developed design spectra. Remarkable differences between the assumed sections and those obtained in the design could also restrict the applicability of the developed spectra.

The design methodology presented here considers the MID, $C_{y,}$ and NSC-loss parameters simultaneously. The NSC losses are presented in terms of repair cost and repair time parameters. The design spectra are developed for six chevron and TSX

SCBF structures with 3, 6, and 12 stories. These spectra are intended to be used for interpolating the NSC losses of a structure designed for specific $C_y$ and MID values. The design procedure employing the developed spectra is illustrated in Fig. 4-1 using schematic loss spectra. Further interpolations may also be required for an actual design problem that are not illustrated in this figure.

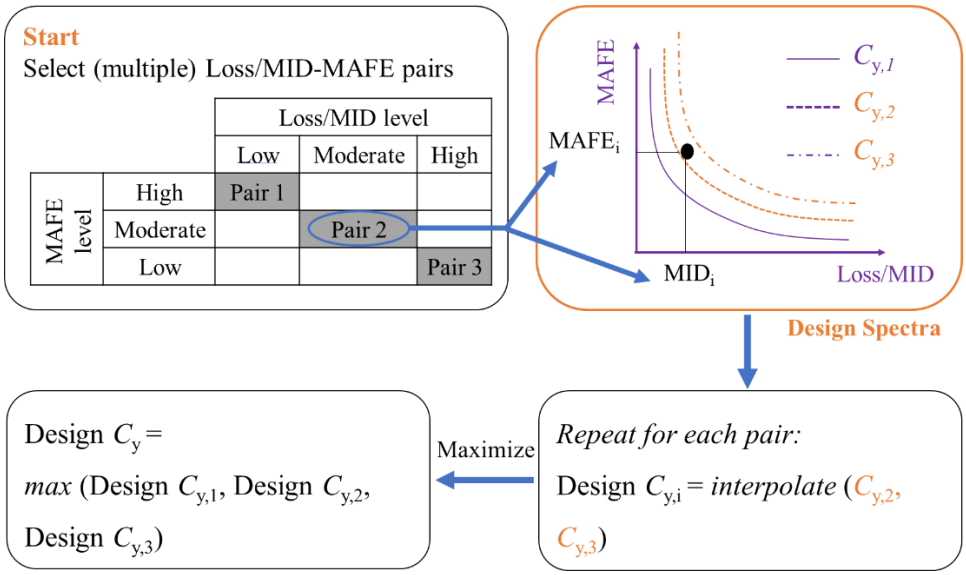


***Fig. 4-1.The proposed flowchart for simplified design based on Loss/MID-MAFE design spectra.***

In addition to the design simplifying application, a comprehensive evaluation of the alternative SPO- and IDA-based demand estimation approaches proposed by FEMA P58 (FEMA-P58, 2018) is also targeted. The flowcharts of the IDA- and SPO-based procedures used for developing the design spectra are graphically illustrated in Fig. 4-2 and Fig. 4-3, respectively. According to Fig. 4-2, the loss estimation procedure starts by taking various $C_y$ values and proportioning the SCBF structures for the strength and drift requirements of the current American design standards (AISC, 2016; ASCE-7, 2022). The second step includes inelastic modeling of the designed structures and is the only step affected by the structural system under consideration. The procedure then performs IDA for reaching two goals: extracting structural demands at different intensity levels and establishing the collapse fragility curve. Developing the design spectra considered in this paper involves extracting the MAFE of MID levels, which is also achieved through performing the IDA. The collapse fragility, estimated demands, seismic hazard curve (SHC), and building occupancy data are provided to the PACT program developed by FEMA P58 (FEMA-P58, 2018) to estimate the seismic losses.

In the simplified SPO-based approach (Fig. 4-3), demand approximation uses empirical methods that are presented in Fig. 4-2. One approximation is provided by the SPO2IDA tool developed by (Vamvatsikos & Cornell, 2005) and suggested by FEMA P58 (FEMA-P58, 2018) to estimate the median MID-$S_a$ curve from a normalized inelastic SPO curve. The median collapse $S_a$ extracted from this curve is combined with suggested dispersion values to approximate the collapse fragility. An elastic SPO is finally performed to extract drifts and displacements at equivalent base shear levels and adjust them to obtain peak story drift ratio (PSDR) and peak floor acceleration (PFA) demands.

The selected structures are only intended to represent typical building layouts and plan areas. As will be described later, the plan area of these buildings will be used for interpolating the losses with respect to the designed building's area. The selected layouts are those previously used by NIST GCR 10-917-8 (NIST, 2010) and (Salari et al., 2022) (Fig. 4-4) and consist of a 2005 $m^2$ office area in each story. The buildings are subjected to the gravity loads formerly used by (NIST, 2010) and employ two perimeter SCBF frames to withstand the lateral loads acting on the 3- and 6-story structures in each direction. For the 12-story structures, these are increased to four frames to enhance the lateral stiffness and help in controlling the design lateral drifts. The nonlinear modeling procedure described in a previous study by the authors (Salari et al., 2022) is employed again here. The range of $C_y$ values considered for the design of various structures is listed in Table 4-1. These values represent the range of base shear coefficients (DBSC) commonly used in practical designs following ASCE 7-22 (ASCE-7, 2022) for various seismic design categories and soil types (ASCE-7, 2022). The DBSC required by ASCE 7 is considered as a minimum requirement in the design of the subject buildings. Therefore, the proposed $C_y$ values (Table 4-1) also represent DBSCs that are higher than the ASCE 7 prescription. Overall, 36 structures are designed, nonlinearly modeled, and subjected to the SPO and IDA procedures.

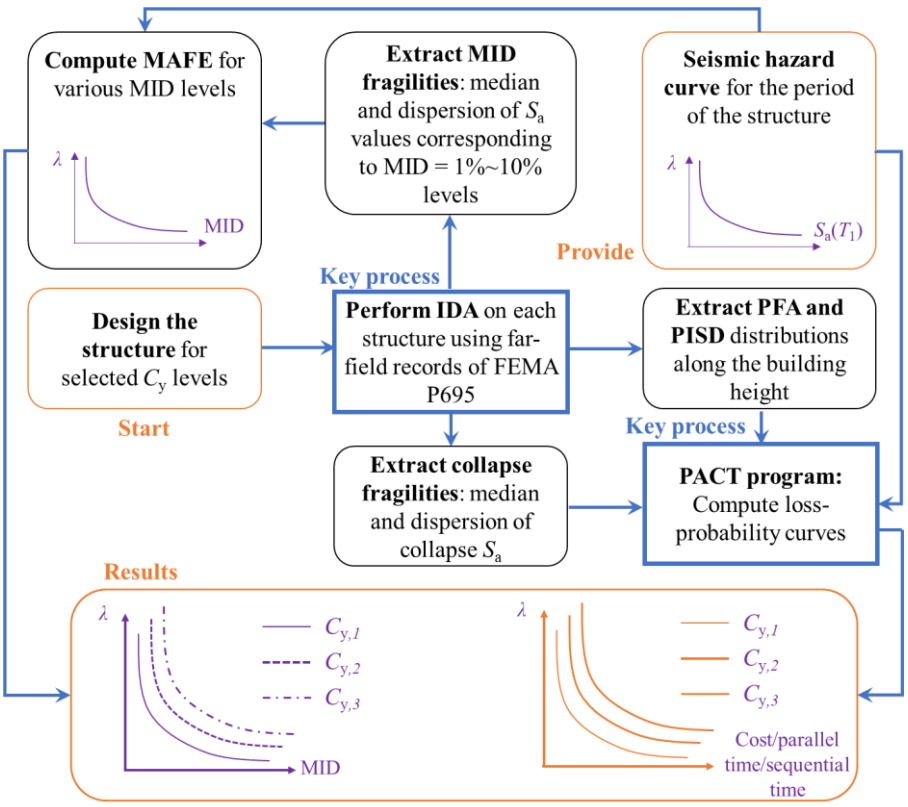


***Fig. 4-2. The IDA-based procedure used for generating the design spectra.***

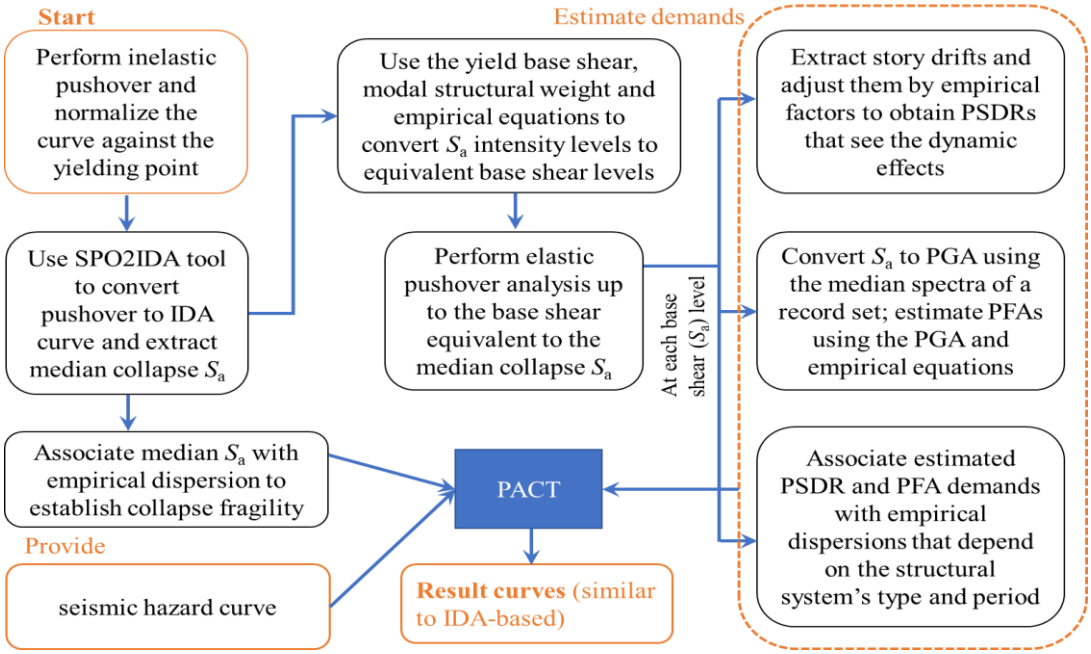


***Fig. 4-3. The simplified pushover-based approach used for extracting structural demand distributions.***

***Table 4-1. $C_y$ values regarded for developing the design maps.***

| Num. of stories | Selected $C_y$ values |
|---|---|
| 3, 6 | 0.10, 0.15, 0.20, 0.25, 0.30, 0.35 |
| 12 | 0.03, 0.05, 0.07, 0.10, 0.15, 0.20 |

For performing IDA, the two horizontal components of the 22 ground motion records proposed by FEMA P695 (FEMA-P695, 2009) are scaled to multiple intensities expressed by the $S_a(T_1, 5\%)$ parameter, shortly denoted as $S_a$ in this study. $S_a$ scaling ends up with collapse identification following the FEMA P695 criterion according to which an 80% softening in the $S_a$-MID curve and exceeding the 10% MID level are considered simultaneously.

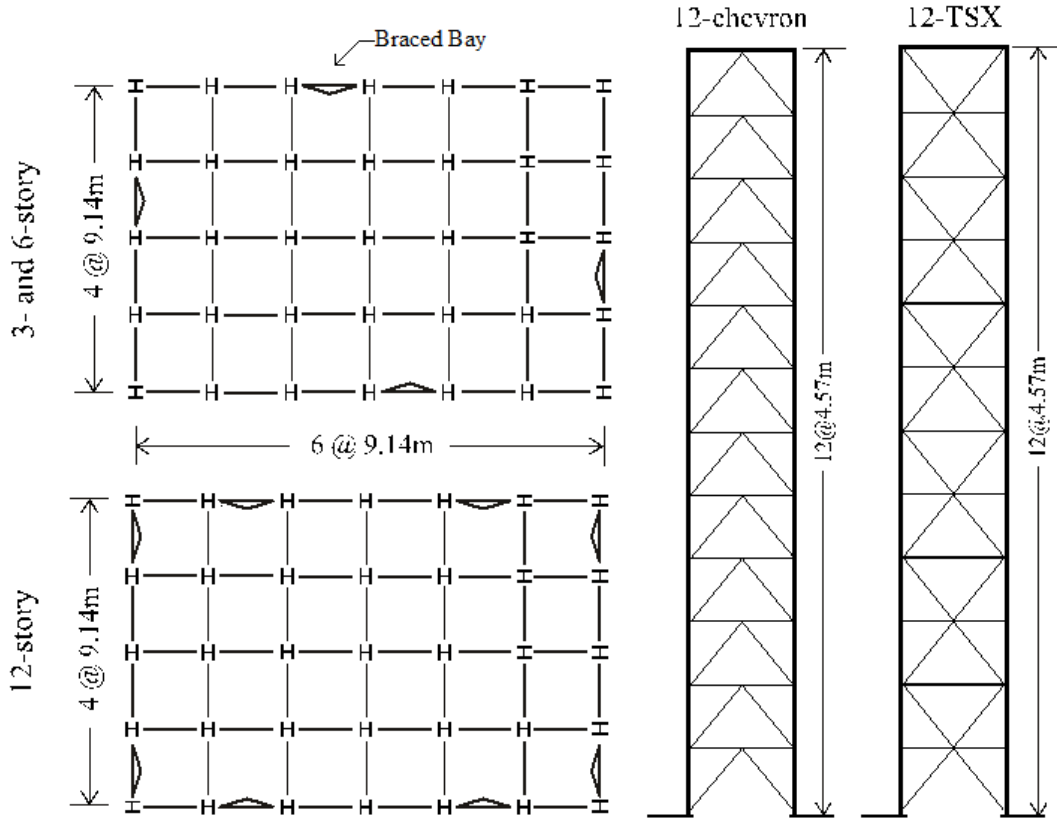


***Fig. 4-4. Plan layout of the SCBF archetypes along with the elevation layout of the 12-story SCBFs (Salari et al., 2022).***

While the IDA-based approach is characterized with the accuracy provided by the performed nonlinear dynamic analyses, the SPO-based procedure is featured with a considerable level of simplicity. In addition to the faster implementation, the SPO-based method is completely consistent with the $C_y$ parameter used for representing the

structural strength level. This consistency is due to the common reliance of the SPO-based and ASCE 7-22 (ASCE-7, 2022) methods on the equivalent lateral force (ELF) procedure. Unlike the SPO-based demands that are directly extracted at the given $C_y$ levels, the IDA-based demands are not directly related to the selected $C_y$ values. That is, elevating the strength level by using a larger $C_y$ does not necessarily lead to increased ductility and energy dissipation capacity (EDC), which are the parameters that directly affect the demands estimated by the IDA. These differences and features are highlighted in this research by incorporating both methods and evaluating the obtained results. In general, the selection of the loss estimation procedure should account for implications made by the design method. Although relying on the ELF procedure restricts the employment of the accurate IDA-based method (as will be shown later), it is advantageous in terms of simplicity and relevance to the current design practice. To highlight this advantage, we should emphasize that the audience of the proposed simplified PBSD method is the engineering community involved in routine design problems. The final goal is to enhance the seismic resilience of society by supporting the utilization of loss measures in common design problems.

The developed spectra should account for the variability in the structural response values, the types and quantities of NSCs (depending on the plan area, occupancy type, and the number of stories,) and the SHC. To account for structural response variability, the story number is selected to vary in the 3-12 range, the brace configuration is considered to be either chevron or TSX, and the strength level is reflected using six different $C_y$ values. The quantity of the NSCs is assumed to be proportional to the plan area. Considering that the computed losses have a linear relation with NSCs quantity, the loss spectra can be scaled to match the plan area of the designed building, based on the prototype area which is 2005 $m^2$. The variation in the NSC types utilized within a building is only addressed in terms of the accommodation of the installation methods to seismic effects. Accordingly, two "seismic" (unaffected by the seismic response of the adjacent structural members) and "non-seismic" categories are considered for components based on the FEMA P58's NSC database (FEMA-P58, 2018). Regarding NSCs with varying material quality levels, the variations are neglected and the components with moderate quality levels are selected (see Appendix I). Due to the time limitations of the study, the design spectra provided here are not

considered to provide a complete answer to the PBSD requirements. As previously mentioned, extending the design spectra to consider the variations in the performance groups requires a repetition of the analyses performed in this study. Although the sample design maps provided in this paper (see Appendix II) are based on a specific hazard curve, a set of companion MATLAB® (MathWorks, 2022) tools and data files are provided that allow using alternative hazard files for regenerating the design spectra. These codes only repeat the final step of the loss estimation procedure described in Fig. 4-2 and Fig. 4-3 flowcharts. This step integrates the provided $S_a$-conditioned loss fragility data with the new SHC and regenerates the design spectra.

The PACT program uses the cost and the time corresponding to total building replacement (TBR) when the random process identifies a collapse occurrence according to the collapse fragility and the intensity level. In order to maintain the continuity of the loss curve, in the non-collapse scenario, the losses associated with the most severe damage states should equal the BTR-based losses. This means that, just before the intensity reaches a level that leads to collapse occurrence, the building is expected to undergo an almost complete loss. To assure this continuity, the standard TBR costs and times suggested by FEMA P58 (FEMA-P58, 2018) by including the structural losses are not used here. Due to the neglection of the structural losses, this study estimates TBR as the sum of the most severe damage states defined in the NSC fragilities.

### 4.3. Initial design evaluations

The numerical models developed for the designed structures have to be validated before subjecting them to the later steps of the procedure. For this purpose, the SPO and median IDA curves are comparatively studied. These evaluations are also expected to help later interpretation of the findings that stem from the characteristics of the SPO and IDA curves. SPO analyses are carried out by applying displacement-controlled static analyses under ASCE 7-22's (ASCE-7, 2022) lateral load pattern. The obtained SPO curves are illustrated in Fig. 4-5 for various SCBF configurations and building heights. The curves show a gradual increase in the structures' strength when they are proportioned for larger $C_y$ values. It is however seen that the first significant yielding occurs at an almost equal global drift for all the buildings. This has led to an increase in the lateral stiffness as the strength level has been escalated using $C_y$. While not

quantitatively shown, the overstrength factor (the ratio of the yielding $C_y$ to the design $C_y$) is around 1.3, 1.7, and 2.5 for the 3-,6- and 10-story SCBFs, respectively. The higher factors obtained for the taller structures are caused by the allowable drift limits controlling their design.

The sequential buckling of the braces located in different stories has led to fluctuations in the base shear of the curves' region following the yield point. These fluctuations can result in a premature collapse (early and rapid decline of the post-yield branch) if the beam members do not provide adequate lateral support for the buckling braces. Such support and the lateral stiffness of the story columns allow the survival of the story from a local collapse mode and allow other story braces to complete the yielding sequence by entering into the inelastic response range. Therefore, in addition to proportioning the structures against the intended $C_y$ level, the practical rule of thumbs controlling the size of members as we traverse toward the upper stories should be considered. Although not required by the design codes, these practical rules are empirically applied by the designers to prevent drift concentration in one or a few stories and are particularly important for tall structures.

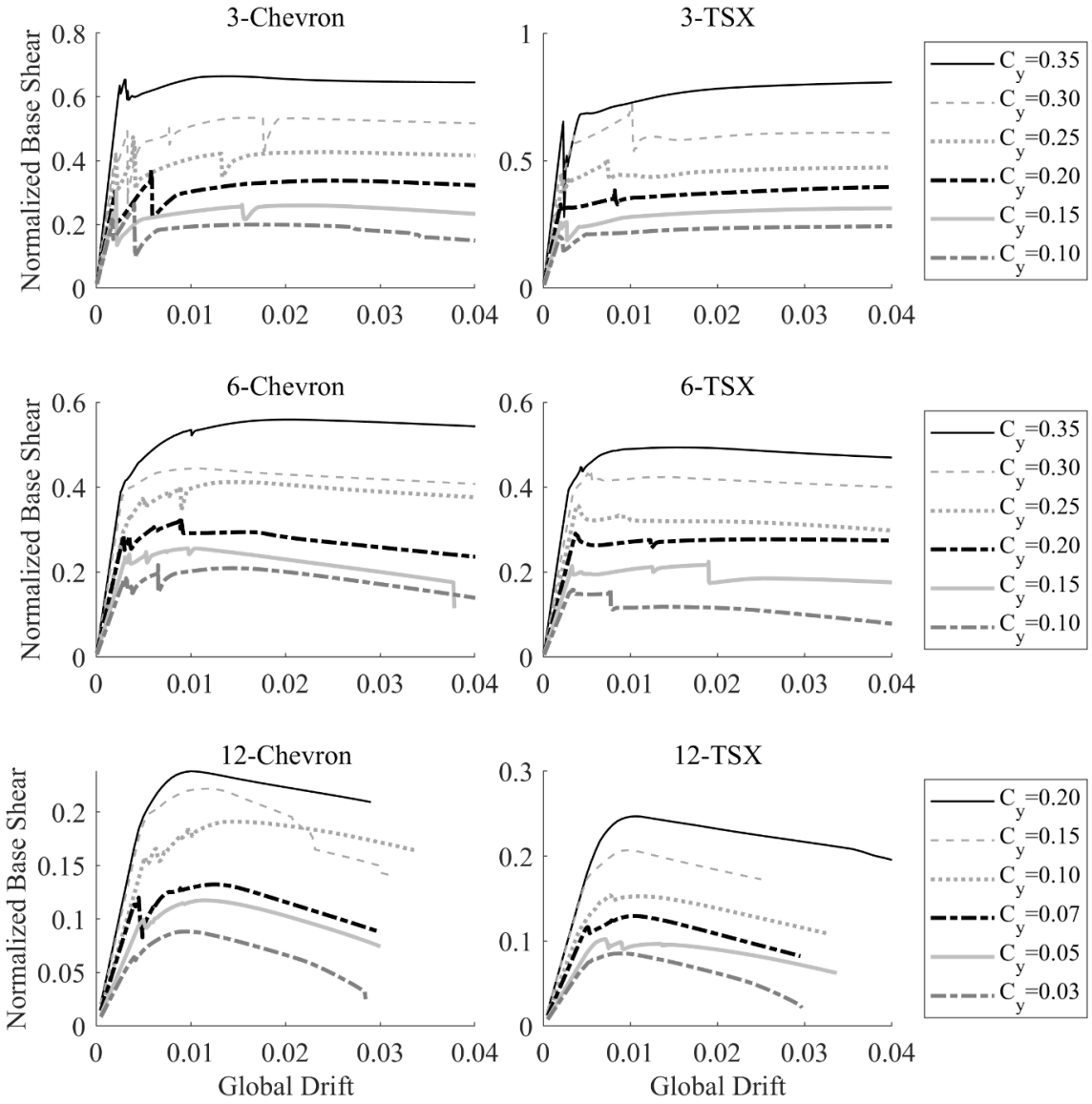


***Fig. 4-5. Static pushover curves obtained for the structures.***

The median $S_a$-MID curves obtained from IDA and SPO for the chevron SCBFs designed versus different $C_y$ values are plotted in Fig. 4-6. The data related to the TSX configuration are not included in the figure for brevity's sake.

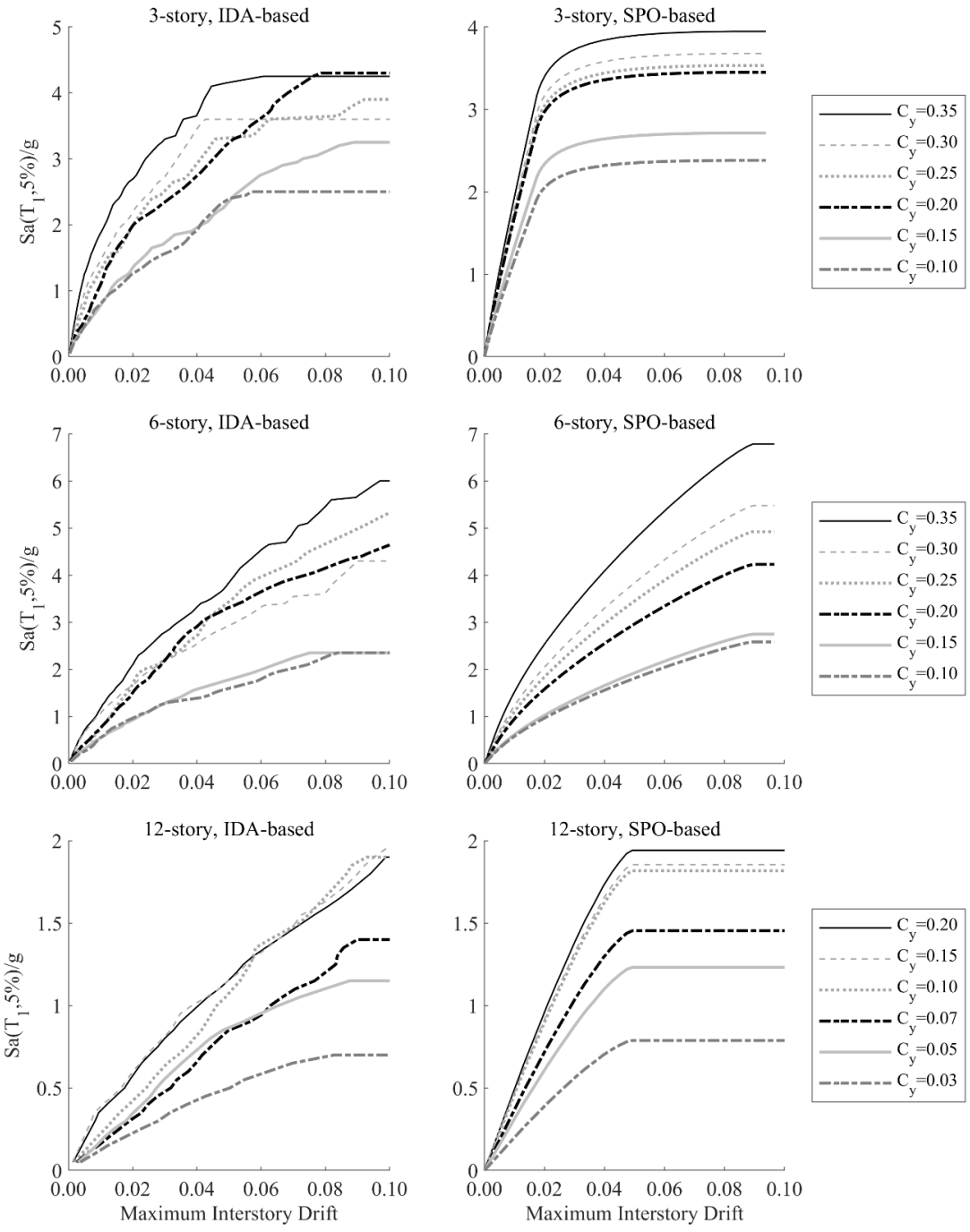


***Fig. 4-6. Median MID-$S_a$ curves obtained for the chevron SCBFs obtained using IDA and SPO methods.***

The IDA-based curves capture the higher-mode and the dynamic effects such as the hysteretic and inherent viscous energy absorption capabilities of the models. The SPO-based $S_a$-MID curves are obtained using the SPO2IDA numerical tool proposed by Vamvatsikos and Cornell (Vamvatsikos & Cornell, 2005) and also suggested by

FEMA P58 (FEMA-P58, 2018). Similar to the SPO curves, the initial elastic slopes of the median $S_a$-MID curves follow the increasing order of the utilized $C_y$ values. The sideway collapse plateaus of these curves denote the $S_a$ values at which a large MID value is observed as a sign of dynamic instability. While the heights of the SPO-based collapse plateaus obey the increasing order of the design $C_y$ values, the IDA-based plateaus show irregular orders when the $C_y$ values of the buildings are considered. These irregularities tend to interrupt the monotone correlation between the $C_y$ values and the collapse capacities of the structures and stem from the inconsistency between the $C_y$-based elastic design of the archetypes and the IDA's nonlinear dynamic method, as described in the previous section.

The IDA-based results reflect higher accuracy in estimating the seismic demands of the studied structures. However, as stated before, these results are not consistent with the $C_y$-based design applications. On the other hand, the simplicity sought by the current study can only be provided by the $C_y$-based method already utilized in the design standards as the ELF procedure.

The median PSDR demands obtained at various stories and for the $S_a$ intensities corresponding to 50% of the median collapse capacity (MCC) of the chevron SCBFs are studied in Fig. 4-7. As for the $S_a$-MID curves, these curves are also generated using the IDA- and SPO-based methods. According to the figure, the SPO method is able to predict the maximum value of PSDR demands computed using IDA. However, the relation between $C_y$ values representing the design strength level and the demand values is not monotone for the IDA results. This is while a monotone relation exists between these parameters when the SPO-based method is utilized. For taller buildings, more fluctuations appear in the IDA-derived $C_y$-PSDR relationship. In general, the common load pattern incorporated for the lateral static design of the buildings generates similar PSDR profiles for the structures designed for various $C_y$ values. In conducting the IDAs, however, the complications not foreseen in the static design process appear to play a role and deviate the computed demands from their design-time predictions. While not shown here, the two chevron and TSX configurations equally suffer from these irregularities. These findings can also be reported for other intensity levels (e.g., 30% and 100% of the MCC).

Similar plots are also provided in Fig. 4-8 regarding the PFA demands. The non-monotone trend observed for the MID-$C_y$ relation in the case of MID shows a better regularity for the PFA observations. The PSO-based PFAs are estimated from the story displacement demands through empirical regression equations suggested by FEMA P58 (FEMA-P58, 2018). As so, these curves increase by getting closer to the roofs of the buildings. Unlike the SPO-based PFAs, the IDA-derived results observed at the base floor, which is equal to the peak ground acceleration, have the largest value among the various floors, irrespective of the story height, design $C_y$ and intensity level. Nonetheless, the absolute overall maximum of the PFA demands estimated via IDA and SPO are in an acceptable agreement.

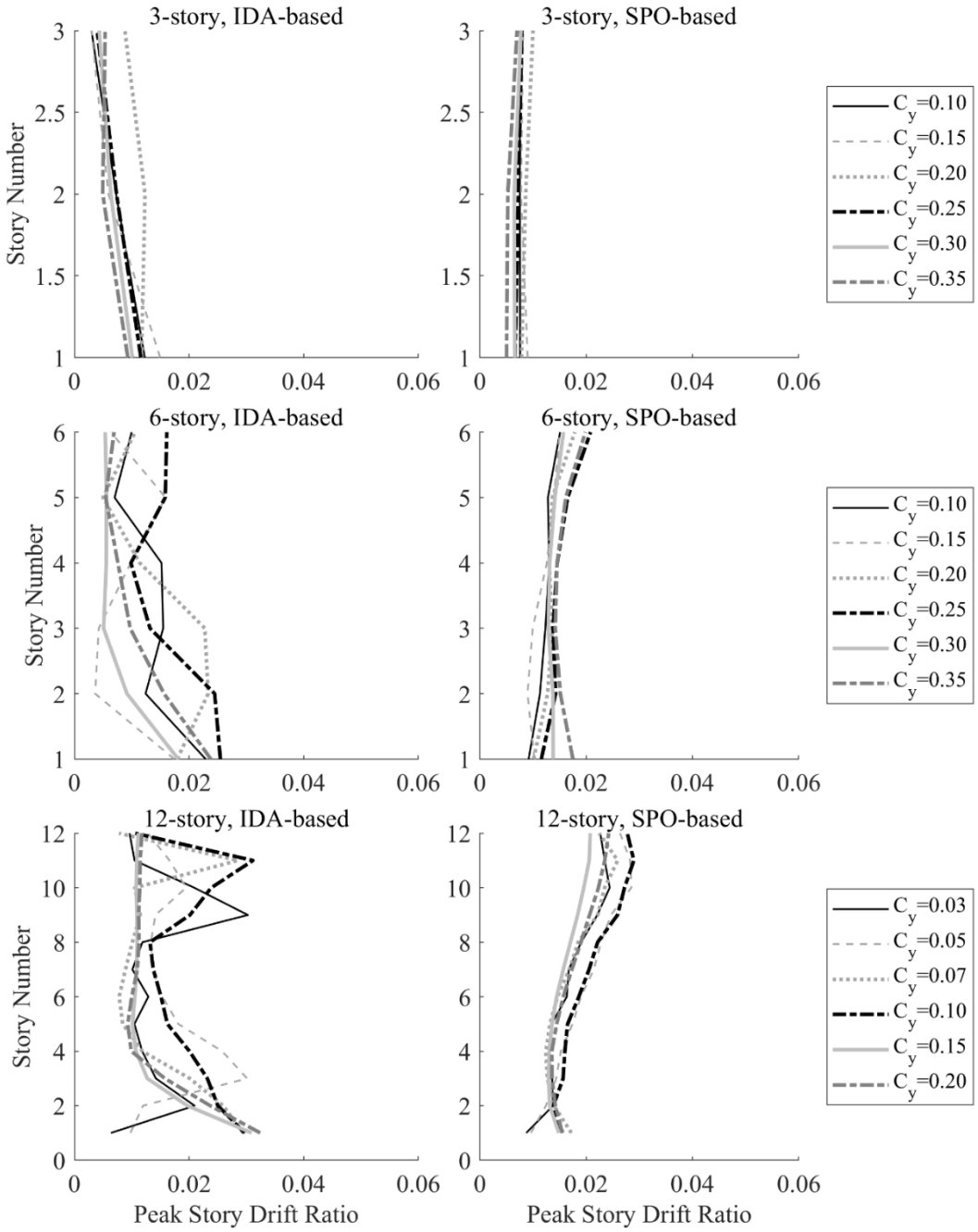


***Fig. 4-7. Median PSDRs obtained for the chevron SCBFs at the 0.5MCC $S_a$ level using IDA and SPO methods.***

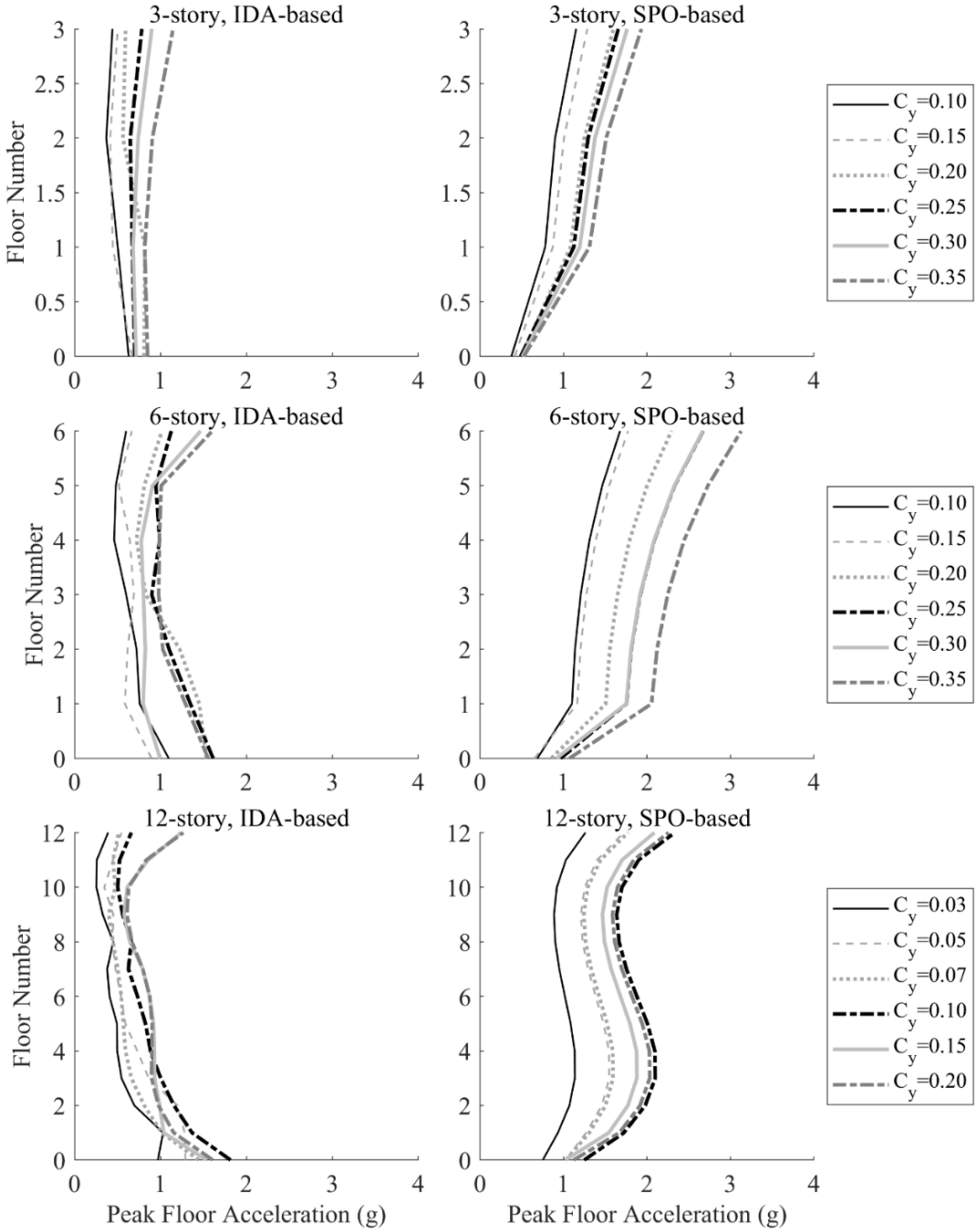


***Fig. 4-8. Median PFAs obtained for the chevron SCBFs at the 0.5MCC $S_a$ level using IDA and SPO methods.***

### 4.4. The loss and MID spectra

The IDA- and SPO-based methods presented in Section 4.2 are employed in this section to extract the MAFE plots for various MID levels and different loss parameters. For clarity purposes, only sample results are presented here and the complete set of design spectra is provided in Appendix 3-I. The example seismic hazard curves expressing the

MAFE of various $S_a$ values of a site in the Los Angeles area for the empirical fundamental periods of the studied structures are presented in Fig. 4-9. These curves are utilized for computing the total MAFE values presented in the design curves. As stated before, for the design of new buildings, these hazard curves should be replaced with the actual curves representing the building's region. To allow this replacement, a set of companion MATLAB® codes and databases are provided that can re-generate the design plots for the supplied user hazard curve. The instructions on using these codes are provided in appendix III. To extract MAFE plots of $MID > MID_0$ limit states (LSs), $MID_0$ values that range from 0.01 to 0.1 are considered. For each $MID_0$ limit, a $S_a$-conditioned fragility is first extracted and is then multiplied by the hazard curve and integrated over the full range of $S_a$ values. Extraction of the LS fragilities varies for the two IDA and SPO-based procedures. Using IDA data, the $S_a$ intensities corresponding to the given $MID_0$ value are interpolated from the IDA results and are then assigned a log-normal probability distribution. Considering the SPO results, the $S_a$ data set representing the record-to-record variability are missing. Instead, the median and dispersion of the MIDs can be approximated, using empirical equations, at different $S_a$ levels. Thus, an extra step is required to generate a data set representing the $S_a$-MID relation using empirical approximations. This is done by sampling the MID values corresponding to a $S_a$ level via random generation.

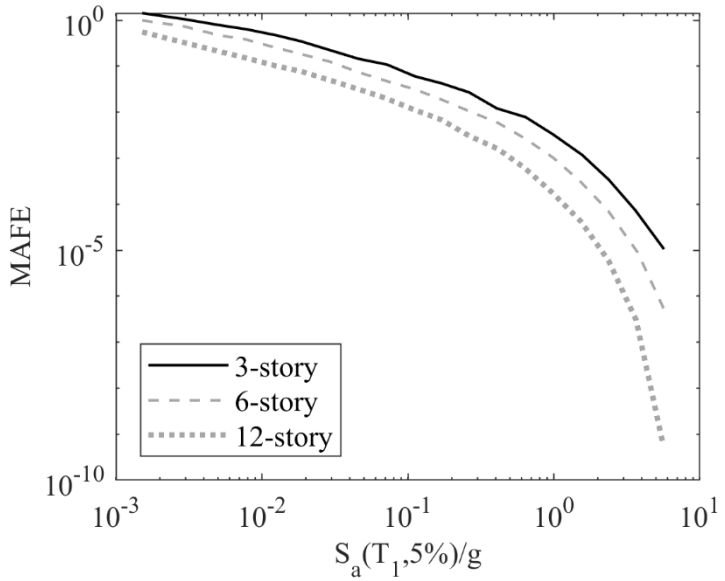


***Fig. 4-9. The utilized seismic hazard curves.***

The MID-MAFE plots are presented in Fig. 4-10 for the chevron SCBFs and the IDA- and SPO-based methods. Similar to the previous IDA-based results, the MID-MAFE plots do not exactly obey the increasing manner of the $C_y$ values. That is, the MAFE corresponding to a constant MID does not always decrease when the strength is increased by using a larger $C_y$. This irregularity is more obvious for the 3-story SCBFs and is minor for the 12-story buildings. As before, the SPO-based plots show a more predictable trend with respect to the increasing manner of the utilized $C_y$ values. Therefore, these plots are more appropriate for determining the design $C_y$ when specific MAFEs are targeted for one or more MID levels.

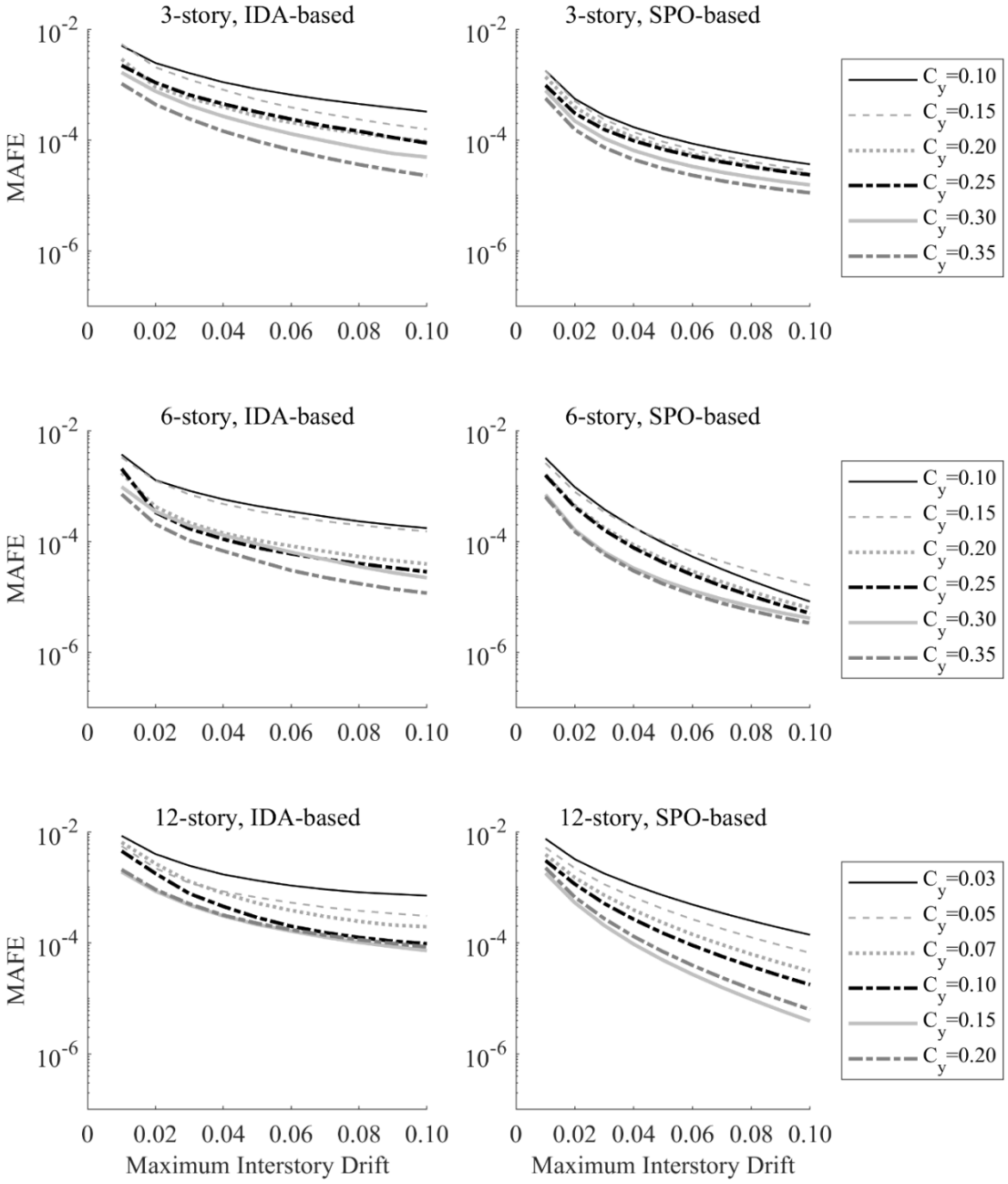


***Fig. 4-10. MID-MAFE spectra obtained for the chevron SCBFs at the 0.5MCC $S_a$ level using IDA and SPO methods.***

For generating the loss-MAFE plots, the seismic loss is represented by the repair cost and the repair time parameters. Regarding the repair time parameter, the time computation can be either sequential or parallel when the repair times of multiple components are aggregated. A "sequential" method indicates that the tasks are performed one after the other, and the components' repair times are algebraically added.

Various scenarios can be considered for parallelizing the repair tasks. One practically rational "parallel" method is to conduct the tasks related to different stories in parallel while within each story the tasks are serially managed. These two basic scenarios are considered by FEMA P58 in implementing the PACT program and are considered here for developing the loss-MAFE plots. Overall, the three loss measures: repair cost, sequential repair time, and parallel repair time are considered in developing the loss spectra.

As was stated in section 4.2, the NSCs typical to office buildings are considered in this study and are categorized based on their response to the lateral deformations of the structure. Accordingly, two "seismic" and "non-seismic" NSC categories are separately used for computing the total NSC loss measures of the structures. The seismic drift-dependent NSCs are associated with less severe damage states at a given lateral drift level, compared to the non-seismic NSCs. However, considering a given damage level, higher costs and times are required for the seismic NSCs due to the more complicated installation method used for them. Sample loss-MAFE plots are presented in Fig. 4-11 and Fig. 4-12 for the repair cost and parallel repair time losses of the seismic NSCs and the complete set of plots is provided in Appendix I. Since the loss probability curves are generated through a Monte-Carlo procedure (with 1000 simulations in this study), the resulting curves are not completely smooth and can be divided into the three regions schematically shown in Fig. 4-13. The identification of these regions helps in a better description of the differences between the observations made for various buildings and by using the alternative IDA and SPO-based methods.

The first initial flat region of Fig. 4-13 is related to the minimum loss value numerically simulated in the Monte-Carlo simulations. Since no loss values are generated between the zero and the minimum loss values, the first exceedance probability computed for the minimum loss is also attributed to the lower loss values while drawing the curve. This leads the initial segment of the loss curve to appear as a flat line. According to Fig. 4-11 plots, the minimum loss level is a function of the story's number and not of the employed design $C_y$. This is because the minimum loss is determined by the lowest damage level defined by the NSC fragilities as well as the NSC quantities, with the latter being changed when more stories are added to the buildings.

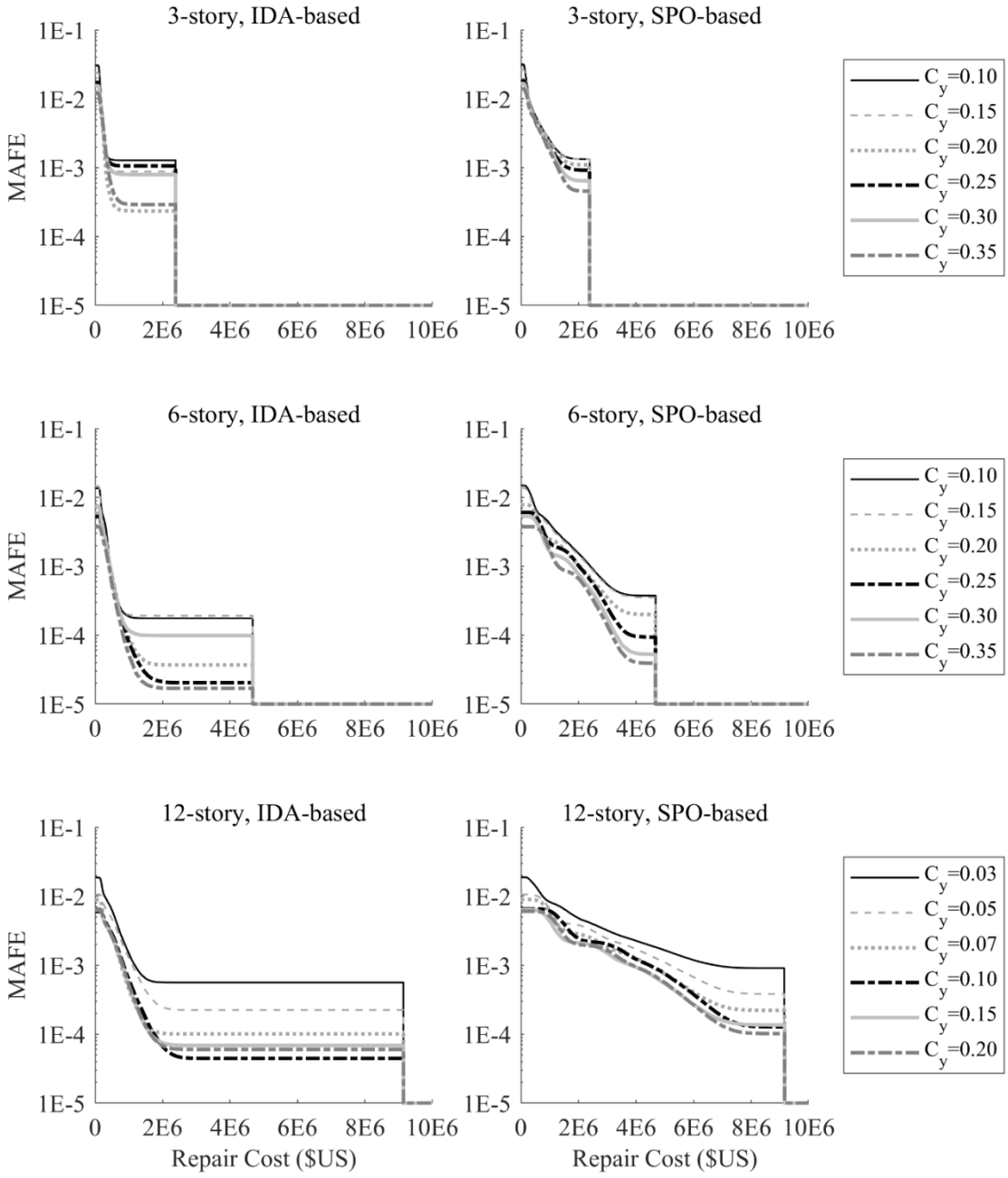


***Fig. 4-11. Spectra of repair cost MAFE obtained for seismic NSCs using the IDA and SPO-based methods.***

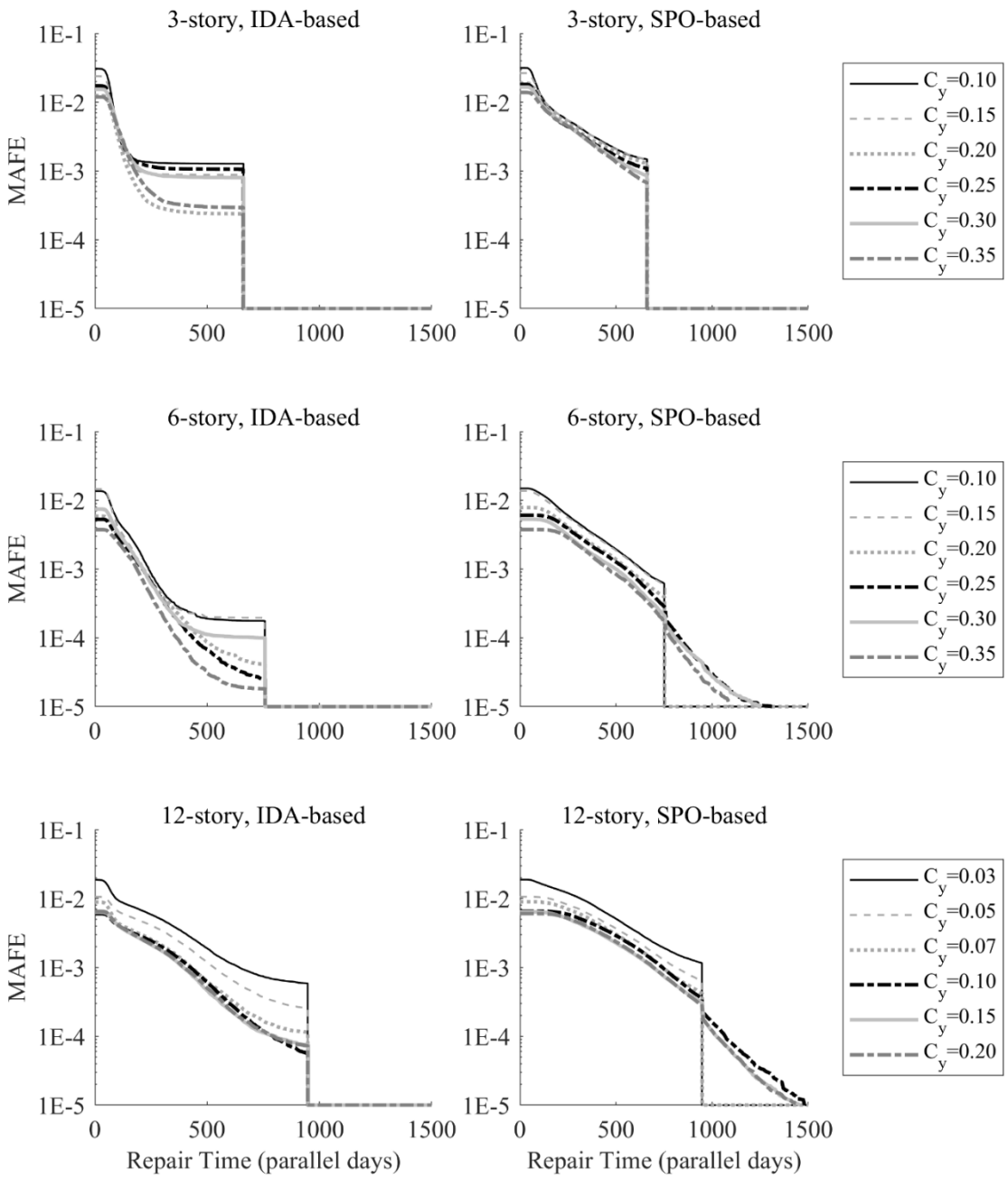


***Fig. 4-12. Spectra of parallel repair time MAFEs obtained for seismic NSCs using the IDA and SPO-based methods.***

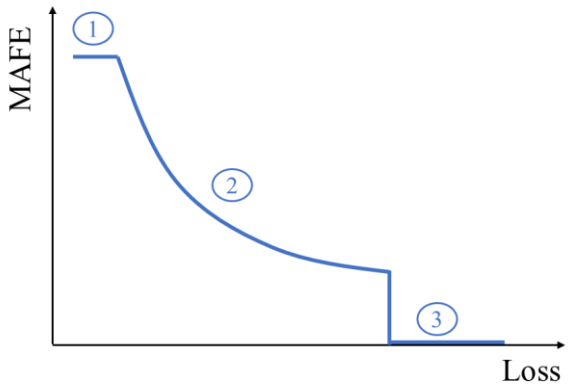


***Fig. 4-13. Regions of the loss-MAFE curves.***

By moving beyond the minimum limit along the loss axis, the exceedance probability gradually decreases and the descending region, called as region 2 in Fig. 4-13, is obtained. The slope of this region is maximum at the beginning and scales down by moving toward its tail. This is due to the fact that the lower loss values are more frequent and increasing the loss threshold by a constant step leads to a larger drop in the ratio of the observations in the initial segment of region 2. This region ends by the maximum loss value observed in the Monte-Carlo simulations. This limit is also a function of the TBR loss computed based on the NSCs and their quantities and does not change by altering the design $C_y$. By moving beyond this limit, the exceedance probability undergoes a sudden drop to zero. This non-smooth behavior, as was seen for region 1, is a result of the loss discretization in the Monte-Carlo simulation, which zeros the ratio observed for losses larger than the maximum value.

Having identified the regions of the loss-probability curves, we are now able to evaluate the effect of design $C_y$ values on either of these regions. To simplify this evaluation, we focus on region 2 and compare the MAFEs corresponding to the various $C_y$ values associated with this area of losses.

As described before, the loss-MAFE curve is a function of the strength level, represented via $C_y$, and the non-quantified ductility and EDC. Neglect of the ductility and EDC parameters is an inevitable feature of the ELF procedure on which the ASCE 7 standard, this article, and many other studies rely. Therefore, structures designed for similar $C_y$ values may show various levels of losses since the ductility and EDC parameters may differ. The fact is that the SPO-based loss estimation procedure also

neglects these dynamic characteristics in estimating the seismic demands. This leads to a consistency between the ELF-based designs and the SPO-based loss curves.

The pushover-based repair cost plots shown in Fig. 4-11 are seen to change regularly when different $C_y$ values are used. Regarding the IDA-based plots, this regularity is observed, to a good extent, by the results obtained for the 12-story SCBFs (Fig. 4-11). However, regarding the IDA-based repair cost plots of the 3 and 6-story SCBFs, a considerable level of randomness is observed for the trend governing MAFEs related to various $C_y$ values. These show again that for a $C_y$-based design, the SPO-based method is a more-practical alternative even though it is not as accurate as IDA. In addition, it can be inferred that the ability of the SPO and ELF methods in predicting the ductility and EDC characteristics depends on the structures' heights. However, evaluating this dependence is beyond the scope of this article.

### 4.5. Design example

In this section, a 5-story building with a plan area equal to 3500 $m^2$ is designed using the chevron SCBF system. The NSCs mounted on this structure are assumed to be selected from the "seismic" category of FEMA P58 performance groups, as listed in Appendix II. In addition, the building's site location is considered to be different from that regarded in developing the Appendix I design spectra. Thus, the design plots are regenerated using the companion MATLAB tools and the new SHC. For the sake of brevity, the SHC and the new spectra are not provided here. As mentioned in the previous sections, the design process does not require deciding on the number of SCBF frames resisting the lateral loads since this selection is assumed not to affect the seismic demands and the subsequent losses when the employed design $C_y$ is constant. Therefore, the design $C_y$ should be interpolated from the design plots with respect to the building's number of stories and plan area.

To simplify evaluating the performance of the designed structure versus the predicted values estimated using the design plots, a single limit state is regarded in this example. This limit state is defined by considering a $2\times10^6$ \$US repair cost threshold and an acceptable MAFE equal to 0.002 (corresponding to a 500-year return period). As described in Appendix III, the accompanying MATLAB codes also provide tools for interpolating the loss spectra and estimating the design $C_y$ based on a target MAFE-

loss/MID pair. The design $C_y$ corresponding to the mentioned target performance is computed as 0.22 by utilizing this tool. This value is used for the design of the structure following the ELF procedure of ASCE 7-22. The inelastic pushover and the repair cost MAFE curves obtained using the SPO-based method for the designed structure are presented in Fig. 4-14. According to this figure, the design process has successfully met the target performance objective.

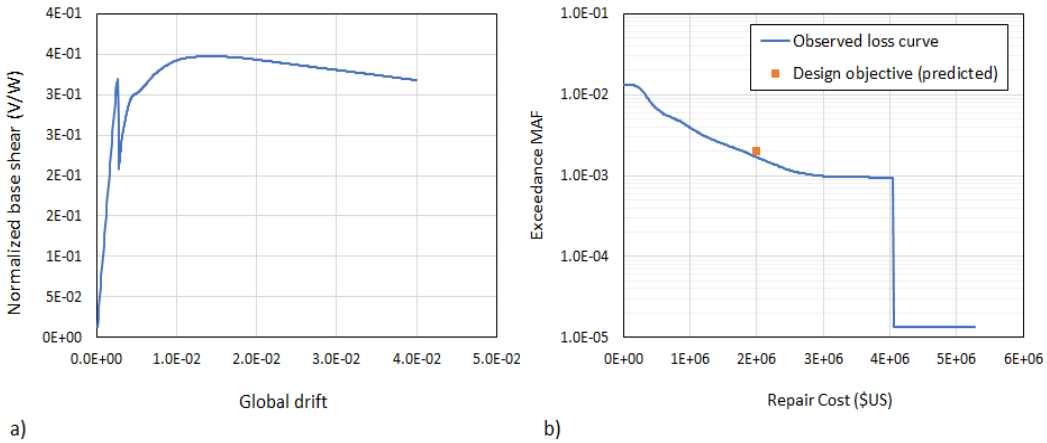


***Fig. 4-14. a) the pushover curve and b) the NSC repair cost probability curve, of the 5-story chevron SCBF designed versus $C_y$=0.22.***

### 4.6. Conclusions

In this study, two alternative approaches relying on IDA and static pushover (SPO) methods were evaluated for use in developing simplified design tools based on NSC losses. These tools helped in predicting the probabilistic seismic NSC losses of SCBF structures with 3, 6, and 12 stories. The design tools provided the mean annual frequency of exceedance (MAFE) of various loss and maximum interstory drift (MID) levels for SCBFs designed for varying design base-shear coefficients ($C_y$). Using these plots, one could simply approximate the design $C_y$ according to the target loss or MID thresholds and the allowable MAFEs. The application of the design spectra is currently limited to office buildings equipped with FEMA P58 non-seismic components (NSCs), employing SCBFs with chevron and two-story-X configurations, and with heights ranging from 3 to 12 stories. The theoretical and applicational aspects of the design tool development process were demonstrated. In addition, the study focused on the impacts made by alternating the demand estimation method between IDA and SPO.

The following remarks can be made according to the obtained results:

- The higher accuracy of the IDA-based demand estimations, as compared to the SPO-based, was accompanied by a high sensitivity of the results to the dynamic characteristics of the models. The inability of the $C_y$ parameter to fully reflect the dynamic characteristics of the structures did not match well with the sensitivity of the IDA method. Thus, the effect of dynamic parameters that affected the IDA-based results but were not reflected by the $C_y$ parameter led to random fluctuations in these results irrespective of the $C_y$ changes. These fluctuations made the IDA-derived design plots suffer from an irregularity that made them not appropriate for a $C_y$-selection process.

- Despite the IDA-based results, the static nature of the SPO-based method made it consistent with the variations in the $C_y$ parameter. This led to the selection of the FEMA P58's SPO-based loss estimation method as the basis for developing the loss and MID-based design tools.

- Disregarding the $C_y$-related regimes, an acceptable agreement was observed between the band of demand estimations made by the two SPO and IDA-based methods. This agreement led to consistency between the range of loss and MID predictions provided by these methods.

- The accuracy and applicability of the developed design tool were evaluated using an example design of a 5-story chevron SCBF structure. The designed structure was numerically modeled and subjected to the SPO-based loss estimation process in order to compare the in-advance loss prediction with that obtained using the accurate procedure. Good agreement between these results was considered as an indication of the design tool's accuracy.

***References***

ANSI, AISC 341-16: Seismic Provisions for Structural Steel Buildings, (2016).

Anajafi, H., & Medina, R. A. (2018). *Effects of Supporting Building Characteristics on Nonstructural components Acceleration Demands.* Paper presented at the 11th US National Conference on Earthquake Engineering.

Anajafi, H., Medina, R. A., & Santini-Bell, E. (2020). Inelastic floor spectra for designing anchored acceleration-sensitive nonstructural components. *Bulletin of Earthquake Engineering*, 18(5), 2115-2147.

ASCE 7-22: Minimum design loads and associated criteria for buildings and other structures, (2022).

Aschheim, M. (2002). Seismic design based on the yield displacement. *Earthquake Spectra*, 18(4), 581-600.

Calvi, G., & Kingsley, G. (1995). Displacement-based seismic design of multi-degree-of-freedom bridge structures. *Earthquake Engineering & Structural Dynamics, 24*(9), 1247-1266.

Chopra, A. K., & Goel, R. K. (2001). Direct displacement-based design: use of inelastic vs. elastic design spectra. *Earthquake Spectra*, 17(1), 47-64.

Cornell, A., & Krawinkler, H. (2000). Progress and challenges in seismic performance assessment. *PEER newsletter*.

FEMA-P58. (2018). Seismic Performance Assessment of Buildings. FEMA p58. Retrieved from

Quantification of Building Seismic Performance Factors, (2009).

FEMA. (2006). FEMA-445. In Next-Generation Performance-Based Seismic Design Guidelines: Program Plan for New and Existing Buildings. Washington, D. C.

Filiatrault, A., Perrone, D., Merino, R. J., & Calvi, G. M. (2021). Performance-based seismic design of nonstructural building elements. *Journal of Earthquake Engineering*, 25(2), 237-269.

Fragiadakis, M., & Papadrakakis, M. (2008). Performance-based optimum seismic design of reinforced concrete structures. *Earthquake Engineering & Structural Dynamics*, 37(6), 825-844.

Franchin, P., & Pinto, P. E. (2012). Method for probabilistic displacement-based design of RC structures. *Journal of Structural Engineering*, 138(5), 585-591.

Katsanos, E. I., & Vamvatsikos, D. (2017). Yield frequency spectra and seismic design of code-compatible RC structures: an illustrative example. *Earthquake Engineering & Structural Dynamics*, 46(11), 1727-1745.

Kowalsky, M. J., Priestley, M. N., & Macrae, G. A. (1995). Displacement-based design of RC bridge columns in seismic regions. *Earthquake Engineering & Structural Dynamics*, 24(12), 1623-1643.

Krawinkler, H., Zareian, F., Medina, R. A., & Ibarra, L. F. (2006). Decision support for conceptual performance-based design. *Earthquake Engineering & Structural Dynamics*, 35(1), 115-133.

Lazar, N., & Dolsek, M. (2012). *Risk-based seismic design-An alternative to current standards for earthquake-resistant design of buildings.* Paper presented at the Proceedings of the 15th World Conference on Earthquake Engineering.

Liao, W.-C. (2010). Performance-Based Plastic Design of Earthquake Resistant Reinforced Concrete Moment Frames.

Mackie, K., & Stojadinović, B. (2007). Performance-based seismic bridge design for damage and loss limit states. *Earthquake Engineering & Structural Dynamics*, *36*(13), 1953-1971.

MathWorks. (2022). Matlab documentation. Retrieved from https://www.mathworks.com/help/matlab/

Miranda, E., & Taghavi, S. (2003). Response assessment of nonstructural building elements. Pacific Earthquake Engineering Research Center, University of California Berkeley, California, USA.

Moehle, J. P. (1992). Displacement-based design of RC structures subjected to earthquakes. *Earthquake Spectra*, 8(3), 403-428.

NIST. (2010). Evaluation of the FEMA P-695 Methodology for Quantification of Building Seismic Performance Factors. In (Vol. NIST GCR 10-917-8). California: National Institute of Standards and Technology.

Panagiotakos, T., & Fardis, M. (1999). Deformation-controlled earthquake-resistant design of RC buildings. *Journal of Earthquake Engineering*, 3(04), 495-518.

Salari, N., Konstantinidis, D., Mohsenzadeh, V., & Wiebe, L. (2022). Demands on acceleration-sensitive nonstructural components in special concentrically braced frame and special moment frame buildings. *Engineering Structures*, 260, 114031.

Steneker, P., Filiatrault, A., Wiebe, L., & Konstantinidis, D. (2020). Integrated Structural–Nonstructural Performance-Based Seismic Design and Retrofit Optimization of Buildings. *Journal of Structural Engineering*, 146(8), 04020141.

Vafaee, M. H., & Saffari, H. (2017). A modal shear-based pushover procedure for estimating the seismic demands of tall building structures. *Soil Dynamics and Earthquake Engineering*, 92, 95-108.

Vamvatsikos, D., & Aschheim, M. A. (2016). Performance-based seismic design via yield frequency spectra. *Earthquake Engineering & Structural Dynamics*, 45(11), 1759-1778.

Vamvatsikos, D., & Cornell, C. A. (2005). Direct estimation of the seismic demand and capacity of MDOF systems through incremental dynamic analysis of an SDOF approximation. *ASCE Journal of Structural Engineering*, 131(4), 589-599.

Vamvatsikos, D., Kazantzi, A. K., & Aschheim, M. A. (2016). Performance-based seismic design: avant-garde and code-compatible approaches. *ASCE-ASME Journal of Risk and Uncertainty in Engineering Systems, Part A: Civil Engineering*, 2(2), C4015008.

*Appendix* 3-I. Provided design spectra

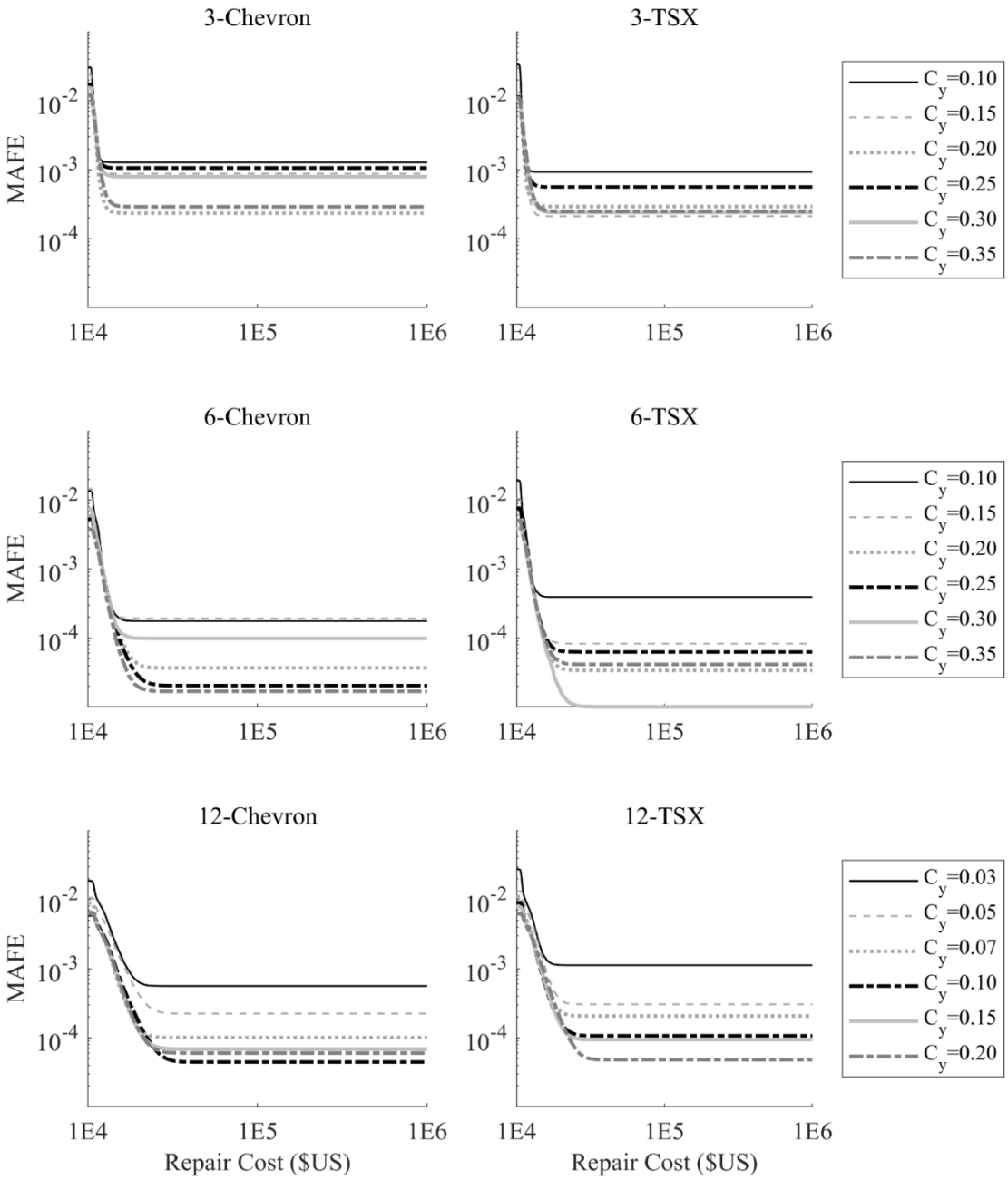


***Fig. 4-15. IDA-based spectra of repair cost MAFEs (seismic NSCs).***

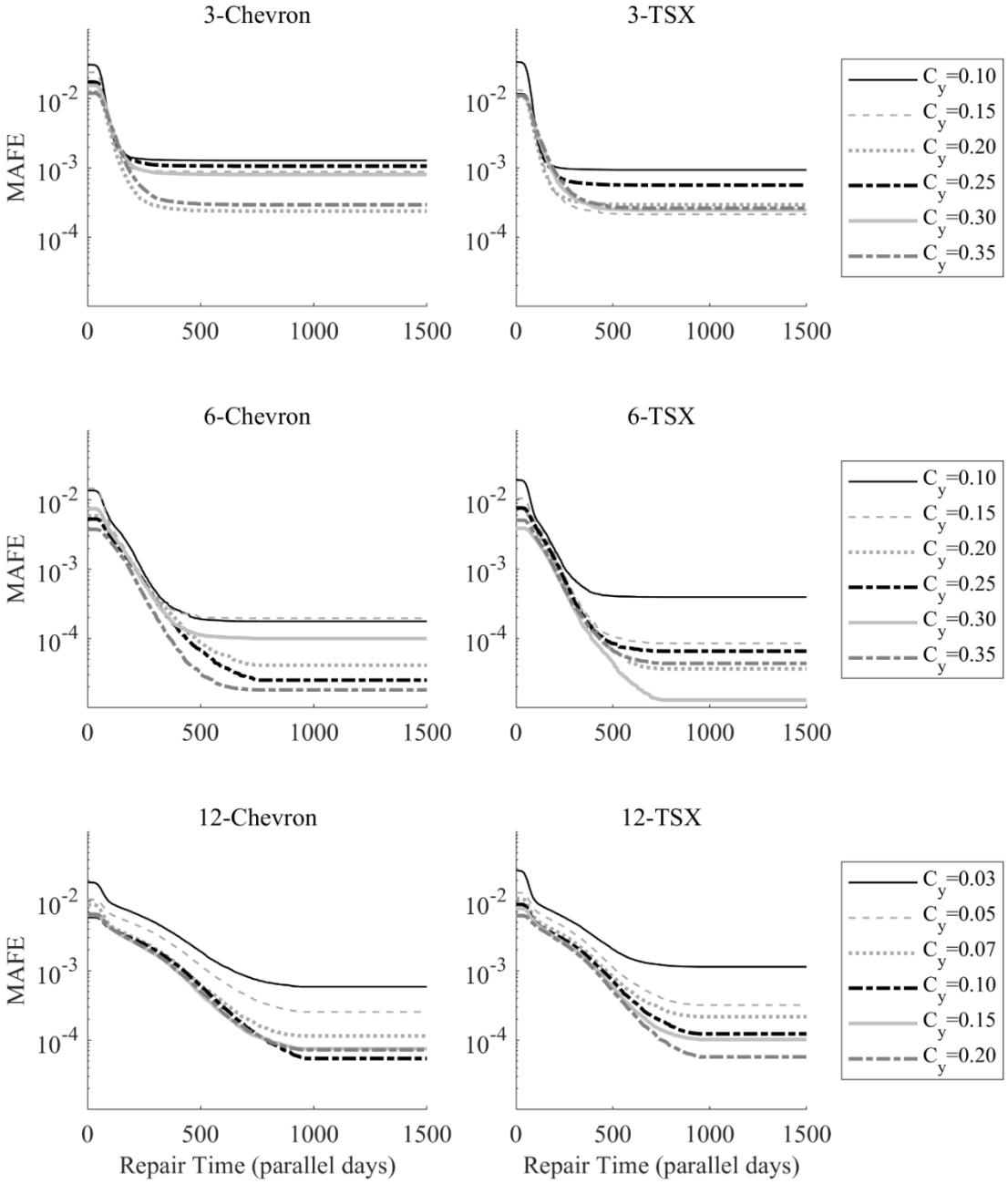


***Fig. 4-16. IDA-based spectra of parallel repair time MAFEs (seismic NSCs).***

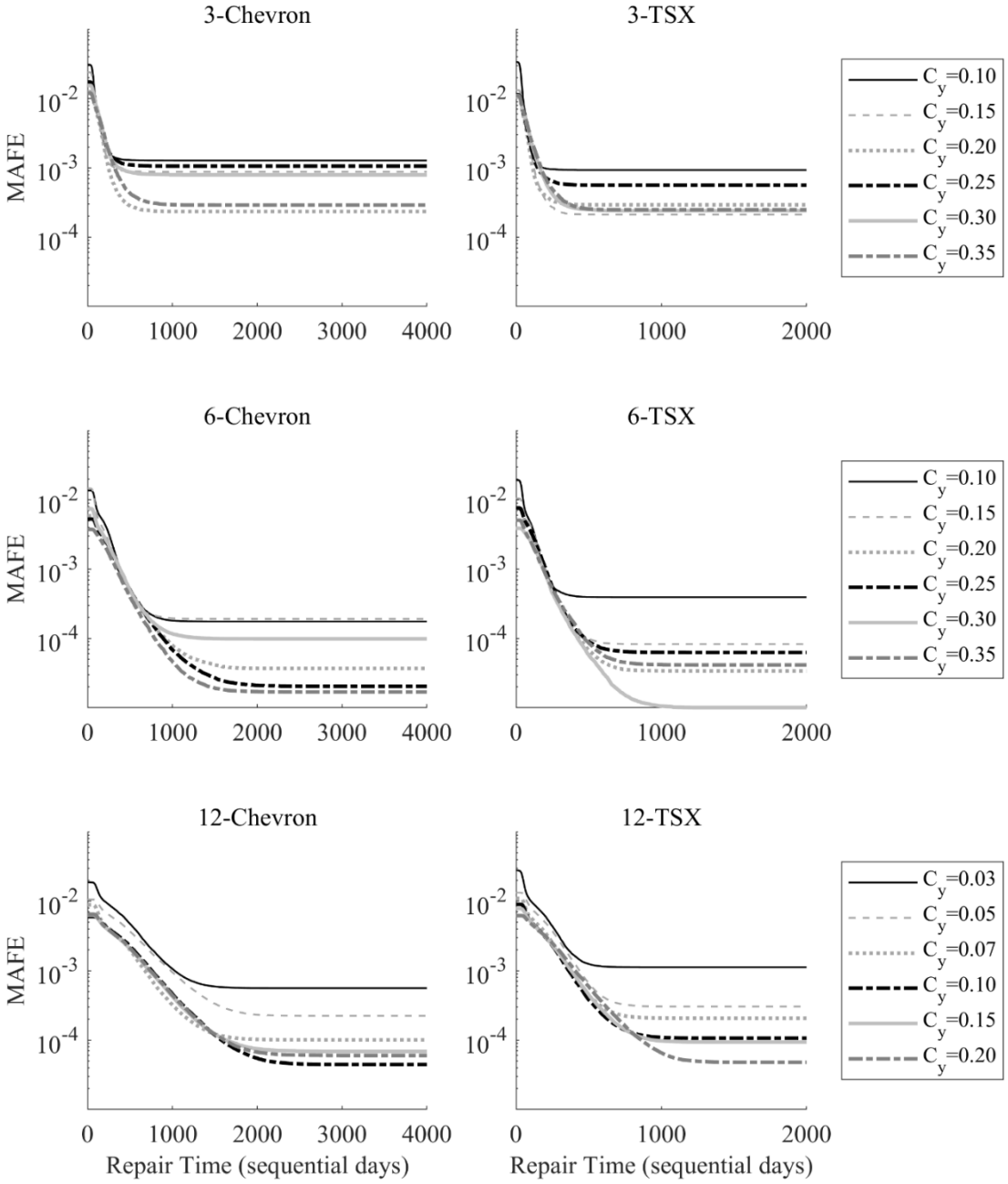


***Fig. 4-17. IDA-based spectra of sequential repair time MAFEs (seismic NSCs).***

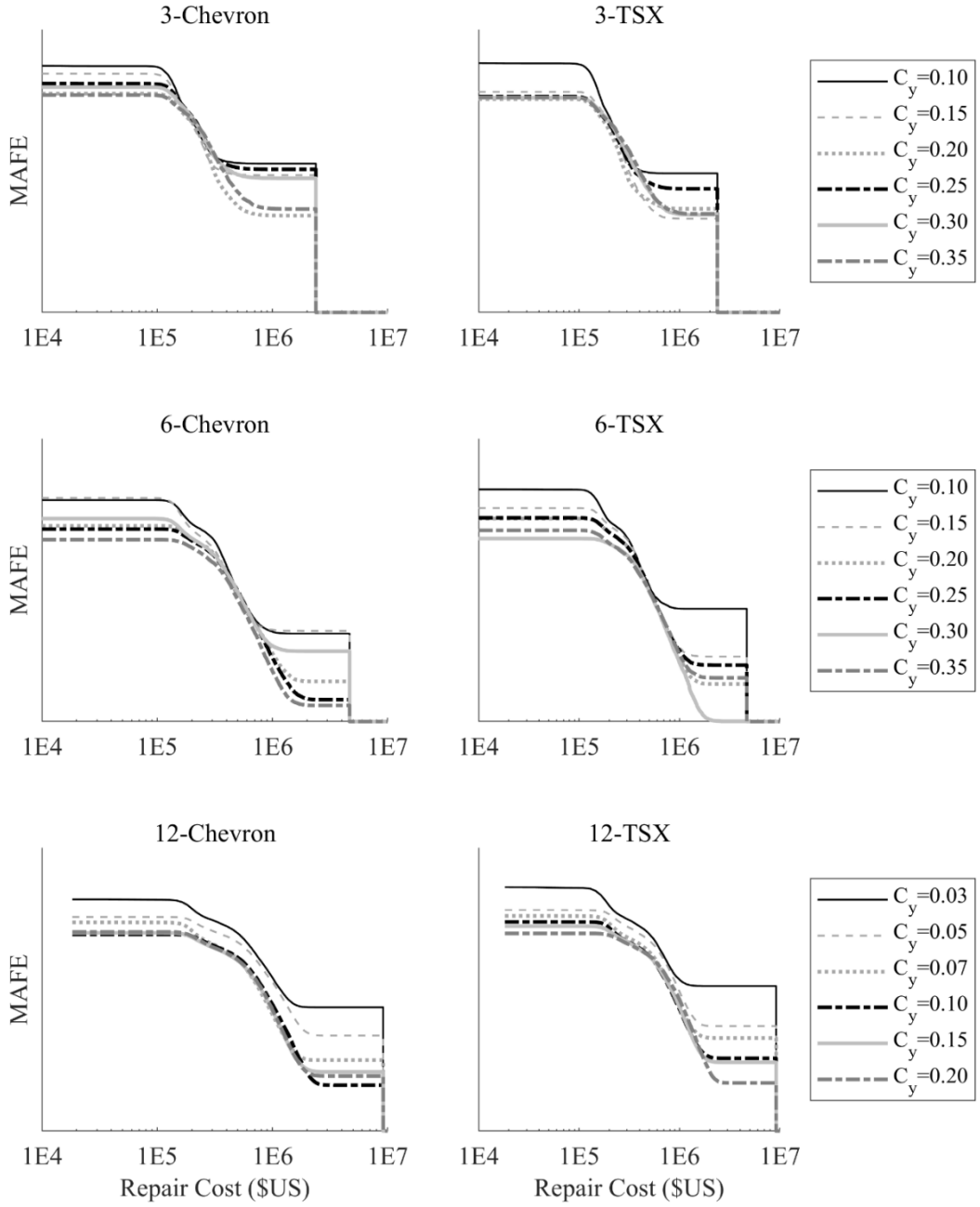


***Fig. 4-18. IDA-based spectra of repair cost MAFE (non-seismic NSCs).***

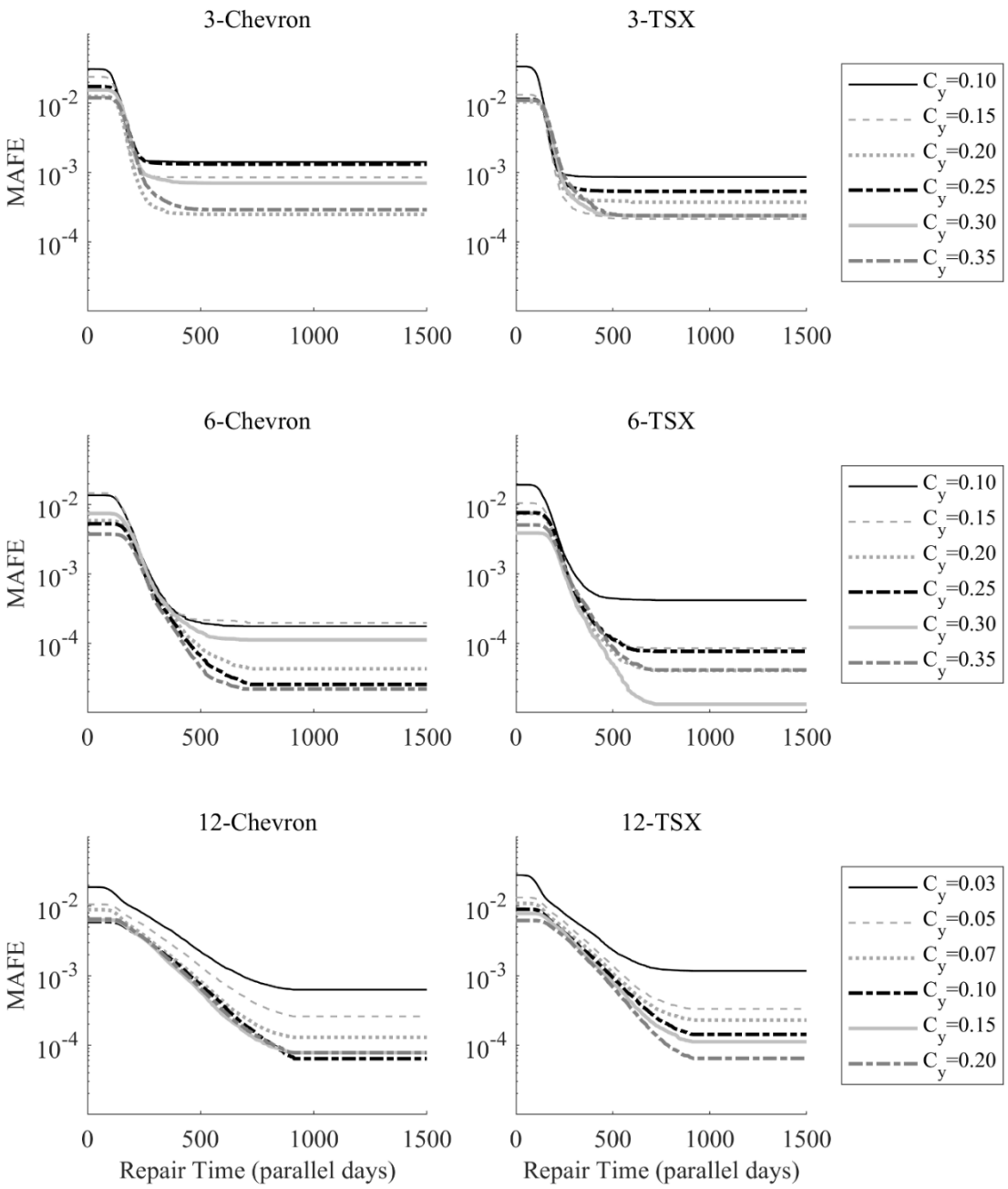


***Fig. 4-19. IDA-based spectra of parallel repair time MAFEs (non-seismic NSCs).***

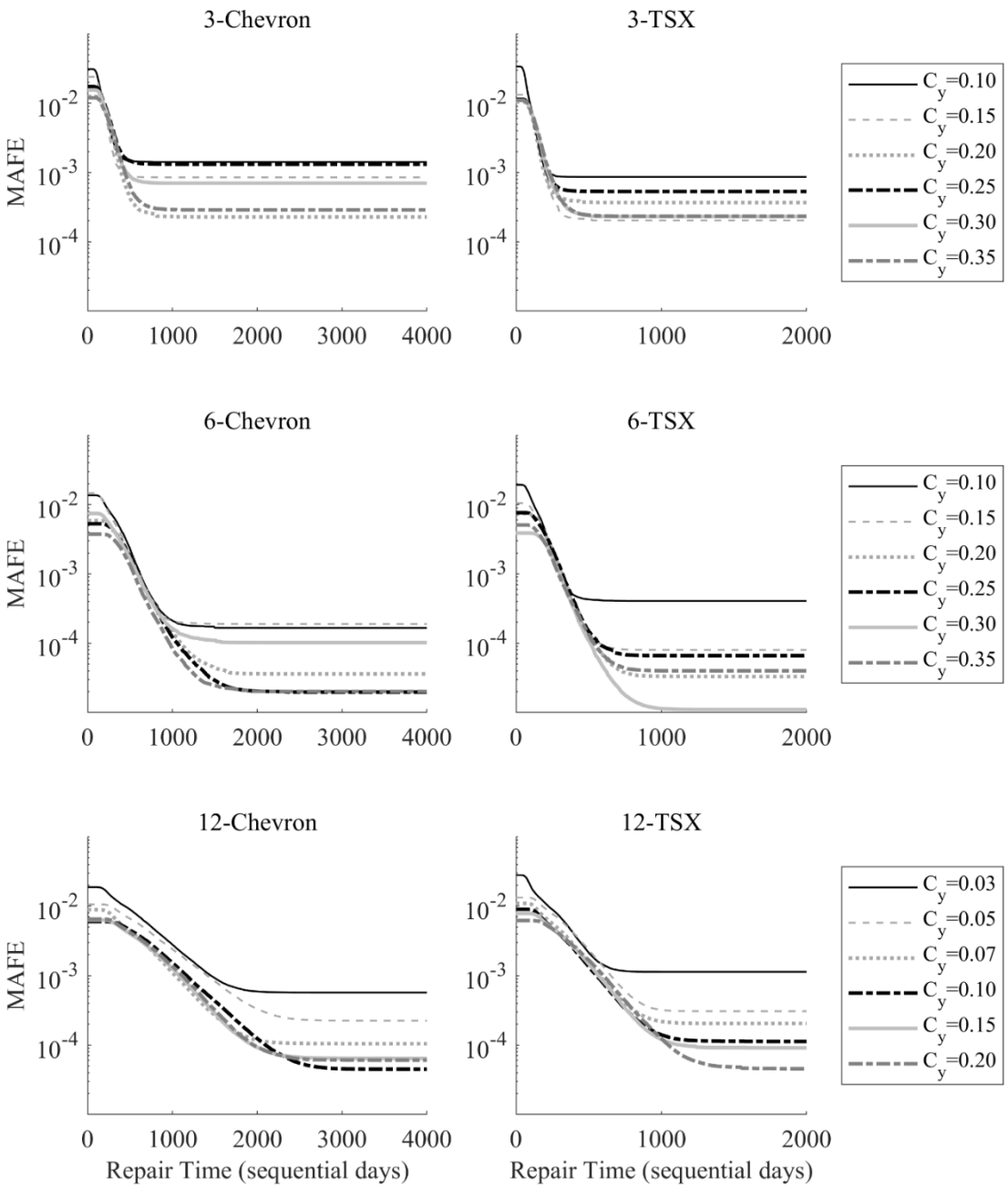


***Fig. 4-20. IDA-based spectra of sequential repair time MAFEs (non-seismic NSCs).***

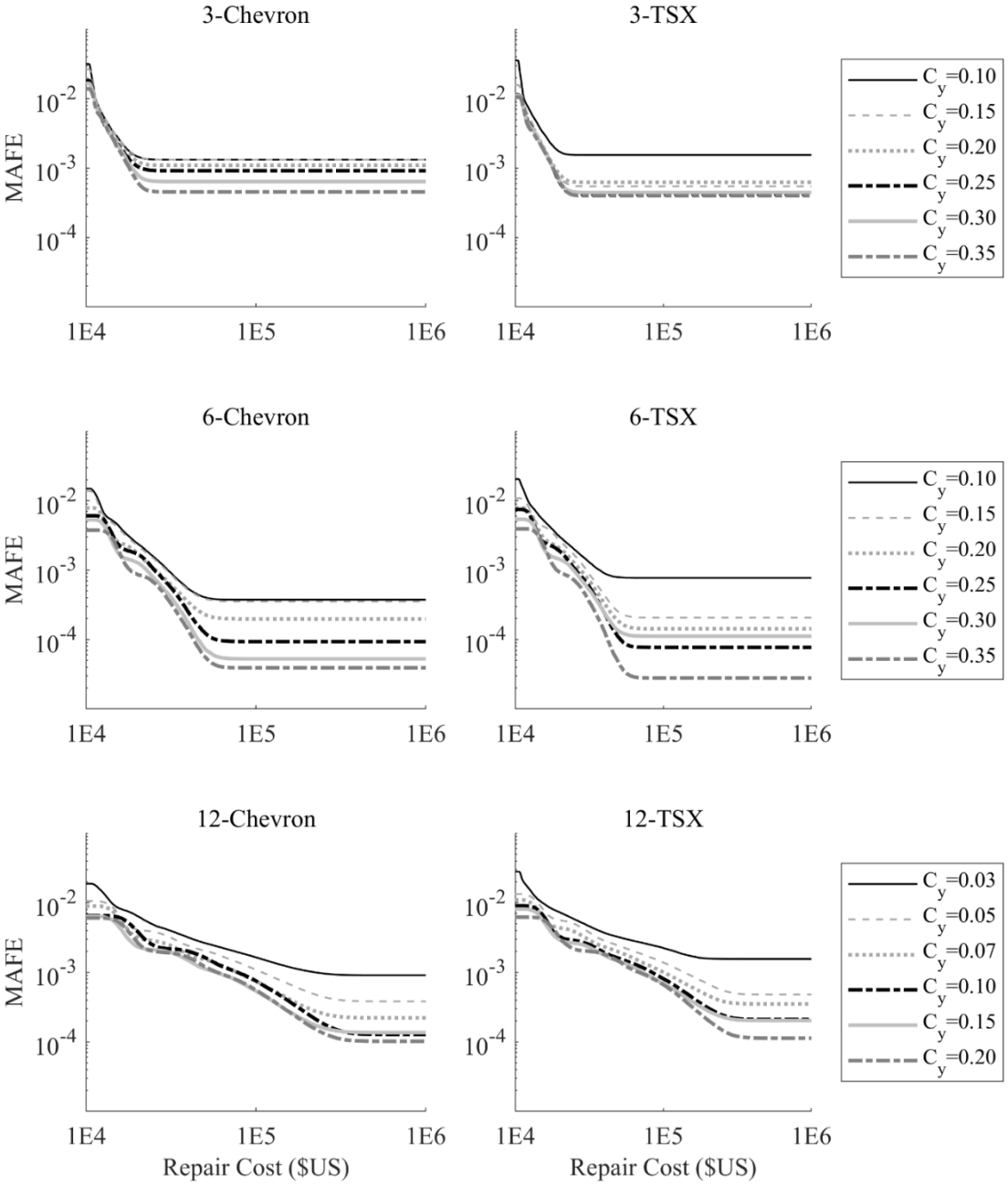


***Fig. 4-21. Pushover-based spectra of repair cost MAFE (seismic NSCs).***

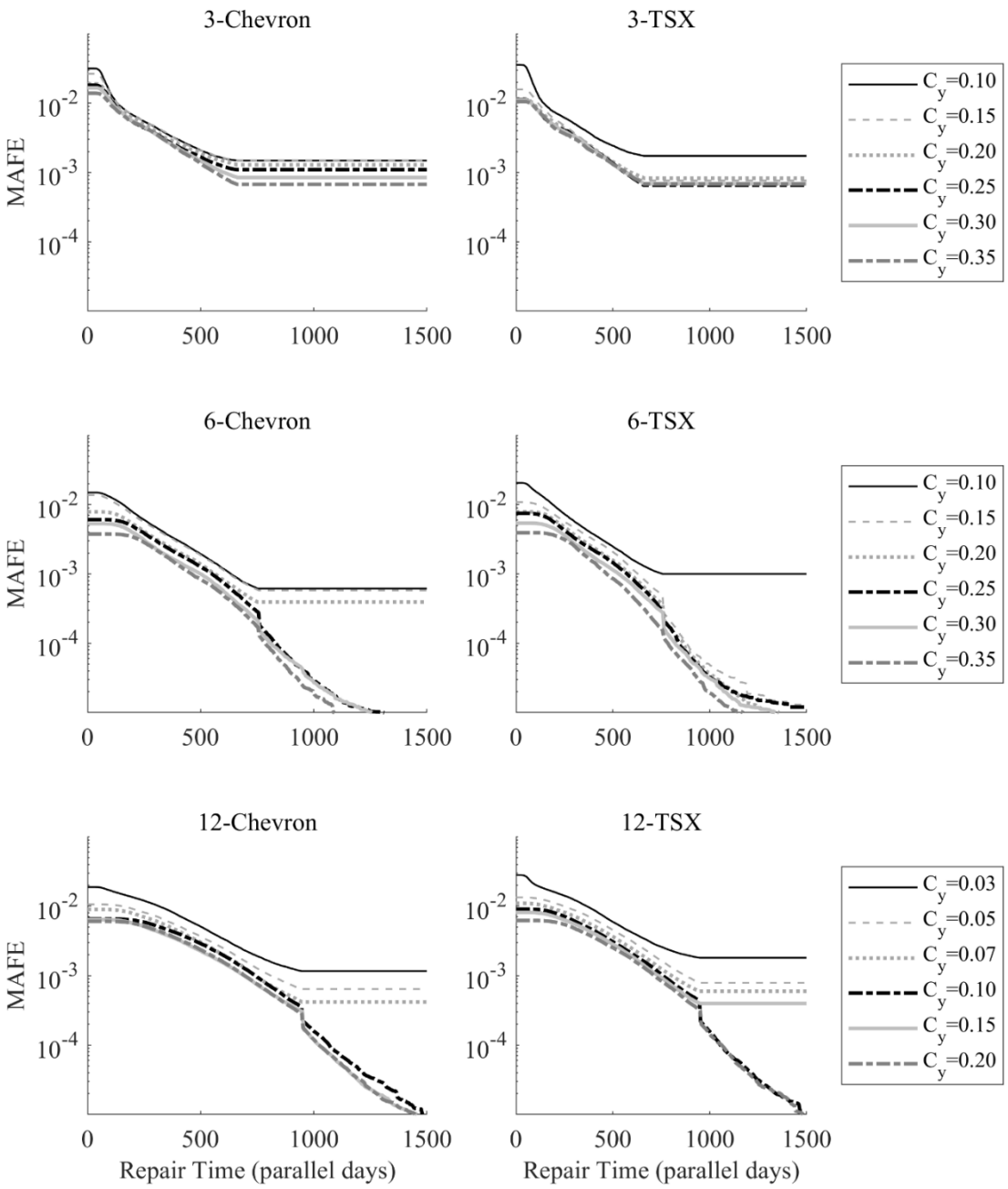


***Fig. 4-22. Pushover-based spectra of parallel repair time MAFEs (seismic NSCs).***

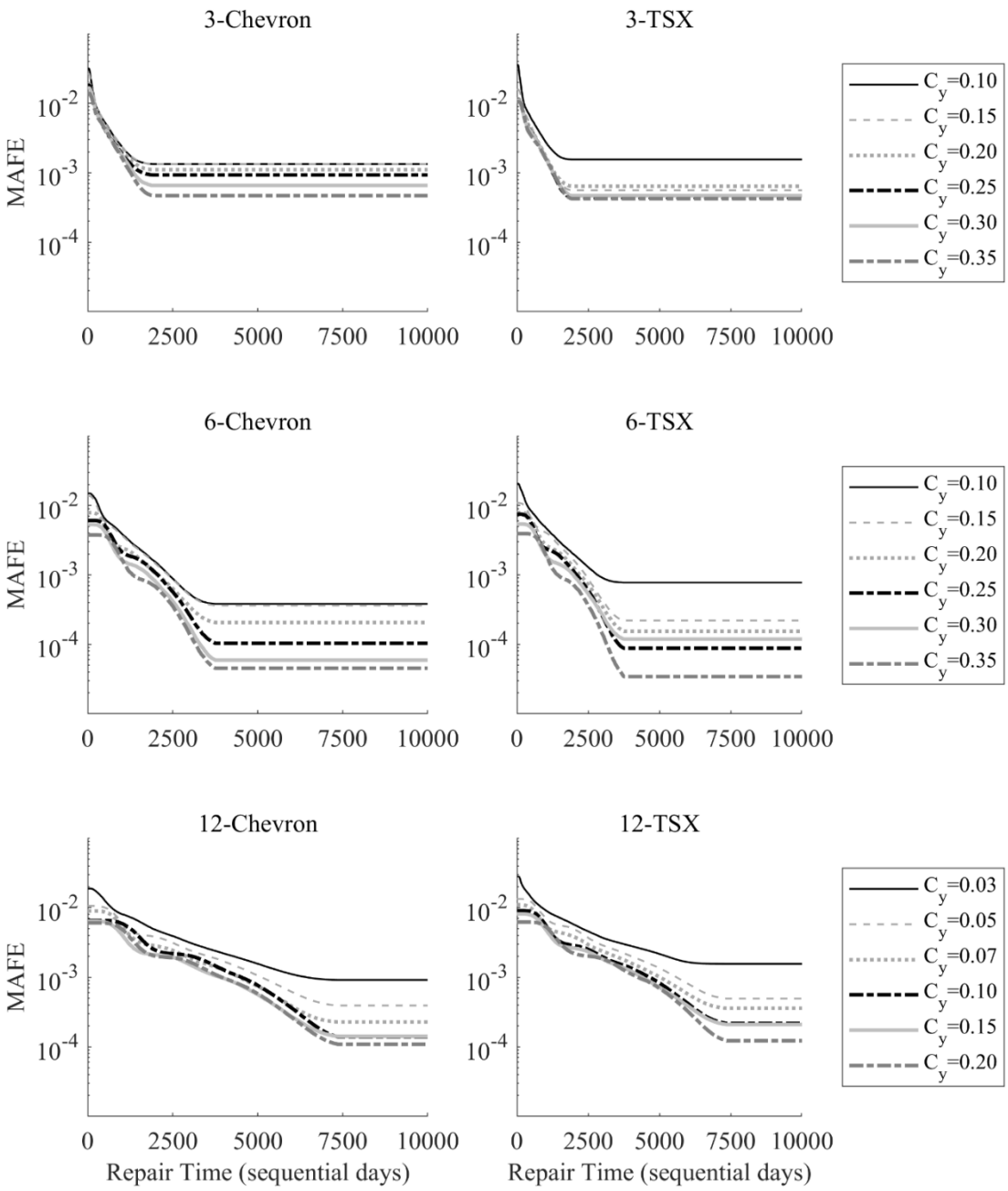


***Fig. 4-23. Pushover-based spectra of sequential repair time MAFEs (seismic NSCs).***

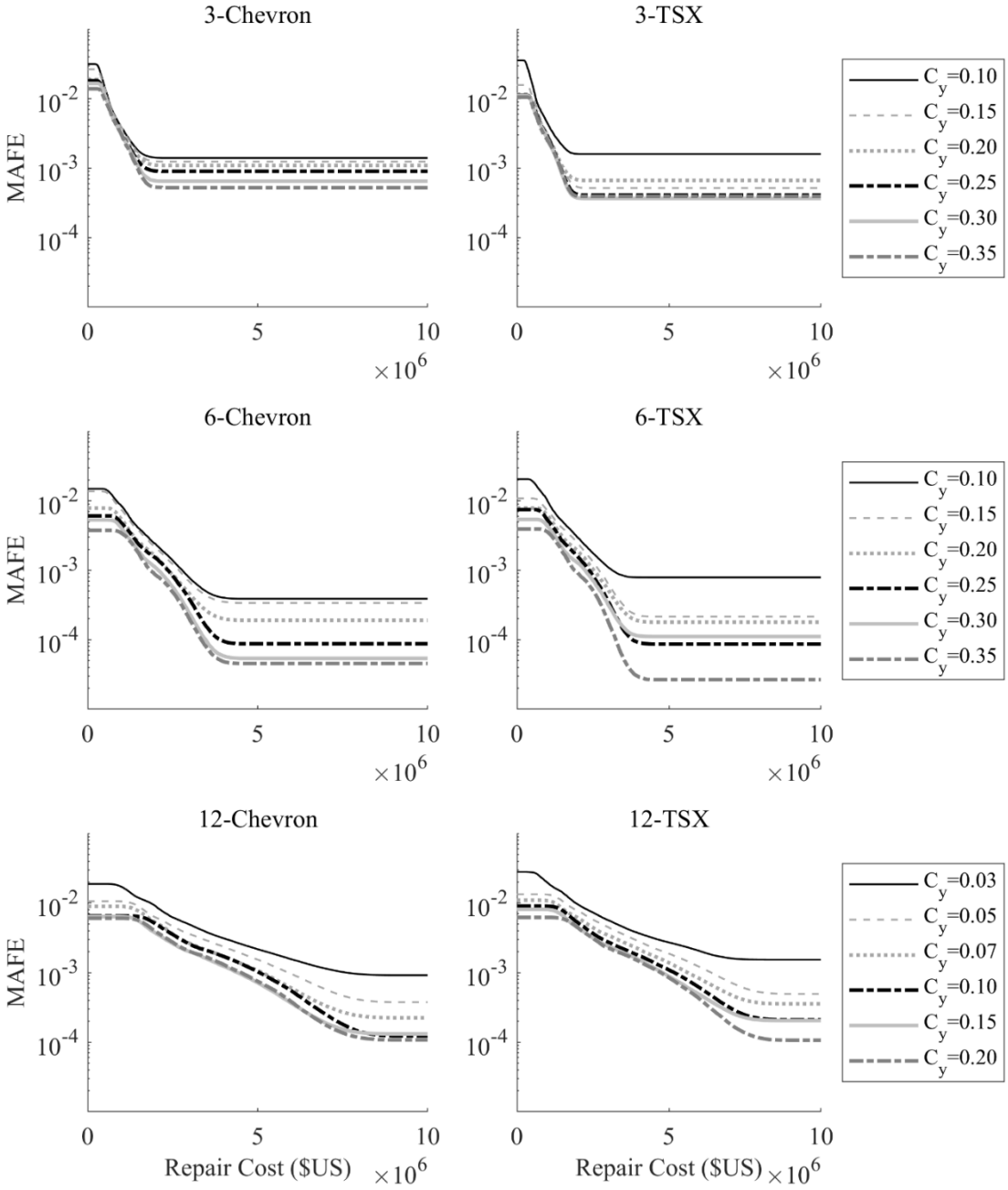


***Fig. 4-24. Pushover-based spectra of repair cost MAFE (non-seismic NSCs).***

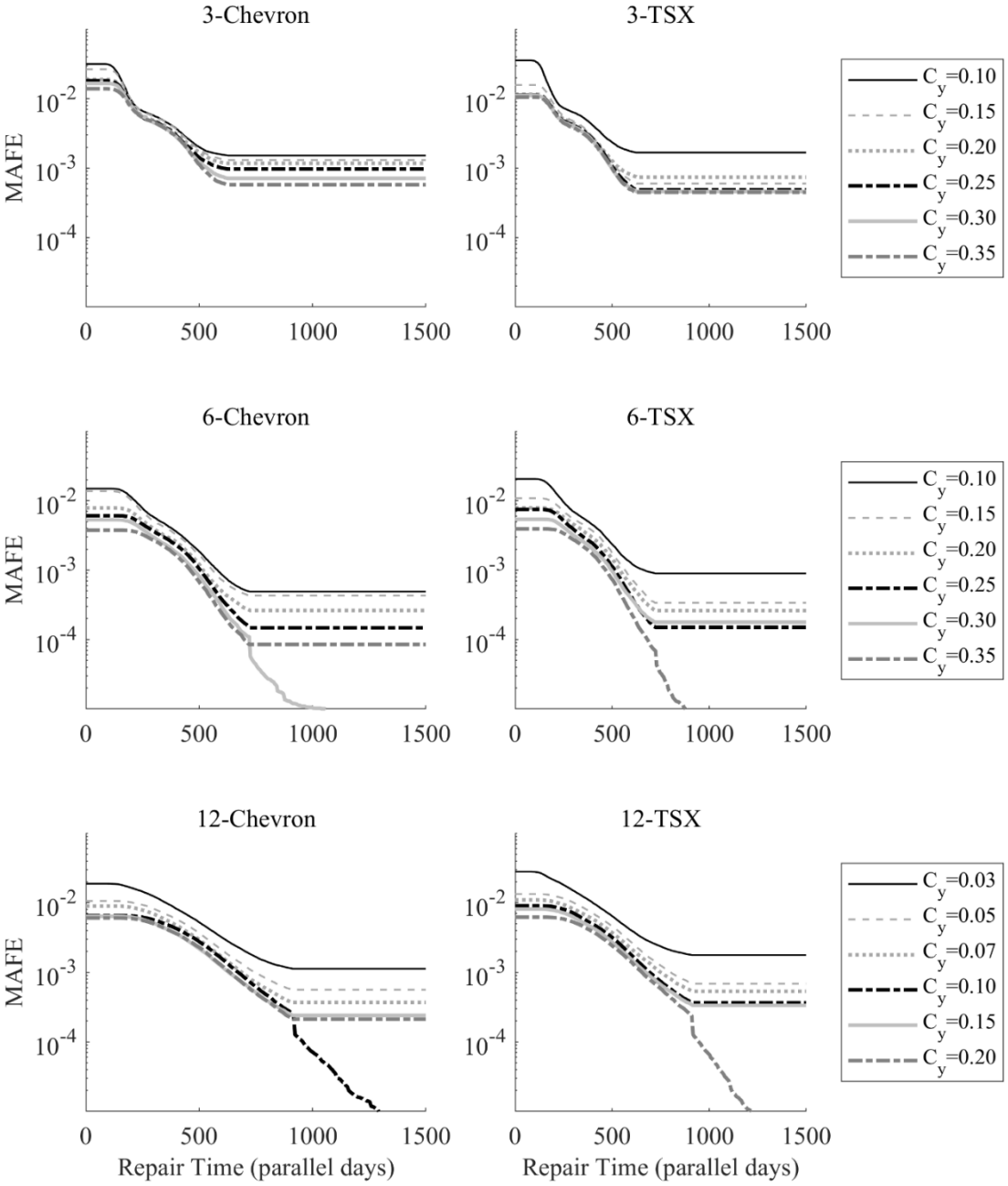


***Fig. 4-25. Pushover-based spectra of parallel repair time MAFEs (non-seismic NSCs).***

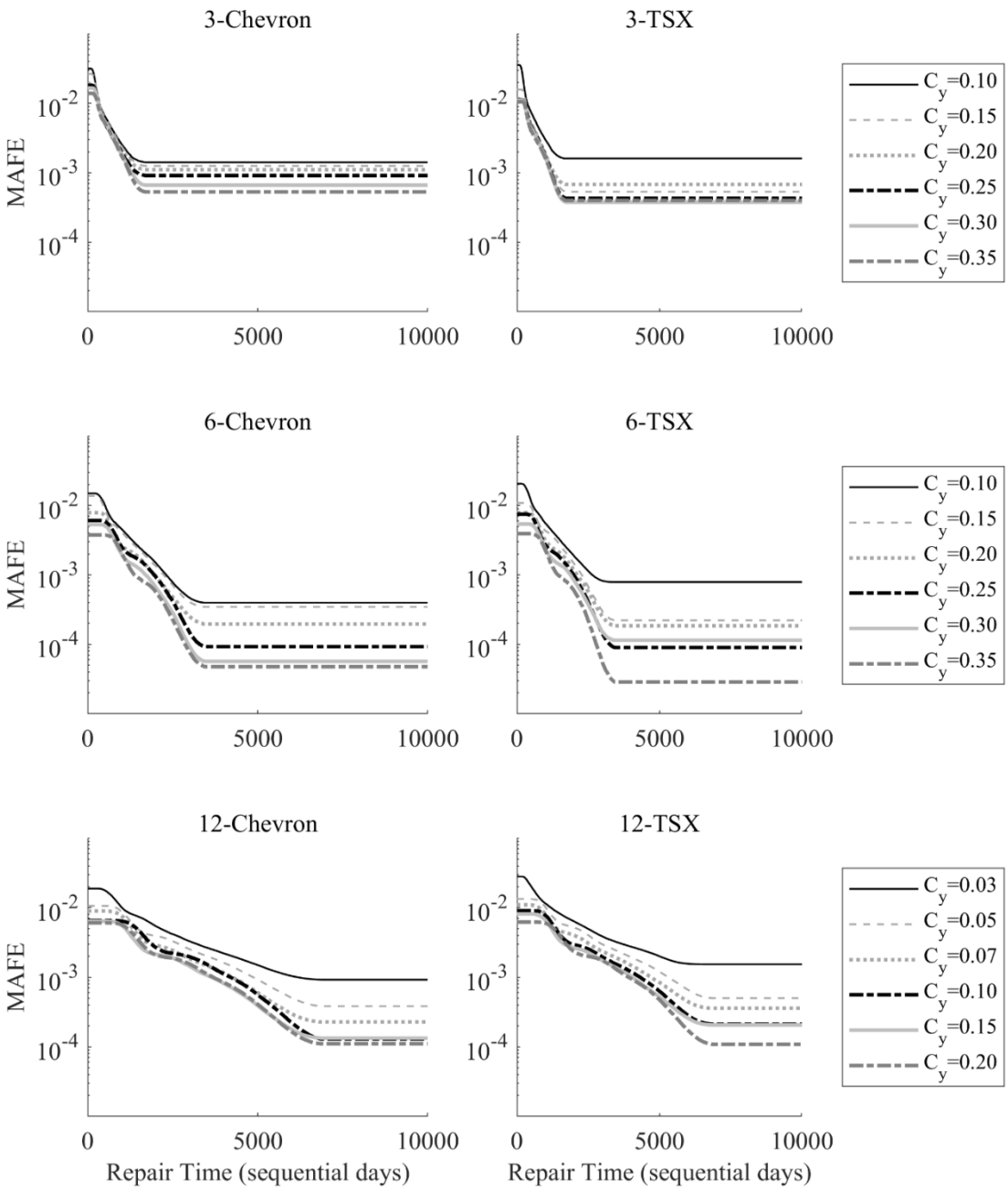


***Fig. 4-26. Pushover-based spectra of sequential repair time MAFEs (non-seismic NSCs).***

*Appendix* 3-II. Performance groups definition for the 3-story office building

a) Seismic components

| NSC ID | Description | Floor | | | |
|---|---|---|---|---|---|
| | | base | Floor-1 | Floor-2 | roof |
| **B3011.011** | Concrete tile roof, tiles secured and compliant with UBC94 | 0.00 | 29.16 | 29.16 | 29.16 |
| **C1011.001d** | Wall Partition, Type: Gypsum with metal studs, Full Height, Fixed Below, Slip Track Above w/o returns (friction connections) | 10.80 | 10.80 | 10.80 | 0.00 |
| **C3011.001c** | Wall Partition, Type: Gypsum + Wallpaper, Full Height, Fixed Below, Slip Track Above w/ returns (friction connection) | 0.82 | 0.82 | 0.82 | 0.00 |
| **C3027.002** | Raised Access Floor, seismically rated. | 81.00 | 81.00 | 81.00 | 0.00 |
| **C3032.003a** | Suspended Ceiling, SDC D, E (Ip=1.0), Area (A): A < 250, Vert & Lat support | 0.00 | 43.20 | 43.20 | 43.20 |
| **E2022.102b** | Bookcase, 2 shelves, anchored laterally | 21.60 | 21.60 | 21.60 | 0.00 |
| **D2021.012a** | Cold or Hot Potable - Small Diameter Threaded Steel - (2.5 inches in diameter or less), SDC C, PIPING FRAGILITY | 0.45 | 0.45 | 0.45 | 0.00 |
| **D3041.012b** | HVAC Galvanized Sheet Metal Ducting - 6 sq. ft cross sectional area or greater, SDC C | 0.22 | 0.22 | 0.22 | 0.00 |
| **D3041.011b** | HVAC Galvanized Sheet Metal Ducting less than 6 sq. ft in | 0.81 | 0.81 | 0.81 | 0.00 |

| | | | | | |
|---|---|---|---|---|---|
| | cross sectional area, SDC C | | | | |
| **D3041.031b** | HVAC Drops / Diffusers in suspended ceilings - No independent safety wires, SDC C | 0.00 | 9.72 | 9.72 | 9.72 |
| **D3041.041b** | Variable Air Volume (VAV) box with in-line coil, SDC C | 7.56 | 7.56 | 7.56 | 0.00 |
| **C3034.002** | Independent Pendant Lighting - seismically rated | 324.00 | 324.00 | 324.00 | 0.00 |
| **D4011.022a** | Fire Sprinkler Water Piping - Horizontal Mains and Branches - Old Style Victaulic - Thin Wall Steel - No bracing, SDC C, PIPING FRAGILITY | 2.16 | 2.16 | 2.16 | 0.00 |
| **D4011.032a** | Fire Sprinkler Drop Standard Threaded Steel - Dropping into unbraced lay-in tile SOFT ceiling - 6 ft. long drop maximum, SDC C | 0.97 | 0.97 | 0.97 | 0.00 |
| **D5012.023a** | Low Voltage Switchgear - Capacity: 100 to <350 Amp - Equipment that is either hard anchored or is vibration isolated with seismic snubbers/restraints - Anchorage fragility only | 0.01 | 0.01 | 0.01 | 0.01 |
| **C2011.001a** | Prefabricated steel stair with steel treads and landings with seismic joints that accommodate drift. | 0.00 | 1.08 | 1.08 | 1.08 |
| **D1014.011** | Traction Elevator – Applies to most California Installations 1976 or later, most western | 0.00 | 1.21 | 0.00 | 0.00 |

| | | | | | |
|---|---|---|---|---|---|
| | states installations 1982 or later and most other U.S installations 1998 or later. | | | | |
| **D3031.012a** | Chiller - Capacity: < 100 Ton - Vibration isolated equipment that is not snubbed or restrained - Anchorage fragility only | 0.00 | 0.00 | 0.00 | 1.64 |
| **D3031.022a** | Cooling Tower - Capacity: < 100 Ton - Vibration isolated equipment that is not snubbed or restrained - Anchorage fragility only | 0.00 | 0.00 | 0.00 | 1.64 |
| **D3052.013a** | Air Handling Unit - Capacity: <5000 CFM - Equipment that is either hard anchored or is vibration isolated with seismic snubbers/restraints - Anchorage fragility only | 0.00 | 0.00 | 0.00 | 7.56 |
| **D5012.013c** | Motor Control Center - Capacity: all - Equipment that is either hard anchored or is vibration isolated with seismic snubbers/restraints - Equipment fragility only | 0.00 | 0.00 | 0.00 | 1.73 |

b) Non-seismic components

| **NSC ID** | **Description** | **Floor** | | | |
|---|---|---|---|---|---|
| | | base | Floor-1 | Floor-2 | roof |
| **B3011.011** | Concrete tile roof, tiles secured and compliant with UBC94 | 0.00 | 29.16 | 29.16 | 29.16 |
| **C1011.001a** | Wall Partition, Type: Gypsum with metal studs, Full Height, Fixed Below, Fixed Above | 10.80 | 10.80 | 10.80 | 0.00 |

| | | | | | |
|---|---|---|---|---|---|
| **B3011.013** | Concrete tile roof, unsecured tiles | 0.82 | 0.82 | 0.82 | 0.00 |
| **C1011.001a** | Wall Partition, Type: Gypsum with metal studs, Full Height, Fixed Below, Fixed Above | 81.00 | 81.00 | 81.00 | 0.00 |
| **C3027.001** | Raised Access Floor, non seismically rated. | 21.60 | 21.60 | 21.60 | 0.00 |
| **C3032.001a** | Suspended Ceiling, SDC A,B,C, Area (A): A < 250, Vert support only | 0.45 | 0.45 | 0.45 | 0.00 |
| **E2022.102a** | Bookcase, 2 shelves, unanchored laterally | 0.22 | 0.22 | 0.22 | 0.00 |
| **D2021.011a** | Cold or Hot Potable - Small Diameter Threaded Steel - (2.5 inches in diameter or less), SDC A or B, PIPING FRAGILITY | 0.81 | 0.81 | 0.81 | 0.00 |
| **D3041.012a** | HVAC Galvanized Sheet Metal Ducting - 6 sq. ft cross sectional area or greater, SDC A or B | 0.00 | 9.72 | 9.72 | 9.72 |
| **D3041.011a** | HVAC Galvanized Sheet Metal Ducting less than 6 sq. ft in cross sectional area, SDC A or B | 7.56 | 7.56 | 7.56 | 0.00 |
| **D3041.031a** | HVAC Drops / Diffusers in suspended ceilings - No independent safety wires, SDC A or B | 324.00 | 324.00 | 324.00 | 0.00 |
| **D3041.041a** | Variable Air Volume (VAV) box with in-line coil, SDC A or B | 2.16 | 2.16 | 2.16 | 0.00 |
| **C3034.001** | Independent Pendant Lighting - non seismic | 0.97 | 0.97 | 0.97 | 0.00 |
| **D4011.021a** | Fire Sprinkler Water Piping - Horizontal Mains and Branches - Old Style Victaulic - Thin Wall Steel - No bracing, SDC A or B, PIPING FRAGILITY | 0.01 | 0.01 | 0.01 | 0.01 |
| **D4011.031a** | Fire Sprinkler Drop Standard Threaded Steel - Dropping into unbraced lay-in tile SOFT ceiling - 6 ft. long drop maximum, SDC A or B | 0.00 | 1.08 | 1.08 | 1.08 |
| **D5012.021a** | Low Voltage Switchgear - Capacity: 100 to <350 Amp - Unanchored equipment that is not vibration isolated - Equipment fragility only | 0.00 | 1.21 | 0.00 | 0.00 |
| **C2011.001b** | Prefabricated steel stair with steel treads and landings with no seismic joint. | 0.00 | 0.00 | 0.00 | 1.64 |
| **D1014.012** | Traction Elevator – Applies to most California Installations prior to 1976, most western states installations prior to 1982 and most other U.S installations prior to 1998. | 0.00 | 0.00 | 0.00 | 1.64 |
| **D3031.011a** | Chiller - Capacity: < 100 Ton - Unanchored equipment that is not vibration isolated - Equipment fragility only | 0.00 | 0.00 | 0.00 | 7.56 |
| **D3031.021a** | Cooling Tower - Capacity: < 100 Ton - Unanchored equipment that is not vibration isolated - Equipment fragility only | 0.00 | 0.00 | 0.00 | 1.73 |
| **D3052.011a** | Air Handling Unit - Capacity: <5000 CFM - Unanchored equipment that is not vibration isolated - Equipment fragility only | 0.00 | 0.00 | 0.00 | 7.56 |
| **D5012.013a** | Motor Control Center - Capacity: all - Unanchored equipment that is not vibration isolated - Equipment fragility only | 0.00 | 0.00 | 0.00 | 1.73 |

c) Un-categorized components

| NSC ID | Description | Floor | | | |
|---|---|---|---|---|---|
| | | base | Floor-1 | Floor-2 | roof |
| **B2022.001** | Curtain Walls - Generic Midrise Stick-Built Curtain wall, Config: Monolithic, Lamination: Unknown, Glass Type: Unknown, Details: Aspect ratio = 6:5, Other details Unknown | 0.00 | 108.00 | 108.00 | 108.00 |
| **E2022.001** | Modular office work stations. | 75.60 | 75.60 | 75.60 | 0.00 |
| **B3041.001** | Masonry Parapet - unreinforced, unbraced | 0.00 | 0.00 | 0.00 | 21.00 |

*Appendix* 3-III. Companion MATLAB tools

The companion MATLAB tools are placed inside a folder named "DesignPlotExtract", which is downloadable as a ".rar" archive. This folder is called as the "root folder" in the following descriptions. Inside the root folder, there are two "IDA_based_data" and "SPO_based_data" folders that contain the MID and loss (PACT) outputs obtained using IDA and SPO methods, respectively. As described in this article, these data are in the form of $S_a$-conditioned fragilities and should be multiplied by the seismic hazard curve in order to produce the final loss/MID-MAFE spectra. The contents of these folders need not be manipulated by the user and are only used by the MATLAB scripts provided inside the "MATLAB_scripts" folder.

To use these tools, all the user needs is to customize the "extractPlots.m" file placed in the root folder. The variables used in this script and their meanings/usages are explained in Table 4-2**Error! Reference source not found.**

***Table 4-2. The variables used in the accompanying "extractPlots.m" MATLAB script.***

| Variable Name | Meaning/Usage | Allowable/Example Values |
|---|---|---|
| **model_type** | The SCBF configuration for which the plots are to be extracted | either V (chevron) or X (two-story-X) |
| **result_path** | the folder name inside the root folder in which hazard-specific plots for all 3-12 story SCBFs will be placed in | "IDA_based_plots", "SPO_based_plots" |
| **hazard_path** | Name of the hazard files folder placed in the root folder; should contain three files named "T_0.5.txt", "T_1.0.txt" and "T_2.0.txt" providing the hazard curves for three 0.5s, 1.0s and 2.0s $T_1$ values respectively. | "LA_hazard_curves" |
| **method** | Reflecting the demand estimation method related to the input data | either 1: IDA_based, or 2: SPO_based |
| **num_of_floors** | Number of floors of the structure to be designed | In 3-12 range |
| **plan_area** | The plan area of the structure to be designed | Any value in units of $m^2$ |
| **resp_type** | The response type for which the structure should be | RC: repair cost, |

| | | |
|---|---|---|
| | designed. When multiple target performances are considered, the user should change the response type and its target value and re-run the script multiple times and consider the minimum $C_y$ value for the design. | PRT: parallel repair time,<br>SRT: sequential repair time,<br>MID: maximum interstory drift |
| **targ_resp** | The target (allowable limit) of the response parameter is defined through the resp_type variable | $2x10^6$ $US as RC<br>250 days, as PRT or SRT<br>0.02 as MID |
| **targ_MAF** | Allowable MAFE for the limit state defined using resp_type and its targ_resp value. | 0.002 (equivalent to 500 years return period) |
| **NSC_compo_category** | The type of NSCs contained in the structure to be designed (not required when resp_type is set as MAF) | either "seismic" or "nonseismic" values given as string values (surrounded by "") |
| **des_Cy** | The output of the MATLAB scripts (along with the design spectra provided in the result_path folder): the $C_y$ value corresponding to the provided resp_type, targ_resp and targ_MAF values. | See the descriptions provided for the resp_type variable |

# Chapter 5. Summary and Recommendations

## 5.1. Summary

This study focused on generating response data, establishing design procedures and evaluating them in order to improve the seismic performance of nonstructural components in steel buildings. Its findings aimed at informing the development of a new generation of either prescriptive or performance-based design approaches for nonstructural components. Demand estimation of acceleration-sensitive nonstructural components (NSCs) and development of NSC-loss based design methods were the two subjects the thesis followed throughout the previous chapters. Regarding the NSC demand estimation, the focus of the study included a number of areas that are briefly described in this section.

Unlike previous studies on NSC demands, which used single-degree-of-freedom (SDOF) or generic multi-DOF models to represent the supporting structures, this study focused on special concentric braced frame (SCBF) and special moment frame (SMF) archetypes. This was intended to reflect the structure-specific inelasticity distribution and damage-induced deterioration in behavior, which vary from structure to structure. Numerical models were developed for SCBF and SMF archetypes with varying heights and vibration properties in OpenSees.

Chapters 2 and 3 were devoted to evaluating and enhancing the prescriptive force-based design methods of NSCs. Subjected the models to a suite of design-level ground motions, the absolute floor acceleration response of these structures was obtained. The simulated floor responses were next used to generate the acceleration spectra of NSCs in conditions that varied with respect to NSC damping and inelasticity levels.

In Chapter 2, elastic behavior was assumed for NSCs supported on the SCBF and SMF structures. First, the accurate structural models were employed to extract the

floor acceleration spectra and provide an estimate of peak floor acceleration (PFA) as a factor of peak ground acceleration (PGA). Next, the acceleration spectra of the elastic NSCs excited by the floor shakings were computed by assuming different NSC damping ratios. These spectra were then subjected to regression analysis in order to generate formulas that predicted peak component acceleration (PCA) to PFA ratio. The developed spectra were also used for evaluating the NSC design spectra proposed by ATC-120, Eurocode-8 and ASCE 7-16.

The ATC-120 findings were based on data from instrumented buildings and under earthquake levels that were much weaker than the design earthquake (DE). In addition, ATC-120 assumed constant ductility for NSC to occur at various stories throughout the height and used a height-independent $R_\mu$ factor when estimated the maximum NSC force. The results showed that the design force equation recommended by ATC-120 was conservative for the SCBF archetypes, with differences of up to 33%. In contrast, the ATC-120 seismic design force underpredicted the demands in the SMFs, with a maximum difference of 9%. Lastly, the values of the NSC seismic forces estimated in this study were smaller than those obtained by the Eurocode 8 design formula, irrespective of the lateral force resisting system type. The Eurocode 8 values were increasingly conservative as the building height increased, especially in the SCBF archetypes.

Evaluating the ASCE 7-16 provisions for estimating the PCA using the PFA revealed a considerable level of conservatism. In addition, the variation in the floor response by moving through the structure height was not properly addressed by ASCE 7-16's formula. The regression equations presented in this study allowed precise prediction of PCA/PFA ratio in terms of various NSC periods normalized to the resonance period of the building.

In line with the efforts made in Chapter 2 to estimate prescriptive design forces, inelastic NSC behavior was assumed in Chapter 3. Similar to Chapter 2, this chapter investigated the effect of NSC damping ratio, NSC location in the building, and the modal periods of the buildings on acceleration demands on inelastic NSCs. Considering varying NSC ductility levels, it was shown that NSC inelasticity, even in low ductility levels such as 1.25 or 1.5, results in a considerable reduction in the spectral acceleration of the NSCs. Results indicated that increasing the NSC ductility level from 1.0 to 6.0

results in a larger reduction in NSC response at the resonance period of the flexible structures (SMFs) compared to the stiff structures (SCBFs).

To allow estimation of NSC acceleration demands from known acceleration of the floor, a formula was proposed for PCA/PFA factor also known as NSC amplification factor. The values obtained from this formula in this study were compared with the values recommended by ATC-120 and provided by ASCE 7-22. Results highlighted that the differences between the NSC amplification factor values in the ASCE 7-22/ATC-120 and this study are large for the NSC "supported above grade plane" (ASCE 2022), while it is small for NSCs "supported at grade plane". The predictive regression equation proposed in Chapter 2 for elastic NSCs was also developed in Chapter 3 considering the NSC ductility parameter. The observations implied that the structural nonlinearity can reduce the seismic demand forces in the NSCs. Accounting for this reduction can lead to a more economical design of the NSCs and their attachment/anchorage. The outcome of this study can be incorporated into technical aspects of the design of the secondary systems.

After evaluating the prescriptive NSC design forces in Chapters 2 and 3, Chapter 4 focused on performance-based design of buildings in terms of NSC loss risk. The methodology utilized in this chapter was shifted towards NSC loss estimation using the empirical and judgment-based NSC damage and loss prediction methods that rely on floor responses instead of NSC response. This shift was unavoidable due to lack of appropriate experimental observations or expert opinions for predicting NSC damage and losses using their responses.

To establish applicable performance-based design tools that account for NSC losses, the methodology proposed by FEMA P-58 was used. A simplified design approach was proposed and implemented for the SCBF structures. This approach was based on NSC loss spectra that expressed the exceedance probability for various NSC loss levels when different design base shear coefficients, denoted by $C_y$, were considered. Thus, these plots allowed in-advance selection of the design base shear coefficient so that multiple target losses and the corresponding acceptable exceedance probabilities could be met.

To develop the loss spectra, a total number of 36 SCBF structures with 3, 6 and 12 stories were designed for a range of $C_y$ values and the FEMA P-58 procedure was

followed for estimating the probabilistic NSC loss curves. Two demand estimation approaches proposed by FEMA P-58 relying on incremental dynamic analysis (IDA) and static pushover (SPO) were considered simultaneously. The accuracy and applicability of these alternative methods were evaluated and discussed. The SPO-based approach was finally adopted for developing the NSC loss-based design spectra, according to its better consistency with the $C_y$-based procedure used in proportioning the structures.

Although the irregular $C_y$-related trends governed the IDA-based loss spectra, acceptable agreement was observed between the range of demand estimations made by the two SPO and IDA-based approaches. An example of 5-story chevron SCBF was designed using the proposed design spectra in order to evaluate the accuracy and applicability of the developed design tool. The interpolated $C_y$ factor was used for proportioning the structure following AISC 341-16 standard. Then, the designed structure was subjected to the SPO-based loss estimation procedure in order to compare the in-advance loss prediction with that obtained using the accurate procedure. Good agreement between the predicted and observed results was considered as an indication of the accuracy of the proposed design tool.

### 5.2. Recommendations for Future Study

The reviews provided in Chapters 2-4 highlight the knowledge and tools that should be provided to allow the practical performance-based design of the structures with respect to NSC losses. Although some of these requirements were addressed throughout this thesis, there are areas requiring further study. These areas mainly include:

- Experimental and judgment-based fragility curves and loss functions of NSCs that are based on the acceleration/velocity/displacement response of NSC instead of the floor response.

As discussed earlier, estimating NSC losses calls for defining multiple damage levels that reflect the extent of effort required to return the component back to its operational status. This needs precise consideration of the mechanism through which the component responds to the imposed excitation. As also discussed in FEMA P-58, experimental tests may be required for components such as partition walls or glazing systems. However, many electrical or machinery equipment can be supported by the data from repairmen.

When performing experimental tests is not affordable due to time or budget limitations, the judgment-based data can be derived using questionaries that collect expert opinions. The reliability of these data is much lower than the experimental data. To account for this lower reliability, the estimated mean values are commonly associated with large dispersion values such as 0.6. Respecting this large dispersion enforces taking enough conservatism so that the reliability of the final design becomes acceptable.

For relatively rigid components, the seismic fluctuation can be acceptably taken as that experienced by the supporting floor. However, as was shown in Chapters 2-3, the accurate value of acceleration response (as well as the other response measures) of the component is a function of its period, damping ratio and yield strength. Thus, relying on floor response for prediction of the component damage, as is currently done in FEMA P-58, may lack the required accuracy. Correlating the pre-defined damage levels to the NSC response is also associated with uncertainties that should be accounted for. Establishing probabilistic damage-response (fragility) models for the wide range of NSCs utilized in various occupancy types and the different disciplines (e.g., electrical and mechanical) of the buildings is an extensive work. This work would require participation of different professionals engaged with manufacturing, repairing and installing of the NSCs.

Having established the fragility models that are based on NSC response, additional work is also required to predict the probabilistic losses associated with each damage level. The probabilistic repair cost, repair time, environmental effects and the likely life losses consequent to each damage level are currently quantified for limited NSCs. This data should also be provided for the wide range of NSCs mentioned above. To allow the NSC loss estimation, the state-of-the-art FEMA P-58 guideline has provided damage and consequence models for a limited number of NSCs used in office and residential buildings. As mentioned before, these models are approximate since they do not rely on the responses predicted for the NSCs considering their interaction with the supporting floor.

- Extending and fine-tuning the performance-based design tools considering NSC losses

The design plots provided in Chapter 4 of this dissertation should be revised and improved in terms of accuracy and applicability. Considering different structural

systems rather than SCBF, addressing various structural properties, e.g., height, bracing configuration, and incorporating accurate NSC damage and loss models that would hopefully become available, form the future perspective of the design tools.
[53]